OXFORD UNIVERSITY PRESS | Carcinogenesis

FIBROBLAST GROWTH FACTOR RECEPTOR 4: A PUTATIVE KEY DRIVER FOR THE AGGRESSIVE PHENOTYPE OF HEPATOCELLULAR CARCINOMA

Journal:	*Carcinogenesis*
Manuscript ID:	CARCIN-2014-00086.R1
Manuscript Type:	Original Manuscript
Date Submitted by the Author:	13-Jun-2014
Complete List of Authors:	Gauglhofer, Christine; Medical University Vienna, Department of Medicine I Paur, Jakob; Medical University Vienna, Austria, Department of Medicine I Schrottmaier, Waltraud; Medical University Vienna, Austria, Department of Medicine I Wingelhofer, Bettina; Medical University Vienna, Austria, Department of Medicine I Huber, Daniela; Medical University Vienna, Austria, Department of Medicine I Naegelen, Isabelle; Medical University Vienna, Austria, Department of Medicine I Pirker, Christine; Medical University Vienna, Austria, Department of Medicine I Mohr, Thomas; Medical University Vienna, Austria, Department of Medicine I Heinzle, Christine; Medical University Vienna, Austria, Department of Medicine I Holzmann, Klaus; Medical University Vienna, Austria, Department of Medicine I Marian, Brigitte; Medical University Vienna, Austria, Department of Medicine I Schulte-Hermann, Rolf; Medical University Vienna, Austria, Department of Medicine I Berger, Walter; Medical University Vienna, Austria, Department of Medicine I Krupitza, Georg; Medical University Vienna, Department of Clinical Pathology Grusch, Michael; Medical University Vienna, Austria, Department of Medicine I Grasl-Kraupp, Bettina; Medical University Vienna, Department of Medicine I
Keywords:	fibroblast growth factor receptor 4, hepatocellular carcinoma , aggressive phenotype

FIBROBLAST GROWTH FACTOR RECEPTOR 4: A PUTATIVE KEY DRIVER FOR THE AGGRESSIVE PHENOTYPE OF HEPATOCELLULAR CARCINOMA

Christine Gauglhofer[1)], Jakob Paur[1)], Waltraud C. Schrottmaier[1)], Bettina Wingelhofer[1)], Daniela Huber[1)], Isabelle Naegelen[1)], Christine Pirker[1)], Thomas Mohr[1)], Christine Heinzle[1)], Klaus Holzmann[1)], Brigitte Marian[1)], Rolf Schulte-Hermann[1)], Walter Berger[1)], Georg Krupitza[2)], Michael Grusch[1)], Bettina Grasl-Kraupp[1)]

[1)] Department of Medicine I, Division: Institute of Cancer Research, Comprehensive Cancer Center, Vienna Medical University of Vienna, Borschkegasse 8a, A-1090 Vienna, Austria

[2)] Institute of Clinical Pathology, Medical University of Vienna, Waehringer Guertel 18-20, A-1090 Vienna, Austria

Correspondence: Bettina Grasl-Kraupp, Department of Medicine I, Division: Institute of Cancer Research, Comprehensive Cancer Center, Vienna Medical University of Vienna, Borschkegasse 8a, A-1090 Vienna, Austria; e-mail: bettina.grasl-kraupp@meduniwien.ac.at, Tel: +43-1-40160-57564

ABSTRACT

Recently, we found upregulation of fibroblast growth factor receptor 4 (FGFR4) in a subset of hepatocellular carcinoma (HCC). Here, we provide mechanistic insight into the role of FGFR4-mediated signaling for the aggressive behaviour of HCC cells.

To overexpress FGFR4, hepatoma/hepatocarcinoma cells were transfected with a construct coding for FGFR4. For down-modulation of endogenous FGFR4 we used siRNA or adenoviral infection with dominant-negative FGFR4 constructs being either kinase dead (kdFGFR4) or coding for the auto-inhibitory soluble domain (solFGFR4).

FGFR4 overexpression in non-tumourigenic hepatocarcinoma cells significantly reduced cell-matrix adhesion, enabled cells to grow anchorage-independently in soft agar, to disintegrate the lymph-/blood-endothelial barrier for intra-/extravasation of tumour cells, and to form tumours in SCID mice. Transcriptome analysis revealed altered expression of genes involved in cell-matrix interactions. Conversely, in highly tumourigenic cell lines kdFGFR4 or solFGFR4 lowered the proportion of cells in S-phase of the cell cycle, enhanced the G0/G1 and G2/M-phase proportions, reduced anchorage-independent growth in vitro, and attenuated disintegration of the lymph-/blood-endothelium and tumour formation in vivo. These findings were confirmed by altered expression profiles of genes being important for late stages of cell division.

Deregulated FGFR4 expression appears to be one of the key drivers of the malignant phenotype of HCC cells. Accordingly, blockade of FGFR4-mediated signaling by soluble dominant-negative constructs, like solFGFR4, may be a feasible and promising therapeutic approach to antagonize aggressive behaviour of hepatoma/hepatocarcinoma cells.

Summary: Here, we found that deregulated FGFR4 expression appears to be one of the key drivers of the malignant phenotype of hepatoma/hepatocarcinoma cells. Accordingly, blockade of FGFR4-mediated signalling may be a promising therapeutic approach to antagonize aggressive behaviour of the cells.

INTRODUCTION

Hepatocellular carcinoma (HCC) is among the five most common cancer entities worldwide, with about half a million new cases diagnosed annually, and an almost equal number of deaths, mostly due to early metastatic spread. About 15% of HCC patients only are candidates for surgical resection or liver transplantation. Standard chemotherapy is not applicable due to the intrinsically high chemoresistance of this tumour type. New strategies offering improvements in therapeutic efficacy and disease outcome are eagerly sought (1-3).

Upregulation of growth and survival factors is an important hallmark of hepatocarcinogenesis and a major driving force for tumour progression and dissemination (1-4). We have recently found over-expression of fibroblast growth factor receptor 4 (FGFR4) in almost 50% of HCC cases investigated, which agrees with observations of another group (5,6). Also, FGFR4-ligands, like FGF2 and FGF8-subfamily members were found to be upregulated in many HCC cases investigated (5-10). FGFR4 belongs to a RTK family of genes with similar protein structures (*FGFR1-4*) (7-11). Upon ligand binding the phosphorylated and dimerized form of FGFR4 recruits several adapter proteins, like FRS2α, and activates several signaling pathways including mitogen-activated protein kinase and phosphoinositide 3-kinase cascades. In dependence on the ligand, a great variety of cell-biological and biochemical processes may be affected, like cell cycle regulation, survival, differentiation, migration, adhesion, and/or bile acid metabolism (8-12). There is some evidence that FGFR4 may contribute to the development and progression of HCC, e.g., siRNA against FGF19 or antibodies targeting the FGF19-FGFR4 axis impaired the tumourigenicity of Huh7-cells, while this approach lacked significant effects in HepG2, SNU182 and SNU423 hepatoma/hepatocarcinoma cells (13-16).

Different FGFR ligands may impact in a specific way on one and the same receptor, as shown by the highly divergent molecular and biological effects of FGF7 and FGF10 on FGFR2b-mediated signaling (17). Also FGF19 exerts unique features with regard to FGFR4-activation and metabolic effects in hepatocytes, which are not shared by other FGFR4-ligands (8,11,12). We therefore used several hepatoma and recently established hepatocarcinoma cell lines which show inherent overexpression of FGF8-subfamily members, like 59% of the HCC cases studied (5,18). Since many FGFR4 ligands are upregulated in HCC, we targeted the receptor and applied not only siRNA and kinase-dead FGFR4-construct but also a soluble FGFR4-protein, which may be applicable in the near future, as exemplified by soluble decoy FGFR1c receptor being currently tested in a phase-1 clinical trial to treat solid tumours (19). In addition a novel, 3-dimensional bulk invasion assay was used to analyse the mechanism of tumour cell-mediated disruption of blood or lymphatic vessels (20). For the first time we show that FGFR4 over-expression reduced cell adhesion and enhanced anchorage-

independent growth, and disintegration of the lymph/blood-endothelial barrier. The boosted aggressive phenotype was confirmed by accelerated tumour formation of the HCC cells in SCID mice. In contrast, transfection with FGFR4-targeting siRNA or with kinase-deficient or soluble forms of FGFR4 impaired the malignant cell phenotype in vitro and tumour formation in vivo. Thus, use of soluble FGFR4-protein appeared as promising therapeutic option. In-depth investigations revealed that deregulations in FGFR4-mediated signaling affect genes involved in cell-matrix interactions, chromosome segregation, and/or cytokinesis. These findings together provide mechanistic insight into the role of FGFR4 as one of the key drivers of the malignant phenotype of HCC cells.

EXPERIMENTAL PROCEDURES

Cells. HepG2 and CCl-13 were obtained from ATCC (Rockville, MD). HCC-1.2. and HCC-3 lines, and telomerase-immortalised human lymphendothelial cells (LEC) and blood endothelial cells (BEC) were recently established and characterized (18,21). Authentication of the lines was performed by short-tandem-repeat-analyses, parallel to in-vitro studies. Determination of cell proliferation and cell death followed previous descriptions (5).

siRNA. Silencer®Select siRNA, targeting human FGFR4 and nonsilencing Silencer®Select scrambled siRNA (No AM4390843) were obtained from LifeTechnologies (Vienna/Austria). Further details see (5).

Vectors and adenoviral constructs. pcDNA3.1-vectors with(out) human VSV-tagged FGFR4 were kindly provided by Axel Ullrich (Max Planck Institute, Martinsried/FRG). The constructs were introduced into HCC-1.2 cells via FuGene® (Roche, Graz/Austria). Neomycin (PAA Laboratories, Cölbe/FRG; 0.5mg/ml medium) served to generate clones.

Adenoviral expression vectors for FGFRs have been described previously (22). Plasmids coding for human FGFR4 and solFGR4 were kindly provided by Shereen Ezzat (Ontario Cancer Institute, Canada) (23). The open reading frame was subcloned into pENTR1A (Invitrogen, Carlsbad/CA) with KpnI/XhoI. To generate a kinase-deficient variant (kdFGFR4), the kinase domain was removed by digestion with BglII/NotI and replaced by the Bg1II/NotI-digested sequence of cyan fluorescent protein (CFP). The resulting FGFR4-CFP chimera and the solFGFR4 were transferred into pAd/CMV/V5-Dest by Gateway recombination (Invitrogen). Virus amplification was done as described and an adenovirus expressing GFP was used as control (24). Virus titers were determined with the Adeno-X Rapid Titer Kit (Clontech, Mountain View/CA). Cells were exposed to the constructs at the lowest multiplicity of infection (MOI) leading to 100% cell infection (titrated by a

GFP-adenovirus).

Clonogenicity. 48hrs after transfection cells were plated in medium containing 10% FCS. At clone appearance in controls, cells were fixed in acetone/methanol (v50:50) and stained with 0.01% of crystal violet.

Soft agar assay. 48hrs after transfection cells were suspended in 20% FCS-RPMI containing 0.3% agar (Sigma) and were seeded onto 20% FCS-RPMI with 0.6% agar. Three-four weeks later the number of colonies (>10 cells) was determined.

Cell adhesion assay. 96-well plates were coated with type 1 collagen or fibronectin (Sigma, St.Louis/MO). Cells were plated at a density of $5x10^3$ per well. After incubation for 60, 90, or 120min at 37°C, medium was removed and wells were washed twice with 1xPBS to eliminate non-adherent cells. The number of adherent cells was determined by the EZ4U assay.

CCID (circular chemorepellent-induced defects) assay. $1x10^3$ cells were incubated in 150 µl EGM2-MV medium (Lonza, Walkersville/MD) containing 20% methylcellulose (M-0512, Sigma) in round bottom microtitre plates (BD-Biosciences) to allow spheroid formation within 48hrs. Spheroids were washed in PBS and transferred to confluent LEC/BEC monolayers, kept in EGM2-MV medium and stained by cytotracker green (2µg/ml for1hr, Invitrogen); 4hrs later, the spheroid and the CCID area in the LEC/BEC monolayer underneath were photographed. For each condition, the size of ≥10 spheroids and appendant CCIDs was measured by Image-J-software. For details see suppl.figs.1 and 2.

Gene expression analyses. For qRT-PCR, the extracted RNA was processed and measured by the ABI-Prism/7500 Sequence Detection System (Applied-Biosystems, Foster City/CA) using TaqMan-based assays (Applied-Biosystems), as described (5).

For whole genome expression analyses, the extracted RNA was subjected to quality control (2100 Bioanalyzer-System, Agilent, StClara/CA) and prepared by "Low RNA Input Linear Amplification Kit Plus", the "RNA Spike-In Kit" and the "Gene Expression Hybridization Kit" according to the manufacturer´s instructions (Agilent). The 4x44k microarray (Agilent) was used as a two-color array and was analysed by the G2505B-Microarray-Scanner (Agilent). Samples were analysed in triplicate in each individual experiment. Per run, data were processed by a combination of "Feature Extraction Software" and "GeneSpring-GX" (Agilent). Fold-change cutoffs (≥2/≤0.5) were used to select upregulated and downregulated genes, respectively. Differential gene expression was detected by t-test and Benjamini-Hochberg correction for multiple testing to ensure a false discovery rate less than 0.05. The functional annotation analysis on the selected lists was carried out using (i) gene set enrichment analysis (GSEA) to identify significantly enriched curated gene sets (version 3.0) among those included in the MSigDB database (http://www.broadinstitute.org/gsea/msigdb/index.jsp) and

(ii) Ingenuity Pathway Analysis (IPA, version 8.8; Ingenuity Systems, Redwood City, CA; www.ingenuity.com) (24). Further details see suppl.tab.5 and 6.

Immunoblotting. Protein purification, separation, and detection followed published protocols (5,18). Antibodies used: anti-VSV tag (eBioscience, San Diego/CA); anti-FGFR4 (sc-124 and sc-9006; Santa-Cruz Inc/CA), anti-ß-actin (Sigma, St Louis, MO), anti-phospho-PLCγ1(Tyr783) (Cell Signaling, Danvers, MA), anti-PLCγ1 (Cell Signaling), anti-phospho-p44/42 MAPK (ERK 1/2) (Thr202/Tyr204) (Cell Signaling), anti-ERK1/2 (Sigma), anti-phospho-AKT (Ser437) (Cell Signaling), anti-AKT (Cell Signaling). Band intensities were quantified by densitometry (ImageQuant 5.0-software; GE-Healthcare).

Animal study. $1x10^6$ cells were injected subcutaneously into both flanks of SCID/BALBc mice by standard procedures. HCC-1.2, HCC-3, and HepG2 cells were applied in serum-free medium containing 50% matrigel (Becton-Dickinson). The number and diameter of palpable tumours were determined thrice a week. When the local tumour affected the status of the host, the animal was sacrificed for necropsy. The experiments were performed according to the Austrian guidelines for animal care and protection.

RESULTS

Upregulation of FGFR4 enhances the aggressive phenotype of hepatocarcinoma cells. We recently found upregulation of FGFR4 in a subset of HCC (5). We therefore asked whether FGFR4 expression levels affect growth and aggressive phenotype of malignant hepatocytes. The hepatoma/hepatocarcinoma cell-lines used differ greatly in clonogenicity, anchorage-dependency in vitro, and tumourigenicity in vivo. Thus, CCl-13 cells are highly clonogenic in two different assays and tumourigenic in SCID mice, while HCC-1.2 cells are (almost) incapable of forming clones and tumours. HCC-3 and HepG2 cells rank in between these two extremes (fig.1). Spheroids of these hepatoma/hepatocarcinoma cells, attached to LEC or BEC monolayers, were used to simulate a critical step of metastasis, i.e., the gaps/CCID formed in the monolayer mimic entry gates for intravasating tumour emboli. The cell lines also vary in their capacity to disintegrate these lymph-/blood-endothelial barriers and to form CCID, with CCl-13 being most aggressive in this respect and HCC-1.2 forming only moderate CCID in LEC/BEC monolayers (fig.1D, E, and F; suppl.figs.1 and 2).

We generated HCC-1.2 clones with stable overexpression of FGFR4 (Cl1-Cl4). The resulting cells showed considerably elevated levels of FGFR4 mRNA and protein and enhanced levels of phosphorylated ERK and phosphorylated phospholipase-Cγ1 (PLCG1), which indicates activation of the major FGFR-mediated pathways under our experimental conditions (suppl.fig.3) (8). When analysing the transcriptome profiles of clones 1 and 3, we found significant, ≥2-fold downregulations of 1295 and ≥2-fold upregulations of 1119 genes (suppl.tab.2). Gene set enrichment or Ingenuity showed that many of the deregulated genes are involved in bile acid- and phase I&II-metabolism as well as in lipid and carbohydrate metabolism, confirming that our cells show known, hepatocyte-specific reaction patterns towards FGFR4-mediated signaling (suppl.tab.5 and 6) (11,12). Furthermore, many deregulations affected pathways being directly or indirectly involved in PLCG- and MAPK-mediated signaling. Similar alterations in the expression level of critical genes became evident in human HCC samples with high FGFR4 expression providing evidence that the hepatocarcinoma cells used are a relevant tool to study FGFR4-driven alterations in hepatocarcinogenesis (suppl.tab.7).

In contrast to vector controls, FGFR4-overexpressing cells became capable to form tumours in SCID mice (fig.2C). Studies on the mechanisms confering tumourigenicity to HCC-1.2 cells revealed that FGFR4 upregulation had little effect on viability, cell-cycle, or apoptotic activity of the cells (data not shown), but enhanced dramatically the clone forming capacity of the cells at low density (fig.2A). Transcriptome analysis showed that many of the affected genes are involved in cell adhesion, e.g.,

several members of the collagen, integrin, laminin, lectin, cadherin or protocadherin family were found to be deregulated (tab.1). In line with this observation, adherence of most of the clones to polystyrene, collagen and to some extent also to fibronectin was significantly reduced and growth in soft-agar was greatly increased (fig.2B,E). We also found upregulation of genes involved in metastasis (suppl.tab.2 and 5). Accordingly, the capacity of clones to induce CCID in BEC monolayers was greatly increased (fig.2D). This may indicate that overexpressed FGFR4 confers the ability for anchorage-independent growth and for invasiveness into blood-/lymph-endothelium, one of the hallmarks of a malignant cell phenotype.

Knock-down of FGFR4 reduces clone forming capacity of hepatocarcinoma cell lines. Next, we down-modulated the expression of FGFR4 by siRNA, which significantly reduced mRNA and protein levels in the cells investigated (fig. 3A and 3B). Viability (fig.3C) as well as cell cycle and apoptotic activity of the cells (not shown) was not altered, but the formation of clones at low density and in soft agar was significantly reduced (fig.3D and E). Scrambled siRNA (siSCR) did not impact on any of the test end points (not shown). These results provide further evidence that endogenous FGFR4 is essential for the pro-tumourigenic phenotype of hepatocarcinoma cells.

Blockade of FGFR4-induced signaling antagonizes tumour formation. To further study the relevance of FGFR4 in malignant transformation we interfered with FGFR4-mediated signaling. Cells were infected with adenoviral constructs coding for (i) dominant negative FGFR4, in which the kinase domain had been replaced by CFP (kdFGFR4), or (ii) the soluble part of FGFR4 (solFGFR4) which is also considered to act dominant-negatively by interfering with receptor-ligand interactions (23). This resulted in high expression of the constructs at the protein level and lowered phosphorylation of the FGFR binding adaptor protein FRS2α (supplementary figs.4 and 5). Impaired FGFR4 signaling resulted in dramatic reduction of clonogenicity and anchorage-independent growth in all 4 cell lines (fig.4A, B) and lowered the cells´ capacity to induce gaps in LEC/BEC monolayers (fig.4G). Correspondingly, tumour forming capacity tested with the 2 most tumourigenic lines, HepG2 and CCl-13, was significantly attenuated (fig.4C). These findings suggest that blockade of FGFR4-mediated signaling is a promising approach to antagonize tumour formation by hepatoma /hepatocarcinoma cells.

Blockade of FGFR4-mediated signaling may affect late stages of cell proliferation. Studies on the mechanisms underlying the reduced tumourigenicity of cell lines revealed that solFGFR4, and more strongly kdFGFR4, reduced the viability of the cells and increased the apoptotic activity

(fig.4D,E). Coincidently a considerable percentage of cells was shifted from the S to the G0/G1 and G2/M phase of the cell cycle (fig.4F). Transcriptome profiles revealed that FGFR4 blockade affected mostly genes involved in the formation and/or function of the spindle apparatus or kinetochore complex, as outlined in detail in the discussion (tab.1, supplementary tabs.3 and 4). Furthermore, the transcripts of genes, which are involved in the initiation and propagation of DNA replication (e.g. CDC7, NOL8) were reduced, while negative regulators of cell cycle (e.g. C13ORF15) tended to be expressed at an enhanced level. Many of these alterations occurred in both, kdFGFR4 or solFGFR4-transfected cells, indicating a similar consequence being more or less independent of the mode of FGFR4 blockade.

To conclude, these findings strongly suggest that expression and function of FGFR4 is an important determinant of the aggressive phenotype of the hepatoma/hepatocarcinoma cell lines tested.

Discussion

Here we show that FGFR4 appears to be a key driver of the aggressive phenotype of hepatoma/hepatocarcinoma cells, as outlined in the following.

For our mechanistic studies, we chose a panel of cell-lines, e.g. in barely aggressive HCC-1.2 cells upregulated FGFR4 expression elevated considerably clone formation, anchorage-independent and invasive growth and tumourigenicity. For proof of principle we chose the opposite approach and interfered in aggressive hepatoma/hepatocarcinoma cells with FGFR4 by (i) siRNA-mediated knock-down, (ii) kinase-dead kdFGFR4 for non-functional dimers with endogenous FGFR4, and (iii) solFGFR4 which consists of the IgI-loop/acidic box, lacks ligand-binding domains, and nevertheless neutralizes the mitogenic effects of FGFR4 ligands (23). The IgI–IgII linker region of FGFR1-3 serves as hinge allowing the IgI-loop/acidic box to auto-inhibit the ligand-binding domain (26). Since FGFR4 harbours the shortest IgI–IgII linker, solFGFR4 may compensate for this lack and compete with FGFs for binding (23,27). Here, solFGFR4 lowered phosphorylated FRS2α and altered the expression profiles to a similar extent as kdFGFR4 (suppl.fig.5). When compared to siRNA, solFGFR4 and kdFGFR4 caused more pronounced effects. The dominant-negative constructs decreased viability, anchorage-independent and invasive growth, and tumour formation in vivo. Thus, our data provide strong evidence that up- or downregulation of FGFR4 increases or decreases the aggressive phenotype of malignant hepatocytes, respectively. Furthermore, soluble FGFR4-protein appears as a very promising approach in the therapy of HCC, similar to FP-1039, a soluble decoy FGFR1c receptor being currently applied in a phase-1 clinical trial to treat solid tumours (19; http://www.fiveprime.com/pipeline/fp-1039).

An important hallmark of aggressive tumour cells is their capability to intravasate into the blood or lymphatic vasculature and to extravasate for metastasis formation. Since hepatocarcinoma cells preferably metastasize within the liver, which is hard to simulate in vivo, we established a 3-dimensional co-culture model of hepatoma/hepatocarcinoma cells with LEC/BEC-monolayers. LEC or BEC retracted and generated CCID, which resembles entry gates for tumour emboli through the lymphatic/blood cell wall. CCID formation could be impaired by inhibitors of I-κBα phosphorylation, matrix-metalloproteases, and lipoxygenases 12/15-1 (suppl.tab.1). Thus, the activity of NF-κB and secretion of metalloproteases and 12/15-HETE appear to be critical for the disintegration of the lymph/hemangioendothelial barrier by hepatoma/hepatocarcinoma cells, as reported for MCF-7 cells (20). The CCID formation could be greatly enhanced by overexpressing FGFR4 and impaired by interfering with FGFR4-mediated signaling. Transcriptome analyses revealed upregulation of NFkB-dependent genes by FGFR4 overexpression, such as phospholipase A2, which releases arachidonic acid from the membranes to provide substrate for lipoxygenases-12/15-1 (suppl.tab.2).

The aggressive phenotype is also characterized by altered cell-cell and cell-matrix interactions to enable evasion from organized tissue structures. The increased cloning efficacy of cells overexpressing FGFR4 may indicate a reduced dependency on cell-cell contacts, while the reduced matrix adhesion and the enhanced growth in soft-agar reflect lower requirements on anchorage for survival and proliferation.

In contrast to FGFR1-3 and mutant FGFR4, wildtype FGFR4 seems not to interact with NCAM (28-30). Upregulated FGFR4 reduced the expression of several cadherins, proto-cadherins, and integrins, which serve as docking sites for collagens, vitronectin and/or thrombospondins (31,32). Furthermore, transcript encoding for several collagens, vitronectin and thrombospondins were lowered as well (tab.1). These alterations altogether may explain the reduced adhesion of FGFR4-overexpressing hepatocarcinoma cells to collagen, fibronectin, and polystyrene.

It is becoming increasingly evident that cell-matrix interactions impact profoundly on several steps of cell division (33). At start of mitosis, cells loose attachments, disassemble focal adhesions, and adopt a round morphology. Cell-adhesion molecules, like ß-integrins, regulate centrosome function, spindle formation and orientation, and cytokinesis (34-36). In line with these findings is our observation that dominant negative FGFR4 constructs reduced the proportion of hepatoma/hepatocarcinoma cells in S-phase of the cell cycle and increased the proportion in G2/M. This was accompanied by changed transcription of genes involved in the formation and/or function of cohesins, chromosomal condensation, kinetochores, centrosome separation, the formation, stabilization and function of the spindles, and cytokinesis. Furthermore, impaired FGFR4-activity increased anchorage-dependency,

induced apoptosis and impaired disintegration of the LEC/BEC barrier. On the other hand, overexpressed FGFR4 reduced anchorage-dependency and cell adhesion, facilitated proliferation and probably mitosis in the emerging clones, and affected also indirectly the interaction with LEC/BEC. Thus, disruption of FGFR4-mediated signaling seems to interfere with mechanisms linking cell matrix interactions with late stages of cell division and to impact on several important components of the malignant phenotype of hepatoma/hepatocarcinoma cells.

To conclude, our mechanistic studies demonstrate the oncogenic impact of FGFR4 on the aggressive behaviour of HCC cells. Thus, great potential might lie in FGFR4 as a target for the treatment of this cancer entity and in the application of solFGFR4-protein as therapeutic tool.

Abbreviations: FGF, fibroblast growth factor; FGFR, fibroblast growth factor receptor; HCC, hepatocellular carcinoma; solFGFR4, soluble fibroblast growth factor receptor 4; kdFGFR4, dominant negative fibroblast growth factor receptor 4.

Disclosures: All authors disclose any potential conflict.

Grant support: This study was supported by the FWF (Project No P23491-B12), „Herzfeldersche Familienstiftung“ and the “Fonds für innovative interdisziplinäre Krebsforschung”.

REFERENCES

1. Forner,A. *et al.* (2012) Hepatocellular carcinoma. *Lancet*, **379**, 1245-1255.
2. Ferenci,P. *et al.* (2010) Hepatocellular carcinoma (HCC): a global perspective. World Gastroenterology Organisation Guidelines and Publications Committee. *J. Clin. Gastroenterol.*, **44**, 239-245.
3. Marquardt,J.U. *et al.* (2012) Molecular diagnosis and therapy of hepatocellular carcinoma (HCC): an emerging field for advanced technologies. *J. Hepatol.*, **56**, 267-275.
4. Calvisi,D.F. *et al.* (2012) Deregulation of signaling pathways in prognostic subtypes of hepatocellular carcinoma. *Biochim. Biophys. Acta*, **1826**, 215-237.
5. Gauglhofer,C. *et al.* (2011) Up-regulation of the fibroblast growth factor 8 subfamily in human hepatocellular carcinoma for cell survival and neoangiogenesis. *Hepatology*, **53**, 854-864.
6. Ho,H.K. *et al.* (2009) Fibroblast growth factor receptor 4 regulates proliferation, anti-apoptosis and alpha-fetoprotein secretion during hepatocellular carcinoma progression and represents a potential target for therapeutic intervention. *J. Hepatol.*, **50**, 118-127.
7. Wang,L. *et al.* (2012) A Novel Monoclonal Antibody to Fibroblast Growth Factor 2 Effectively Inhibits Growth of Hepatocellular Carcinoma Xenografts. *Mol. Cancer Ther.*, **11**, 864-870.
8. Turner,N. *et al.* (2010) Fibroblast growth factor signaling: from development to cancer. *Nat. Rev. Cancer*, **10**, 116-129.
9. Heinzle,C. *et al.* (2011) Targeting fibroblast-growth-factor-receptor-dependent signaling for cancer therapy. *Expert Opin. Ther. Targets*, **15**, 829-846.
10. Cheng,A.L. *et al.* (2011) Targeting fibroblast growth factor receptor signaling in hepatocellular carcinoma. *Oncology*, **81**, 372-380.
11. Wu,X. *et al.* (2012) Understanding the structure-function relationship between FGF19 and its mitogenic and metabolic activities. *Adv. Exp. Med. Biol.*, **728**, 195-213.
12. Heinzle,C. *et al.* Is fibroblast growth factor receptor 4 a suitable target of cancer therapy? *Current Pharmaceutical Design* (in press).
13. Nicholes,K. *et al.* (2002) A mouse model of hepatocellular carcinoma: ectopic expression of fibroblast growth factor 19 in skeletal muscle of transgenic mice. *Am. J. Pathol.*, **160**, 2295-2307.
14. Desnoyers,L.R. *et al.* (2008) Targeting FGF19 inhibits tumour growth in colon cancer xenograft and FGF19 transgenic hepatocellular carcinoma models. *Oncogene,* **27**, 85-97.
15. Sawey,E.T. *et al.* (2011) Identification of a therapeutic strategy targeting amplified FGF19 in liver cancer by oncogenomic screening. *Cancer Cell*, **19**, 347-358.

16. French,D.M. *et al.* (2012) Targeting FGFR inhibits hepatocellular carcinoma in preclinical mouse models. *PLoS One,* **7**, e36713.
17. Francavilla,C. *et al.* (2013) Functional proteomics defines the molecular switch underlying FGF receptor trafficking and cellular outputs. *Mol. Cell*, **51**, 707-722.
18. Sagmeister,S. *et al.* (2008) New cellular tools reveal complex epithelial-mesenchymal interactions in hepatocarcinogenesis. *Br. J. Cancer*, **99**, 151-159.
19. Harding,T.C. *at al.* (2013) Blockade of nonhormonal fibroblast growth factors by FP-1039 inhibits growth of multiple types of cancer. S*ci. Transl. Med.*, **5**, 178-189.
20. Kerjaschki,D. *et al.* (2011) Lipoxygenase mediates invasion of intrametastatic lymphatic vessels and propagates lymph node metastasis of human mammary carcinoma xenografts in mouse. *J. Clin. Invest*., **121**, 2000-2012.
21. Schoppmann,S.F. *et al.* (2004) Telomerase-immortalized lymphatic and blood vessel endothelial cells are functionally stable and retain their lineage specificity. *Microcirculation*, **11**, 261–269.
22. Fischer,H. *et al.* (2008). Fibroblast growth factor receptor-mediated signals contribute to the malignant phenotype of non-small cell lung cancer cells: therapeutic implications and synergism with epidermal growth factor receptor inhibition. *Mol. Cancer Ther.*, **7**, 3408–3419.
23. Ezzat,S. *et al.* (2001) A soluble dominant negative fibroblast growth factor receptor 4 isoform in human MCF-7 breast cancer cells. *Biochem. Biophys. Res. Commun*., **287**, 60-65.
24. Losert,A. *et al.* (2006) Monitoring viral decontamination procedures with green fluorescent protein-expressing adenovirus. *Anal. Biochem*., **355**, 310–312.
25. Subramanian,A. *et al.* (2005) Gene set enrichment analysis: A knowledge-based approach for interpreting genome-wide expression profiles. *Proc. Natl. Acad. Sci. USA*, **102**, 15545-15550.
26. Olsen,S.K. *et al.* (2004) Insights into the molecular basis for fibroblast growth factor receptor autoinhibition and ligand-binding promiscuity. *Proc. Natl. Acad. Sci. USA*, **101**, 935–940.
27. Chen,Q. *et al*. (2011) Soluble FGFR4 extracellular domain inhibits FGF19-induced activation of FGFR4 signaling and prevents nonalcoholic fatty liver disease. *Biochem. Biophys. Res. Commun.*, **409**, 651-656.
28. Cavallaro,U. *et al.* (2001) N-CAM modulates tumour-cell adhesion to matrix by inducing FGF-receptor signaling. *Nat. Cell Biol*., **3**, 650-657.
29. Ezzat,S. *et al.* (2004) Pituitary tumour-derived fibroblast growth factor receptor 4 isoform disrupts neural cell-adhesion molecule/N-cadherin signaling to diminish cell adhesiveness: a mechanism underlying pituitary neoplasia. *Mol. Endocrinol*., **18**, 2543-5252.
30. Christensen,C. *et al.* (2011) Berezin V, Bock E. Neural cell adhesion molecule differentially interacts with isoforms of the fibroblast growth factor receptor. *Neuroreport,* **22**, 727-732.

31. Staatz,W.D. *et al.* (1991) Identification of a tetrapeptide recognition sequence for the alpha 2 beta 1 integrin in collagen. *J. Biol. Chem.,* **266**, 7363-7367.

32. Adams,J.C. *et al.* (2004) The thrombospondins. *Int. J. Biochem. Cell. Biol.*, **36**, 961-968.

33. Streuli,C.H. (2009) Integrins and cell-fate determination. *J. Cell Sci.*, **122**, 171-177.

34. Aszodi,A. *et al.* (2003) β1 integrins regulate chondrocyte rotation, G1 progression, and cytokinesis. *Genes Dev.,* **17**, 2465–2479

35. LaFlamme,S.E. *et al.* (2008) Integrins as regulators of the mitotic machinery. *Curr. Opin. Cell Biol.*, **20**, 576-582.

36. Colello,D. *et al.* (2012) Integrins regulate microtubule nucleating activity of centrosome through mitogen-activated protein kinase/extracellular signal-regulated kinase kinase/extracellular signal-regulated kinase (MEK/ERK) signaling. *J. Biol. Chem*., **287**, 2520-2530.

LEGENDS

Figure 1. Cloning efficiency, invasive growth and tumourigenicity differ between hepatoma/hepatocarcinoma cell lines. In (A) cell lines were plated at a low density of 240 cells/cm^2 (HCC-1.2), 100 cells/cm^2 (HepG2, HCC-3), and of 60 cells/cm^2 (CCl-13). Clone numbers were determined after 3 weeks (HCC-1.2, HCC-3, HepG2) or 7 days (CCl-13). In (B) cells were seeded in soft agar at a density of 540 cells/cm^2 (HCC-1.2, HCC-3) or 180 cells/cm^2 (HepG2, CCl-13). Clones were counted after 4 weeks. In (A) and (B) the cloning efficiency was determined as the percentage of the cells seeded that form a clone. In (C) 1x10^6 cells/100µl serum-free medium were injected into flanks of SCID/BALBc mice. In (D,E) 3x10^3 cells were used for spheroid formation (for details see Methods). 48hrs later the spheroids formed were placed on confluent monolayers of LEC or BEC and were incubated for 4hrs. Pictures of spheroids and gap areas underneath were taken and areas were measured by ImageJ software. (D), representative spheroids of untreated HCC-1.2 cells and (E) CCID formed beneath in LEC or BEC. (F) gives the ratio between CCID area and spheroid size. All data are given as mean +/- SD of 3 independent experiments in (A,B,F) or of 4 animals in (C).

Figure 2. Overexpression of FGFR4 enhances anchorage-independency, invasiveness, and tumourigenicity of HCC-1.2 cells. Experiments in (A)–(D) have been performed as described in fig.1. (D), CCID formation of FGFR4-overexpressing clones. For further details on clones see suppl.fig.3. In (E) cells were seeded to petri dishes (made of polystyrene), being uncoated or coated with collagen or fibronectin; 60, 90, or 120min later the number of attached cells was determined. Data are expressed as fold vector control (pcDNA3.1) in (A,B,E) and are given as mean $\pm$ SD of $\geq$3 independent experiments in (A,B,D,E). (C) shows tumour formation in individual animals for each treatment group. Statistics by t-test in (A,B,D) and by Kruskal-Wallis test in (C,E): a) $p < 0.05$; b) $p < 0.01$; c) $p < 0.001$.

Figure 3. FGFR4 knockdown in hepatocarcinoma/hepatoma cell lines lowers clonogenicity and colony formation in soft agar. Cells were transiently transfected with scrambled siRNA (siSCR) or siRNA targeting FGFR4 (siFGFR4) applying 20nM (HCC-1.2, HepG2) or 10nM (HCC-3, CCl-13) of each. (A), the FGFR4 expression level was determined by qRT-PCR. The level of FGFR4 protein was determined 48hrs after transfection by immunoblotting and bands obtained were subjected to densitometry in (B). In (C) cell viability was determined by the EZ4U assay (see Experimental Procedures). In (D) cells were allowed to grow for up to 48hrs after transfection, were re-seeded and cultivated until the formation of colonies. Further details see fig.1. In (E) 48 hrs after transfection cells were replated in soft agar and were cultivated until the appearance of colonies. Further details are given in fig.1. Abbreviation: n.d., not determined. Data in (A-E) are means $\pm$ SD of fold siSCR of 3 independent experiments. Statistical analyses were performed with the t-test for siFGFR4 vs. siSCR: a) $p < 0.05$; b) $p < 0.01$; c) $p < 0.001$; d) $p < 0.0001$.

Figure 4. Blockade of FGFR4-mediated signaling impairs growth of hepatoma/hepatocarcinoma cells. Adenoviral constructs were used to transfect cells with kdFGFR4 or solFGFR4 (see experimental procedures). Untransfected cells (Co) and cells transfected with the adenoviral construct expressing GFP only (Vector) served as controls. (A) gives the clonogenicity and (B) the clone forming capacity in soft agar of untreated and infected cells. In (C) cells were implanted subcutaneously into the flanks of SCID/BALBc mice. In (D) the viability was determined by the EZ4U assay (see Experimental Procedures). FACS analyses served to determine the frequency of apoptosis in (E) and of the relative cell cycle distribution of asynchronous cultures in (F). In (G), 24hrs after transfection, $3x10^3$ cells were used for spheroid formation and were placed on BEC/LEC monolayers for CCID formation. In (A), (B), (D)-(G) the mean +/- SD of $\geq$ 3 independent experiments are given. (C) shows the means of 2 independent experiments each with 4 animals per treatment group. Statistics by t-test in (A,B,D-G) and by Kruskal-Wallis test in (C) for solFGFR4 or kdFGFR4 vs. vector: a) $p < 0.05$; b) $p < 0.01$; c) $p < 0.001$; d) $p < 0.0001$.

FIGURE 1

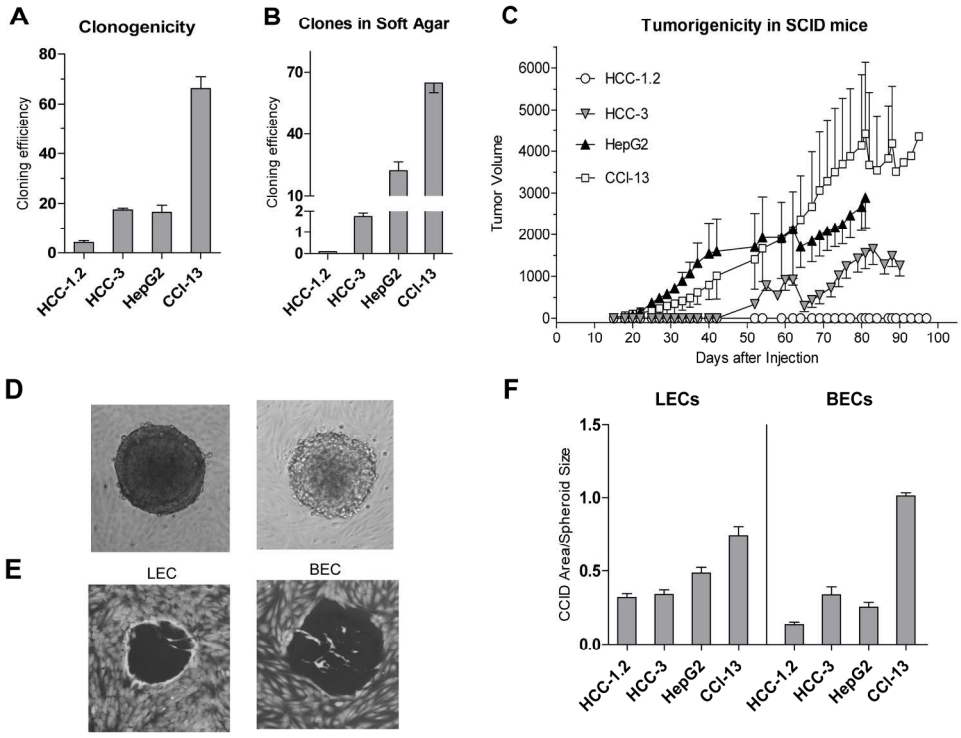

181x152mm (300 x 300 DPI)

FIGURE 2

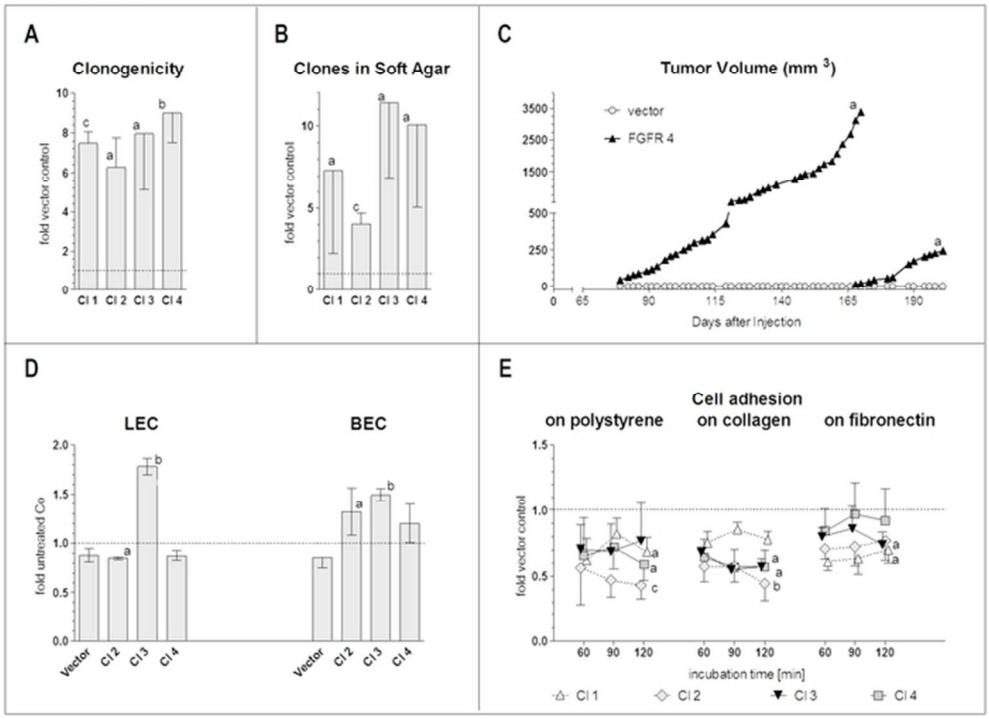

59x44mm (300 x 300 DPI)

FIGURE 3

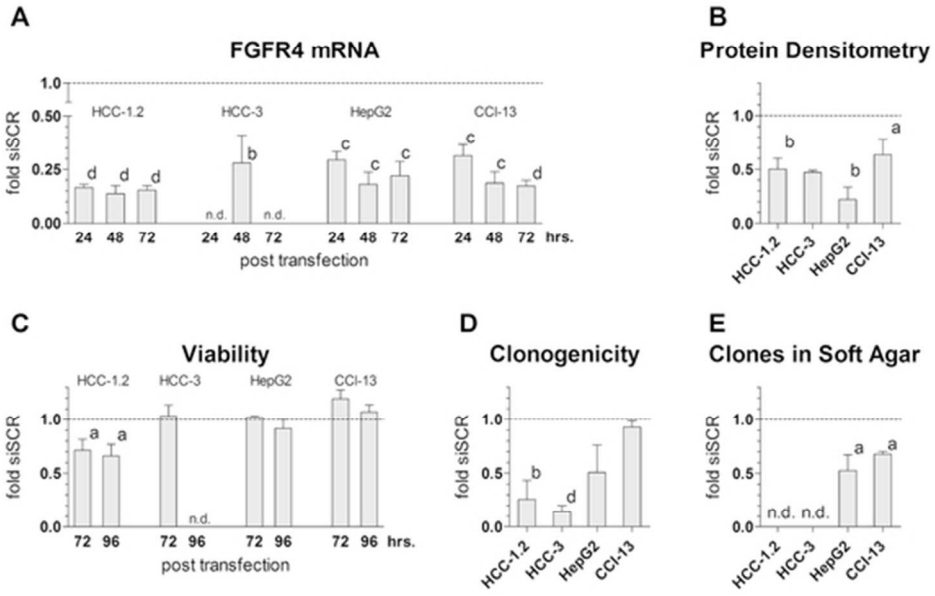

51x33mm (300 x 300 DPI)

FIGURE 4

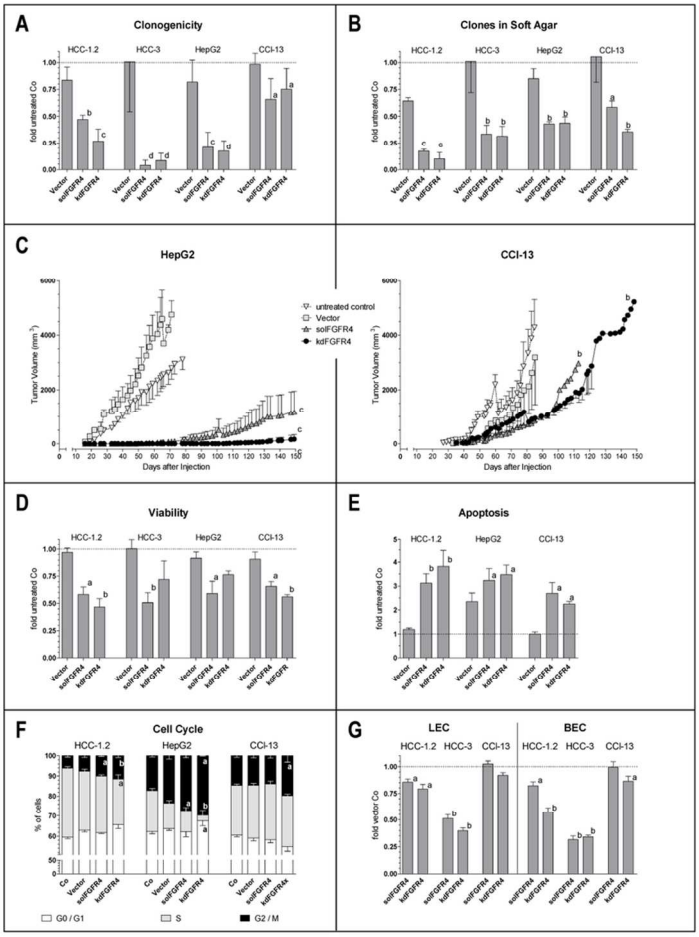

78x124mm (300 x 300 DPI)

Table 1. Selected genes being deregulated at least 2-fold by FGFR4 overexpression or dominant negative FGFR4-constructs. Further information is given in Experimental Procedures. For the significance of gene deregulation see supplementary tabs. 2-4. Gene set enrichment analyses are given in suppl.tab.5.

Type of Reg.	HCC-1.2 expressing **FGFR4**	HepG2 expressing **solFGFR4**	HepG2 expressing **kdFGFR4**
Cell Cycle/Division			
↓	*Genes involved in the function of : G1/S and/or G2/M* (CCAR1,CCNB3, CDKN1A, CLSPN), *M-phase*: MPHOSPH10, *cohesins* (SMC1A), *spindles* (NEK1), *kinetochore* (CENPF,CENPJ), *centrosome* (CEP290, KIF15)	*Genes involved in the function of: cohesins* (SGOL2), *kinetochore* (CENPC1, CENPE, NDC80), *centrosome* (CEP290,TTK), *spindles* (HMMR, DLGAP5)	*Genes involved in the function of: G1/S-Phase* (CDC7, DNA2, RB1CC1), *M-phase* (C14ORF106, MPHOSPH10, CUZD1,CDC40, NCAPG), *cohesins* (ESCO1,SGOL2, SMC2/6), *kinetochore* (CCDC99, CENPE, CENPK, CENPQ,CENPC1, MAD2L1, NDC80,NUF2,PLK4, ZWILCH), *centrosome* (KIF15), *spindles* (HMMR,DLGAP5,NEK7), *cytokinesis* (ANLN,SEPT7), *Other:* G2E3,NOL8, MORC3
↑	*G1/S and/or G2/M:* CDKN1C, PPP2R1B, CCRK, *Spindles* (FEZ1, NEK6), *cytokinesis* (NEK6, SEPT4/5/6)	*G0/G1:* G0S2, *G1/S and G2/M:* RRAD, C13ORF15	*G1/S and G2/M:* RRAD
Cell Adhesion/Extracellular Matrix			
↓	AHR, *cadherins* (CDH11/12 PCDH1), CADM4, CEACAM1/3,CLDN4, *collagens* (COL4A5/6, COL5A2/3,COL8A2,COL9A3,COL21A1), CTHRC1,DST,DTNA,FAT1,FLNC,FLRT3,GJA1, GULP1,HPSE, ICAM5, *integrins* (ITGA1/2/V), KIRREL, *laminins* (LAMA4/B1), LGALS1, LPP, LUM, MMP15, MUC4/15,NRCAM,PARD6A, PECAM1, PPFIBP1,PLXND1,PNN,PRPH2, RELN,ROBO1,ROCK1/2,SSX2IP,STEAP1, *thrombospondins(receptor)* (THBS1/4, THSD4, CD36) ,TRPM7, TSPAN8/13, UNC5B	HMMR	CUZD1,HMMR,SEPP1, TMEM87A,
↑	*cadherins* (CDH16/17,PCDHA1, PCDH24, PCDHB2/5/12), CADM1,CLDN14, CLEC10A, COL4A2,FBLN7,FBN1,FLRT1,GJA3,GPC1/4/5 *integrins* (ITGA3, ITGAM,ITGB2,ITGB1BP2), LAMB3,LOXL2,MPP1/7,NFASC,NPNT, PARVA,PRG4,SDCBP2,TNC,TNN,TNS1/3, TRO,VTN, TPBG	PLXND1,PSG2, RASD1,ROBO3, UNC5B	RASD1

Online Supplement

Studies on interactions of hepatoma/hepatocarcinoma cells with blood and lymphatic endothelium.

Metastasis is one of the primary causes for human mortality by cancer, as is true also for hepatocellular carcinoma (HCC). In particular, HCC most frequently show intrahepatic colonization due to the dense hepatic vasculature in the liver microenvironment (Van Zijl et al., 2011). Blood circulation is considered the main route of metastatic spread of HCC cells although invasion into the lymphatic system is often observed as well (Mitsunobu et al., 1996). In epithelial cancer entities, cells spontaneously form cohesive groups, which directly penetrate lymphatic vessel walls through large discontinuities (Kerjaschki et al., 2004; Christiansen et al., 2006; Friedl et al., 2010).

To gain insight into the mechanisms underlying lymphatic bulk invasion, an in vitro assay was established mimicking some features of the in vivo situation (Kerjaschki et al., 2011). MCF-7 cells were used to form spheroids, which were placed on telomerase immortalized human lymphendothelial cells (LEC) grown to confluent monolayers. Co-cultivation of spheroids on LEC resulted in the formation of circular discontinuities in the monolayers precisely beneath the spheroids, termed as circular chemorepellent-induced defects (CCID).

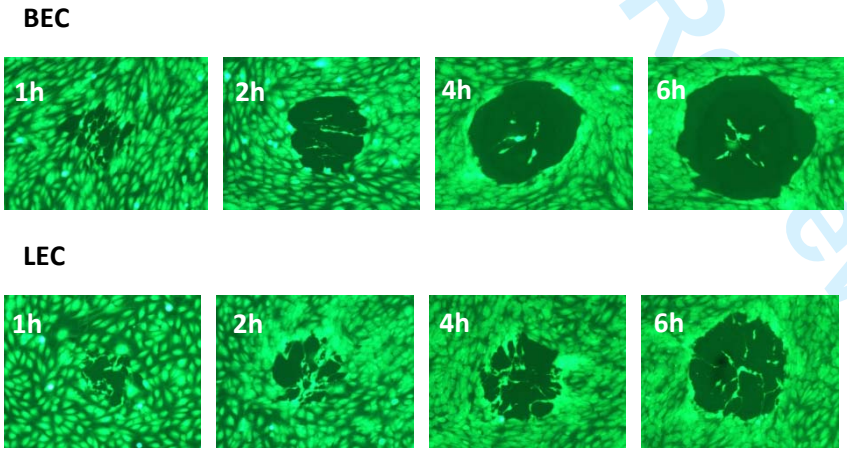

Supplementary Figure 1. Interaction of hepatoma/hepatocarcinoma cell lines with endothelial cells. *$1x10^3$ CCl-13 cells were incubated in 150 µl EGM2-MV medium (Lonza, Walkersville, MD) containing 20% methyl cellulose (M-0512, Sigma Aldrich) in round bottom microtitre plates (BD Biosciences) to allow spheroid formation within 48hrs. Spheroids were washed in PBS and transferred to confluent LEC/BEC monolayers, kept in 24-well plates and EGM2-MV medium and stained by cytotracker green (2µg/ml for1hr, Invitrogen). After 4hrs of incubation, the spheroid size and the CCID area in the LEC/BEC monolayer underneath were photographed at the time points indicated. Magnification (x 100).*

Further, centrifugal migration (retraction) of LEC instead of apoptosis was defined as the mechanism for gap formation (Kerjaschki et al., 2011).

We applied this assay to study the interaction of hepatoma/hepatocarcinoma cells with monolayers of telomerase immortalized LEC and blood endothelial cells (BEC) (Schoppmann et al., 2004). Generally, all cell lines used were able to form spheroids and CCID in endothelial cell monolayers. Pictures, taken at regular intervals, revealed centrifugal retraction of LEC and BEC beneath the spheroids, as has been shown before (suppl.fig.1).

CCl-13 cells had the highest capacity to disintegrate the LEC/BEC barrier, followed by HepG2, HCC-3 and HCC-1.2 cells, which agrees with the highly differing aggressive phenotype of the cell lines (suppl.fig.2 and fig.1 in manuscript). HepG2 spheroids were larger and less compact than those of CCl-13, HCC-1.2, or HCC-3 cells, and tended to fall apart when being transferred to LEC/BEC monolayers. Consequently, we used CCl-13, HCC-1.2, and HCC-3 cells for further experimentation.

A

	Spheroid	*Mean spheroid size (mm^2)*	*CCID in LEC*	*Mean area of CCID in LEC (mm^2)*	*CCID in BEC*	*Mean area of CCID in BEC (mm^2)*
HCC-1.2	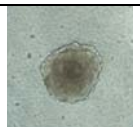	0.108 ± 0.019	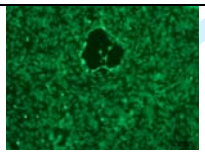	0.041 ± 0.01	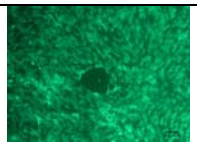	0.017 ± 0.005
HCC-3	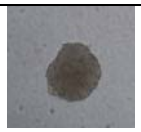	0.127 ± 0.015	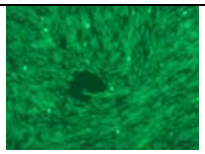	0.035 ± 0.009	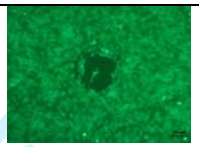	0.036 ± 0.016
HepG2	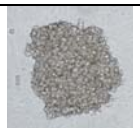	0.170 ± 0.034	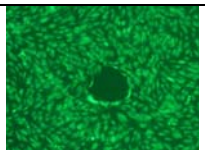	0.081 ± 0.01	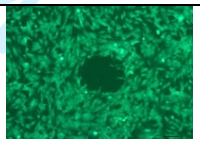	0.044 ± 0.021
CCl-13	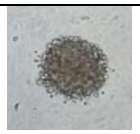	0.098 ± 0.012	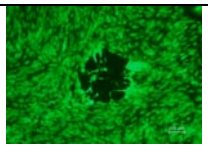	0.073 ± 0.015	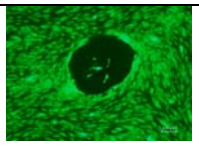	0.099 ± 0.016

Supplementary Figure 2. Interaction of HCC model cell lines with endothelial cells. *Methodical details see suppl.fig.1. After 4hrs of co-culture pictures of spheroids and CCID underneath were taken and the size of spheroids and the area of CCID underneath were measured by ImageJ software. Data are means ± SD of four independent experiments. Magnification x100.*

As shown by Honn et al. (1994) and Kerjaschki et al. (2011), the hypoxia-inducible enzymes lipoxygenases 12 (ALOX12) and ALOX15-1, which metabolize arachidonic acid to 12-hydroxyeicosatetraenoic acid (12(S)-HETE), were identified as mediators of CCID formation by MCF-7 cells. LEC exposed to 12(S)-HETE transiently destabilize VE-cadherin resulting in focal disruption of inter-endothelial adhesions and induction of migration of these cells. NFkB activation and matrix-metalloproteases (MMP) were also found to enhance the process of CCID formation (Vonach et al., 2011). Flister et al. (2010) suggested that activation of NF-κB enhances the motility of LEC which is required for the retraction of the cells. MMP degrade components of the extracellular matrix, modulate cell-cell and cell-matrix interactions, and therefore assist tumour cell metastasis (Deryugina et al., 2006). Accordingly, gap formation by MCF-7 spheroids was decreased by inhibition of MMP, which was assigned to impaired degradation of the VE-cadherin meshwork at inter-endothelial junctions and matrix attachments (Kerjaschki et al., 2011; Deryugina et al., 2006).

To investigate the mechanisms underlying the effects of hepatoma/hepatocarcinama spheroids on endothelial cells, we applied inhibitors of I-κBα phosphorylation (BAY11-7082, Merck, Darmstadt, FRG), MMP (GM6001, Merck), or ALOX12/15-1 (baicalein, Merck) 1hr before spheroids were transferred to LEC or BEC (suppl.tab.1). These pretreatments of spheroids reduced the size of CCID in LEC and BEC, with the exception of baicalein-treated CCl13 cells. Thus, the activity of NF-κB, MMP, and 12/15-HETE appear to be critical for the disintegration of the lymph/hemangioendothelial barrier by hepatoma/hepatocarcinoma cells.

		HCC-1.2.		HCC-3		CCL13	
		LEC	BEC	LEC	BEC	LEC	BEC
BAY	5 µM	99 ± 2	100 ± 11	90 ± 5	80 ± 8	97 ± 7	96 ± 15
BAY	10 µM	73 ± 3[b]	84 ± 15	73 ± 16	75 ± 8[a]	89 ± 1[b]	95 ± 2[a]
GM6001	10 µM	83 ± 9	82 ± 8	98 ± 7	75 ± 3[b]	97 ± 11	94 ± 1[a]
GM6001	20 µM	86 ± 7	83 ± 6[a]	93 ± 6	82 ± 5[a]	87 ± 5[a]	81 ± 8
GM6001	50 µM	83 ± 5[a]	62 ± 6[b]	85 ± 7	80 ± 2[b]	58 ± 5[b]	77 ± 2[b]
Baicalein	10 µM	90 ± 9	78 ± 17	93 ± 5	87 ± 5	104 ± 15	99 ± 9
Baicalein	20 µM	83 ± 3[a]	73 ± 10[a]	87 ± 5[a]	78 ± 6[a]	100 ± 12	100 ± 4
Baicalein	50 µM	76 ± 7[a]	65 ± 12[a]	75 ± 6[a]	67 ± 4[b]	97 ± 5	104 ± 13

Supplementary Table 1. BAY 11-7082, GM6001, and baicalein impair spheroid-induced gap formation in BEC and LEC monolayers. *Methodical details see suppl.fig.1. Spheroids were treated with different concentrations of BAY11-7082, GM6001 and baicalein for 1h and were placed on confluent LEC or BEC monolayers for 4hrs. Pictures of spheroids and gap areas underneath were taken and areas were measured by ImageJ software. Results are shown as % of untreated control and*

are expressed as mean ± SD of 3 independent experiments. Significant differences to untreated controls were determined by t-test: a), $p<0.05$; b), $p<0.01$.

References

Baker AH, Edwards DR, Murphy G. Metalloproteinase inhibitors: biological actions and therapeutic opportunities. Journal of Cell Science 2002;115:3719–3727.

Christiansen JJ, Rajasekaran AK. Reassessing epithelial to mesenchymal transition as a prerequisite for carcinoma invasion and metastasis. Cancer Research 2006;66:8319-8326.

Deryugina EI, Quigley JP. Matrix metalloproteinases and tumor metastasis. Cancer and Metastasis Reviews 2006;25:9-34.

Flister MJ, Wilber A, Hall KL, Iwata C, Miyazono K, Nisato RE, Pepper MS, Zawieja DC, Ran S. Inflammation induces lymphangiogenesis through up-regulation of VEGFR-3 mediated by NF-κB and Prox1. Blood 2010;115:418-429.

Friedl P, Wolf K. Plasticity of cell migration: a multiscale tuning model. Journal of Cell Biology 2010;188:11-19.

Honn KV, Tang DG, Gao X, Butovich IA, Liu B, Timar J, Hagmann W. 12-lipoxygenases and 12(S)-HETE: role in cancer metastasis. Cancer Metastasis Rev 1994;13:365-396.

Kerjaschki D, Regele HM, Moosberger I, Nagy-Bojarski K, Watschinger B, Soleiman A, Birner P, Krieger S, Hovorka A, Silberhumer G, Laakkonen P, Petrova T, Langer B, Raab I. Lymphatic neoangiogenesis in human kidney transplants is associated with immunologically active lymphocytic infiltrates. Journal of the American Society of Nephrology 2004;15:603-612.

Kerjaschki D, Bago-Horvath Z, Rudas M, Sexl V, Schneckenleithner C, Wolbank S, Bartel G, Krieger S, Kalt R, Hantusch B, Keller T, Nagy-Bojarszky K, Huttary N, Raab I, Lackner K, Krautgasser K, Schachner H, Kaserer K, Rezar S, Madlener S, Vonach C, Davidovits A, Nosaka H, Hämmerle M, Viola K, Dolznig H, Schreiber M, Nader A, Mikulits W, Gnant M, Hirakawa S, Detmar M, Alitalo K, Nijman S, Offner F, Maier TJ, Steinhilber D, Krupitza G. Lipoxygenase mediates invasion of intrametastatic lymphatic vessels and propagates lymph node metastasis of human mammary carcinoma xenografts in mouse. J Clin Invest 2011;121:2000-2012.

Mitsunobu M, Toyosaka A, Oriyama T, Nakao N. Intrahepatic metastases in hepatocellular carcinoma: the role of the portal vein as an efferent vessel. Clinical & Experimental Metastasis 1996;14:520-529.

Schoppmann SF, Soleiman A, Kalt R, Okubo Y, Benisch C, Nagavarapu U, Herron GS, Geleff S. Telomerase-immortalized lymphatic and blood vessel endothelial cells are functionally stable and retain their lineage specificity. Microcirculation 2004;11(3):261–269.

Van Zijl F, Krupitza G, Mikulits W. Initial steps of metastasis: cell invasion and endothelial transmigration. Mutation Research 2011;728:23-34.

Vonach C, Viola K, Giessrigl B, Huttary N, Raab I, Kalt R, Krieger S, Vo TPN, Madlener S, Bauer S, Marian B, Hämmerle M, Kretschy N, Teichmann M, Hantusch B, Stary S, Unger C, Seelinger M, Eger A, Mader R, Jäger W, Schmidt W, Grusch M, Dolznig H, Mikulits W, Krupitza G. NF-kB mediates the 12(S)-HETE-induced endothelial to mesenchymal transition of lymphendothelial cells during the intravasation of breast carcinoma cells. British Journal of Cancer 2011;105:263-271.

HCC-1.2. clones overexpress FGFR4 at the transcript and protein level and show enhanced phosphorylation of ERK and phospholipase Cγ (PLCγ).

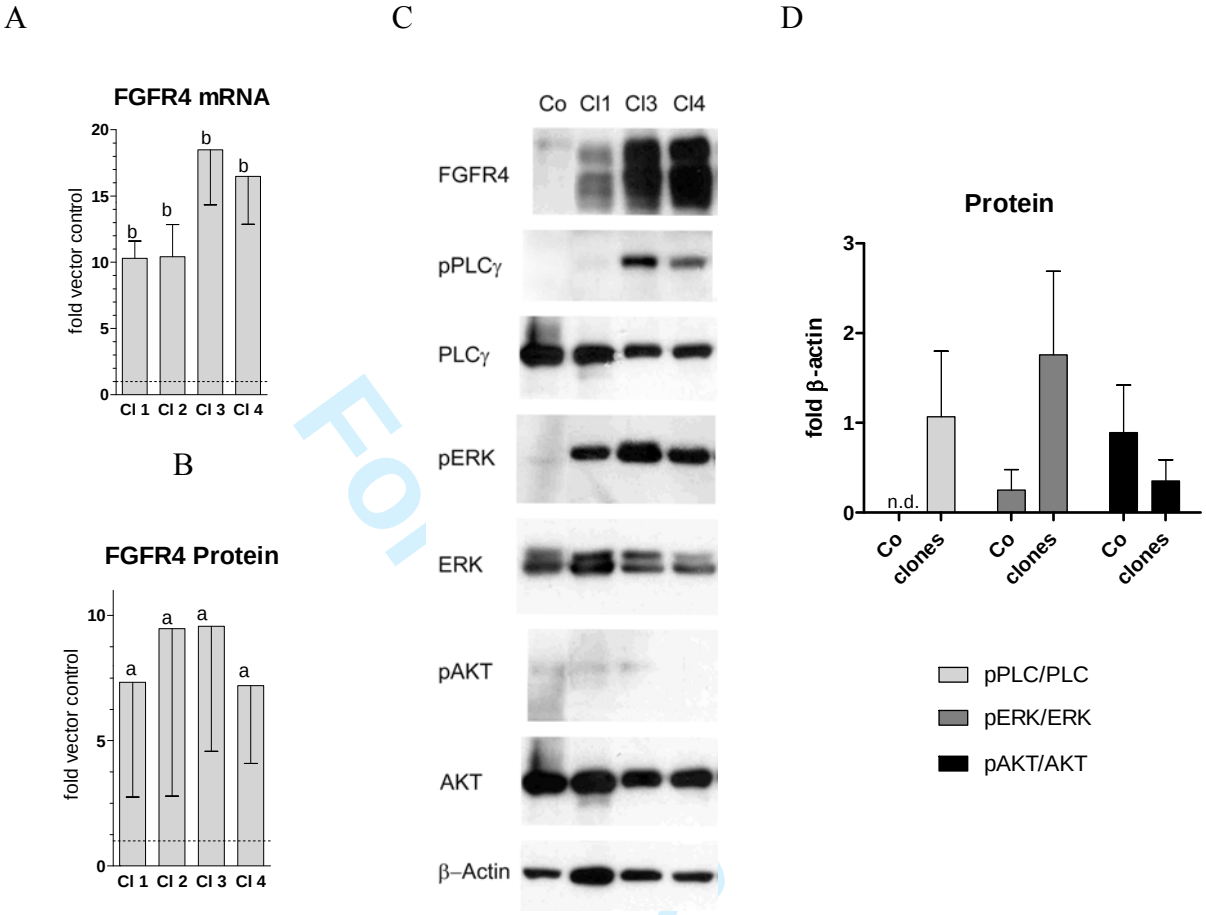

Supplementary Figure 3. *We generated HCC-1.2 clones with stable overexpression of FGFR4 (Cl1-Cl4). In (A) FGFR4 mRNA levels of clones 1-4 (Cl1-Cl4) were determined by qRT-PCR. In (B)- (D) cell lysates of the clones were subjected to immunoblotting to detect proteins. Antibodies used: anti-FGFR4 (sc-124 and sc-9006; Santa-Cruz Inc/CA), anti-ß-actin (Sigma, St Louis, MO), anti-phospho-PLCγ1(Tyr783) (Cell Signaling, Danvers, MA), anti-PLCγ1 (Cell Signaling), anti-phospho-p44/42 MAPK (ERK 1/2) (Thr202/Tyr204) (Cell Signaling), anti-ERK1/2 (Sigma), anti-phospho-AKT (Ser437) (Cell Signaling), anti-AKT (Cell Signaling). Band intensities were quantified by densitometry (ImageQuant 5.0-software; GE-Healthcare). Band intensities were quantified by densitometry and normalized to the ß-actin level. Abbreviation: n.d., not detectable. Data are means ± SD of ≥3 independent (in A, B) and of ≥2 experiments in (D). Statistics by t-test: a) $p < 0.05$; b) $p < 0.001$.*

Expression of dominant negative FGFR4 constructs and interference with downstream signaling.

Hepatoma/hepatocarcinoma cell lines were infected with dominant-negative FGFR4 constructs. The high expression of the constructs is shown in suppl.fig.4.

To investigate interference with FGFR4-mediated signaling, phosphorylation of the FGFR binding adaptor protein Frs2α was determined. On immunoblots signals were obtained at 60-75kDa which conforms to the molecular weights known for Frs2 proteins (suppl.fig.5). The impact of stable FGFR4 overexpression on the amount of phosphorylated Frs2α is shown in suppl.fig.5A. In all three HCC cell lines, the expression of dominant-negative FGFR4 constructs interfered with downstream signaling, as indicated by a reduced amount of phosphorylated Frs2α relative to total Frs2 protein (suppl.fig5B and 5C).

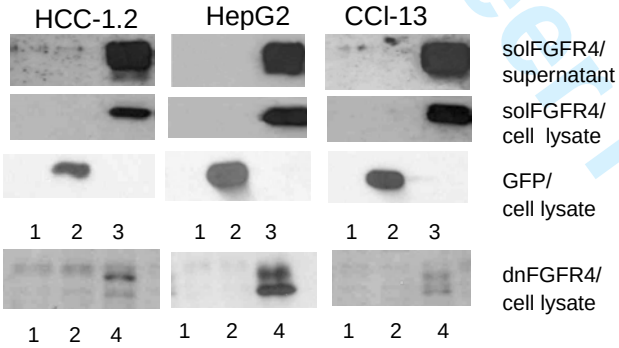

Supplementary Figure 4. Expression of dominant-negative FGFR4-constructs in hepatoma/ hepatocarcinoma cell lines. *Cells were infected with adenoviruses encoding for dn-FGFR4 or sol-FGFR4. Untreated cells and cells infected with a GFP-adenovirus served as controls. Proteins were isolated 24 hrs after infection and determined by immunoblotting. Proteins in the cell supernatants were isolated by EtOH precipitation, as described by Gauglhofer et al (Hepatology, 2011;53:854-864). For further details see Experimental Procedures. Lane 1, untreated; lane 2, GFP; lane 3, solFGFR4; lane 4, kdFGFR4.*

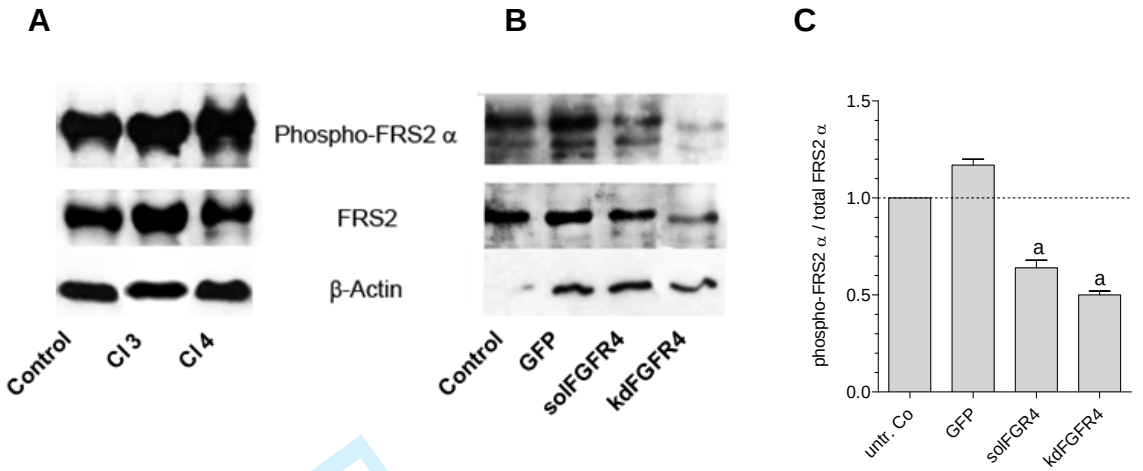

Supplementary Figure 5. Effect of FGFR4 blockade on downstream signaling. *(A), cell lysates of clones overexpressing the vector (control) or FGFR4 (Cl). (B), cell lysates of untreated HCC-1.2 cells (control) or 48hrs after infection with vector (GFP), solFGFR4, or kdFGFR4). Lysates were subjected to immunoblotting to detect total FRS2 and the phosphorylated form of FRS2α. Antibodies: anti-FRS2 (Santa Cruz Biotechnology, St.Cruz, CA) anti-FRS2α (Tyr196) Cell Signaling Technology (Danvers, MA). (C), band intensities were quantified by densitometry and normalized to the ß-actin level. The values, obtained in untreated controls, were arbitrarily set 1. Means and SD of fold control values are given. Statistics by t-test for solFGFR4 or kdFGFR4 vs. GFP: a) $p < 0.05$.*

Impact of FGFR4 overexpression and of intereference with FGFR4-mediated signaling on transcriptome profiles of hepatoma/hepatocarcinoma cells.

Supplementary Table 2. Genes being deregulated in FGFR4-overexpressing HCC-1.2. cells. *Data were processed as described in Experimental Procedures and are means of fold-vector control values of two different clones (clone 1 and 3). Fold-change cutoffs of ≥2 and ≤0.5 were used to select upregulated and downregulated genes, respectively.*

Gene	reg.	Mean x Control	S.D.	p-value
A1BG	up	8,3	6,7	0,1842
A2BP1	down	-2,8	0,1	0,0128
A2M	down	-7,1	6,7	0,2091
AADAC	down	-2,3	1,6	0,2313
AASDH	down	-2,2	0,1	0,0269
ABCA3	up	8,3	5,1	0,1454
ABCC3	down	-2,2	0,2	0,0420
ABCD3	up	2,7	0,7	0,0934
ABCE1	down	-2,1	0,2	0,0466
ABCG5	up	9,3	0,8	0,0209
ABCG8	up	3,8	0,3	0,0248
ABHD12	up	2,4	0,2	0,0334
ABHD2	up	2,0	0,8	0,1548
ACMSD	up	23,9	20,8	0,1817
ACPP	down	-6,3	2,1	0,0862
ACSL3	down	-3,2	0,3	0,0326
ACSL5	up	3,0	0,3	0,0363
ACSL6	down	-9,5	7,6	0,1803
ACSM1	down	-5,3	4,8	0,2126
ACSM3	up	2,5	0,8	0,1201
ACSS1	up	6,7	0,1	0,0043
ACSS2	up	2,5	0,1	0,0211
ACSS3	down	-3,4	1,7	0,1487
ACTG2	down	-3,2	2,2	0,1974
ACVR1C	up	3,1	0,9	0,0923
ACYP1	down	-2,1	0,3	0,0571
ADAM21	up	2,0	0,8	0,1655
ADAM23	down	-2,9	0,6	0,0736
ADAM6	down	-2,6	0,8	0,1101
ADAM8	up	2,8	0,1	0,0074
ADAM9	down	-2,2	0,0	0,0075
ADAMTS2	down	-12,4	4,6	0,0882
ADAMTS9	up	2,8	1,2	0,1441
ADARB1	up	2,3	0,4	0,0679
ADC	up	2,7	0,4	0,0525
ADCY5	up	5,1	0,5	0,0277
ADCY9	up	2,0	0,7	0,1364
ADH1A	up	14,7	14,2	0,2019
ADH1C	up	2,6	0,6	0,0906
ADH4	up	15,7	16,0	0,2089
ADORA1	up	2,9	1,3	0,1445
ADPRHL1	up	2,1	0,1	0,0253
ADRB2	up	6,3	3,7	0,1464
ADRBK2	up	4,5	3,2	0,1849
AFAP1L1	up	2,1	0,4	0,0784
AFF1	down	-2,0	0,4	0,0891
AFM	up	8,9	7,3	0,1857
AFP	up	29,8	35,3	0,2274
AGAP2	up	2,9	0,4	0,0420
AGBL2	up	2,7	1,0	0,1271
AGGF1	down	-2,4	0,4	0,0667
AGK	down	-2,4	0,4	0,0646
AGPAT2	up	2,9	0,4	0,0485
AGPAT4	up	4,1	0,0	0,0013
AGPS	down	-2,3	0,6	0,1111
AGR2	down	-7,0	1,6	0,0608
AGTR1	down	-2,2	0,5	0,0951
AGXT	up	2,2	0,5	0,0862
AHCTF1	down	-3,2	0,4	0,0452
AHCY	up	2,2	0,1	0,0182
AHR	down	-3,2	1,3	0,1302
AHRR	up	2,3	0,0	0,0035
AHSA2	down	-2,0	0,3	0,0680
AIF1	down	-3,9	3,1	0,2076
AIF1L	up	12,0	4,1	0,0816
AIFM3	down	-2,6	0,5	0,0707
AIMP1	down	-2,0	0,4	0,0795
AKAP11	down	-2,3	0,6	0,0961
AKAP12	up	3,2	2,6	0,2201
AKAP14	up	9,6	3,4	0,0880
AKAP9	down	-3,8	1,0	0,0777
AKD1	up	3,2	0,9	0,0871
AKR1B10	down	-2,4	1,3	0,1802
AKR1C1	up	4,7	2,5	0,1417
AKR1C3	up	2,1	0,1	0,0210
AKR1D1	up	5,6	0,6	0,0280
AKT1S1	up	2,0	0,1	0,0319
ALAD	up	2,2	0,0	0,0079

ALB	up	3,9	3,9	0,2442	APOL4	up	2,2	0,6	0,1007
ALDH8A1	up	2,5	1,2	0,1660	APOLD1	up	2,5	0,6	0,0885
ALDOB	down	-2,4	0,6	0,0961	AQP3	up	3,0	0,7	0,0795
ALKBH8	down	-2,2	0,8	0,1495	ARAP1	up	2,1	0,2	0,0431
ALMS1	down	-2,7	0,8	0,1005	ARAP2	down	-10,0	5,2	0,1221
ALMS1P	down	-2,2	0,5	0,0980	ARG2	down	-2,5	0,4	0,0655
ALOX5AP	up	7,1	0,5	0,0186	ARGLU1	down	-2,1	0,2	0,0415
ALPK1	down	-2,6	1,4	0,1773	ARHGAP12	down	-2,7	0,7	0,0868
ALX4	down	-2,3	0,2	0,0391	ARHGAP18	down	-5,2	3,2	0,1587
AMMECR1	down	-2,1	0,0	0,0028	ARHGAP20	up	3,6	2,1	0,1641
AMOTL1	up	7,8	0,1	0,0031	ARHGAP21	down	-2,1	0,1	0,0118
AMPD3	up	10,6	0,2	0,0042	ARHGAP22	down	-6,0	2,3	0,1011
ANG	up	2,2	0,7	0,1265	ARHGAP29	down	-2,6	0,2	0,0310
ANGPT1	down	-4,9	0,0	0,0007	ARHGAP5	down	-2,0	0,4	0,0892
ANGPTL1	down	-3,5	1,0	0,0895	ARHGEF10	down	-2,5	1,0	0,1369
ANK3	down	-2,2	1,0	0,1770	ARHGEF16	down	-3,1	1,7	0,1643
ANKRD10	down	-2,3	0,3	0,0570	ARID4B	down	-2,5	0,1	0,0166
ANKRD12	down	-3,7	0,6	0,0506	ARID5B	down	-2,8	0,1	0,0184
ANKRD18B	up	7,2	1,7	0,0594	ARL10	up	3,0	0,1	0,0093
ANKRD20A2	up	5,1	0,8	0,0424	ARL17	down	-2,1	0,2	0,0464
ANKRD26	down	-3,2	0,7	0,0715	ARL17P1	down	-2,5	0,7	0,1025
ANKRD32	down	-2,4	0,4	0,0680	ARL4C	up	8,0	2,9	0,0921
ANKRD36	down	-2,4	0,4	0,0728	ARMC2	up	3,4	1,2	0,1098
ANKRD36B	down	-2,6	0,5	0,0722	ARMC9	up	2,5	0,4	0,0653
ANKRD58	up	7,2	2,0	0,0729	ARMCX1	down	-4,7	2,1	0,1206
ANKRD6	up	16,8	7,3	0,1004	ARMCX3	down	-3,5	0,3	0,0314
ANKRD62	down	-6,7	4,9	0,1751	ARNTL2	down	-3,6	1,1	0,0890
ANTXR1	up	3,7	1,2	0,0993	ARRDC4	up	2,4	0,5	0,0790
ANTXR2	down	-2,3	0,9	0,1366	ARSJ	down	-39,8	46,0	0,2218
ANXA1	down	-7,8	0,6	0,0196	ART5	up	3,2	0,4	0,0420
ANXA13	up	12,6	0,5	0,0088	ASB2	up	2,9	0,5	0,0558
ANXA3	down	-2,8	1,5	0,1678	ASB9	down	-2,3	1,2	0,1811
AP1AR	down	-2,3	0,2	0,0281	ASH1L	down	-3,6	1,4	0,1126
APBA2	up	9,1	3,1	0,0842	ASMT	down	-3,5	0,3	0,0308
APBB1IP	up	5,6	0,7	0,0321	ASPA	up	5,0	0,1	0,0043
APBB2	down	-2,2	0,2	0,0325	ASPG	up	2,9	0,3	0,0345
APLF	down	-6,5	2,4	0,0951	ASPH	down	-2,9	0,4	0,0431
APLN	up	4,7	1,0	0,0619	ASPHD1	down	-3,8	0,3	0,0219
APOA2	down	-2,0	0,3	0,0711	ASPM	down	-2,6	0,1	0,0209
APOA4	up	3,2	0,0	0,0046	ASS1	up	3,1	0,3	0,0320
APOA5	up	7,4	1,3	0,0468	ATAD2	down	-2,2	0,2	0,0280
APOB	down	-3,4	0,6	0,0593	ATAD4	up	2,2	0,6	0,1000
APOBEC3C	down	-3,3	2,6	0,2139	ATAD5	down	-3,8	1,1	0,0838
APOBEC3G	up	6,4	2,8	0,1127	ATG16L2	down	-2,5	0,4	0,0627
APOC1	up	2,3	0,1	0,0144	ATOH7	up	2,5	1,0	0,1356
APOC3	up	6,6	2,4	0,0948	ATOH8	down	-5,1	1,1	0,0625
APOL2	up	2,2	0,5	0,0811	ATP10D	up	2,6	0,7	0,0928

ATP13A3	down	-2,1	0,3	0,0556	C10orf10	down	-5,5	0,7	0,0368
ATP2B1	down	-2,4	0,4	0,0597	C10orf116	down	-3,7	0,9	0,0756
ATP7A	down	-2,1	0,6	0,1223	C10orf118	down	-2,8	0,8	0,0996
ATR	down	-2,4	0,6	0,0876	C10orf82	up	10,4	10,3	0,2102
ATRNL1	up	5,0	4,0	0,1943	C10orf90	down	-2,3	0,0	0,0043
ATRX	down	-2,9	0,2	0,0292	C10orf93	up	8,3	6,9	0,1864
AUTS2	up	23,9	1,5	0,0150	C11orf60	up	3,2	0,5	0,0508
AVIL	up	4,3	3,3	0,1950	C11orf63	up	7,2	6,7	0,2073
AZGP1	up	3,9	1,8	0,1325	C11orf82	down	-2,0	0,2	0,0361
AZI2	down	-3,1	0,0	0,0034	C11orf86	up	2,6	1,0	0,1366
B3GALNT1	down	-4,0	2,5	0,1676	C11orf92	down	-2,3	0,9	0,1454
B4GALNT3	up	5,3	1,1	0,0546	C11orf93	down	-2,2	0,9	0,1499
BACE1	down	-2,4	0,7	0,1136	C12orf34	up	2,2	0,5	0,0831
BAGE	down	-3,4	0,5	0,0429	C12orf35	down	-2,8	0,0	0,0003
BAT2D1	down	-2,1	0,2	0,0334	C12orf39	down	-6,9	0,7	0,0257
BATF	down	-10,6	9,1	0,1875	C12orf42	up	2,2	0,1	0,0122
BAZ1A	down	-2,5	1,0	0,1349	C12orf70	down	-3,0	0,0	0,0028
BAZ2B	down	-2,8	0,9	0,1141	C13orf15	down	-7,5	0,6	0,0217
BBOX1	up	3,8	0,2	0,0151	C13orf29	down	-2,9	0,5	0,0617
BBS7	down	-2,4	0,3	0,0404	C13orf31	down	-2,6	0,9	0,1173
BCL2A1	up	2,0	0,3	0,0665	C14orf106	down	-2,3	0,7	0,1221
BCL2L11	up	2,2	0,2	0,0373	C14orf132	up	7,8	1,9	0,0613
BCLAF1	down	-2,1	0,8	0,1539	C14orf145	down	-2,3	0,0	0,0076
BDKRB1	down	-14,0	3,8	0,0655	C15orf27	up	9,1	2,2	0,0605
BDP1	down	-2,5	0,4	0,0600	C15orf41	down	-2,8	0,6	0,0730
BEND5	up	10,6	1,6	0,0384	C15orf48	up	15,3	6,0	0,0920
BEST1	down	-3,2	0,7	0,0686	C15orf59	up	4,7	1,9	0,1114
BEX5	up	2,5	0,6	0,0893	C16orf45	up	8,4	1,9	0,0578
BICC1	down	-4,5	3,4	0,1936	C16orf74	up	5,3	2,4	0,1188
BIN3	up	2,4	0,0	0,0009	C17orf108	up	2,1	0,3	0,0626
BIRC3	down	-6,5	0,4	0,0155	C17orf97	up	6,1	0,7	0,0295
BIVM	down	-2,1	0,6	0,1137	C18orf1	up	79,6	2,4	0,0070
BMF	up	4,7	1,4	0,0821	C19orf18	up	4,1	1,5	0,1062
BMP8B	up	2,2	0,3	0,0665	C19orf69	down	-11,4	10,3	0,1949
BNIP3L	up	2,0	0,3	0,0706	C1orf114	down	-3,9	0,7	0,0529
BOD1L	down	-5,3	1,6	0,0833	C1orf115	up	2,2	0,4	0,0698
BPI	up	9,7	0,8	0,0210	C1orf161	down	-2,8	0,5	0,0659
BRCA2	down	-4,5	1,1	0,0716	C1orf162	down	-2,1	0,2	0,0328
BRCC3	down	-2,9	0,6	0,0673	C1orf21	up	6,7	2,2	0,0837
BRF1	down	-2,3	0,7	0,1181	C1orf210	up	3,7	2,0	0,1546
BRIP1	down	-2,4	0,5	0,0875	C1orf226	up	2,5	0,3	0,0486
BRUNOL4	down	-3,5	0,5	0,0436	C1orf27	down	-3,3	0,6	0,0581
BRWD1	down	-4,5	0,8	0,0511	C1orf89	down	-2,2	0,3	0,0620
BRWD3	down	-2,3	0,1	0,0153	C1orf9	down	-3,8	0,7	0,0528
BTBD9	up	2,8	0,2	0,0276	C1R	up	2,3	0,2	0,0337
BTD	up	2,3	0,3	0,0487	C20orf132	up	2,8	0,4	0,0472
BTG1	up	2,3	0,2	0,0345	C20orf29	up	2,3	0,0	0,0013

C20orf3	up	2,2	0,4	0,0720	C9orf123	up	2,2	0,5	0,0996
C20orf94	down	-100,9	102,1	0,1991	C9orf125	down	-3,5	1,4	0,1190
C21orf122	up	2,6	0,8	0,1091	C9orf130	up	2,2	0,3	0,0639
C21orf129	down	-2,3	1,3	0,1962	C9orf150	down	-4,9	0,5	0,0261
C21orf34	down	-11,6	0,0	0,0001	C9orf167	up	2,8	0,8	0,1022
C22orf41	up	2,6	0,1	0,0124	C9orf3	up	2,0	0,0	0,0003
C2CD2	down	-2,2	0,0	0,0002	C9orf43	up	2,9	0,4	0,0443
C2orf60	down	-2,1	0,5	0,1025	C9orf5	up	2,3	0,2	0,0259
C2orf63	down	-2,1	0,7	0,1285	C9orf57	down	-7,4	0,5	0,0167
C2orf77	down	-5,5	0,9	0,0428	C9orf9	up	3,0	0,2	0,0265
C2orf88	up	2,0	0,4	0,0805	CA13	up	16,2	10,3	0,1431
C3	up	2,4	0,4	0,0626	CA14	down	-2,0	0,1	0,0317
C3orf14	down	-2,5	0,8	0,1143	CA5A	up	2,2	0,4	0,0669
C3orf15	down	-6,9	0,0	0,0015	CA9	down	-2,9	0,5	0,0575
C3orf32	down	-2,6	0,9	0,1125	CACHD1	up	4,8	2,3	0,1281
C3orf57	down	-4,1	2,6	0,1704	CACNA1D	down	-2,7	0,2	0,0223
C3orf63	down	-2,4	0,4	0,0675	CACNG1	down	-4,1	0,2	0,0166
C4B	up	5,5	2,6	0,1240	CACNG4	down	-3,0	0,7	0,0759
C4orf21	down	-4,2	1,5	0,0978	CADM1	up	2,3	0,7	0,1235
C4orf41	down	-2,1	0,0	0,0003	CADM4	down	-2,6	0,3	0,0361
C4orf49	down	-2,5	0,3	0,0407	CADPS2	down	-3,2	1,1	0,1055
C5orf24	up	2,5	0,0	0,0013	CALR3	up	2,0	0,5	0,1053
C5orf32	down	-13,5	12,4	0,1950	CAMK2D	down	-2,1	0,5	0,0995
C5orf42	down	-3,2	0,1	0,0075	CAMKK1	up	2,9	1,2	0,1366
C6	down	-5,0	3,9	0,1927	CAMSAP1L1	down	-2,3	0,2	0,0311
C6orf114	up	2,1	0,3	0,0684	CAMTA1	down	-2,8	0,1	0,0158
C6orf132	up	4,9	0,1	0,0073	CAMTA2	down	-2,1	0,1	0,0127
C6orf134	down	-4,7	0,0	0,0006	CAPN2	up	4,6	3,0	0,1672
C6orf141	down	-11,4	10,5	0,1971	CASC5	down	-2,2	0,6	0,1095
C6orf145	up	2,0	0,3	0,0691	CASK	down	-2,2	0,1	0,0273
C6orf154	up	2,3	0,1	0,0181	CASP8	down	-3,3	0,7	0,0637
C6orf168	up	3,1	1,7	0,1618	CASP8AP2	down	-2,6	0,6	0,0868
C6orf208	up	2,5	0,6	0,0842	CCAR1	down	-2,1	0,5	0,1032
C6orf225	up	2,9	0,8	0,0922	CCBL2	down	-2,1	0,2	0,0367
C6orf26	down	-2,5	0,0	0,0075	CCDC11	down	-8,0	1,9	0,0611
C6orf59	up	4,2	0,5	0,0344	CCDC116	up	2,1	0,2	0,0501
C7orf10	up	2,5	0,6	0,0932	CCDC122	down	-2,0	0,3	0,0604
C7orf53	down	-2,9	1,3	0,1444	CCDC125	down	-2,2	0,3	0,0595
C7orf58	down	-7,3	1,2	0,0417	CCDC132	down	-2,0	0,1	0,0201
C8B	up	4,1	2,0	0,1320	CCDC135	up	3,6	1,1	0,0891
C8orf38	down	-2,0	0,1	0,0134	CCDC144A	up	2,3	0,6	0,0964
C8orf4	down	-20,8	0,3	0,0031	CCDC150	down	-2,9	0,4	0,0423
C8orf47	up	2,7	0,7	0,0930	CCDC151	up	2,9	0,1	0,0102
C8orf58	up	2,1	0,2	0,0512	CCDC155	up	5,7	2,8	0,1279
C9orf109	up	3,0	0,0	0,0006	CCDC28B	down	-2,1	0,5	0,1042
C9orf114	up	2,0	0,1	0,0141	CCDC34	down	-2,2	0,2	0,0370
C9orf122	up	3,6	1,3	0,1086	CCDC36	up	4,8	0,0	0,0007

CCDC41	down	-2,1	0,4	0,0747
CCDC46	down	-2,9	1,5	0,1612
CCDC47	down	-2,0	0,3	0,0706
CCDC50	down	-2,0	0,1	0,0188
CCDC55	down	-2,4	0,7	0,1039
CCDC66	down	-3,1	0,0	0,0006
CCDC68	down	-3,8	1,0	0,0784
CCDC69	up	5,6	1,3	0,0612
CCDC74B	down	-2,9	0,2	0,0248
CCDC82	down	-2,9	0,2	0,0213
CCDC88A	down	-3,6	1,3	0,1085
CCL20	down	-3,1	0,8	0,0854
CCL27	up	2,9	0,2	0,0199
CCL28	down	-4,2	1,2	0,0838
CCNB3	down	-2,9	0,1	0,0122
CCNJL	down	-2,4	1,5	0,2001
CCNL1	down	-2,7	0,0	0,0053
CCNT2	down	-2,0	0,6	0,1196
CCPG1	down	-2,5	0,2	0,0260
CCR6	down	-2,6	0,7	0,0986
CCRK	up	3,0	0,1	0,0096
CD163	down	-10,4	7,8	0,1696
CD163L1	down	-3,8	0,3	0,0247
CD2	up	3,0	1,8	0,1773
CD244	up	3,8	2,8	0,1920
CD36	down	-21,4	19,2	0,1866
CD72	up	3,3	0,5	0,0440
CD83	down	-2,1	0,1	0,0206
CD86	up	4,0	0,8	0,0621
CD8A	up	7,0	3,3	0,1190
CD9	up	5,1	2,1	0,1081
CD99L2	up	3,6	0,9	0,0746
CDC42BPA	down	-2,7	0,7	0,0954
CDCA7L	up	8,2	3,6	0,1101
CDH11	down	-3,6	0,0	0,0005
CDH12	down	-6,9	0,3	0,0114
CDH16	up	3,0	1,9	0,1881
CDH17	up	23,5	8,8	0,0861
CDKN1A	down	-2,1	0,6	0,1205
CDKN1C	up	4,2	1,2	0,0849
CDS1	down	-6,7	2,4	0,0904
CDYL2	up	4,6	0,7	0,0437
CEACAM1	down	-3,1	0,2	0,0208
CEACAM3	down	-2,5	0,2	0,0314
CEBPB	up	2,0	0,3	0,0571
CEBPE	up	2,3	0,2	0,0296
CEBPZ	down	-2,3	0,5	0,0836
CECR2	up	2,9	0,1	0,0094
CECR6	up	4,5	0,3	0,0167
CENPC1	down	-2,7	0,8	0,0983
CENPE	down	-4,8	1,7	0,0999
CENPF	down	-3,2	0,3	0,0356
CENPJ	down	-2,7	0,7	0,0905
CEP110	down	-2,3	0,2	0,0318
CEP120	down	-2,1	0,0	0,0029
CEP135	down	-2,3	0,5	0,0881
CEP152	down	-2,4	0,3	0,0481
CEP170	down	-3,5	0,4	0,0328
CEP192	down	-2,1	0,4	0,0784
CEP290	down	-4,6	1,6	0,0995
CEP350	down	-2,6	0,1	0,0193
CEP63	down	-2,1	0,3	0,0645
CES4	down	-4,6	2,9	0,1632
CFB	up	6,4	3,8	0,1473
CHAC2	down	-2,0	0,5	0,1034
CHADL	up	2,4	0,4	0,0620
CHD1	down	-3,3	0,4	0,0418
CHD2	down	-2,6	0,6	0,0797
CHD9	down	-3,0	0,9	0,0950
CHIC1	down	-2,6	0,4	0,0559
CHM	down	-2,2	0,3	0,0477
CHML	down	-3,1	1,1	0,1125
CHMP7	up	2,2	0,0	0,0063
CHN1	up	2,1	0,6	0,1083
CHP2	up	2,2	0,6	0,1039
CHPT1	up	2,2	0,4	0,0786
CHRDL2	down	-2,2	0,2	0,0279
CHRM3	up	10,2	1,3	0,0307
CHST14	up	2,1	0,2	0,0440
CHST7	up	2,3	1,5	0,2193
CIDEB	up	2,0	0,1	0,0231
CIDEC	up	2,1	0,6	0,1218
CIZ1	up	2,1	0,1	0,0260
CKMT1A	up	2,3	0,4	0,0709
CLDN14	up	2,2	0,4	0,0649
CLDN4	down	-3,7	2,0	0,1585
CLEC10A	up	2,3	0,4	0,0761
CLK1	up	3,7	0,0	0,0024
CLMN	up	4,0	0,8	0,0612
CLOCK	down	-2,3	0,7	0,1105
CLRN3	up	2,1	0,1	0,0198
CLSPN	down	-2,6	0,4	0,0581
CMAH	down	-2,1	0,6	0,1183
CNNM2	up	3,3	0,2	0,0165

CNTNAP3	up	8,4	3,6	0,1053	CXCL2	down	-7,1	4,5	0,1533
COBLL1	down	-2,1	0,7	0,1331	CXCL3	down	-12,3	3,4	0,0676
COG6	down	-2,1	0,3	0,0685	CXCL5	down	-14,1	3,8	0,0647
COL21A1	down	-66,0	30,2	0,1011	CXCR7	up	122,0	152,7	0,2319
COL4A2	up	2,3	0,6	0,0972	CXorf15	down	-2,4	0,9	0,1421
COL4A5	down	-3,9	0,1	0,0099	CXorf48	up	2,5	0,3	0,0413
COL4A6	down	-3,3	0,1	0,0141	CXorf61	up	9,5	8,3	0,1918
COL5A2	down	-8,0	0,0	0,0013	CXorf65	down	-13,9	0,4	0,0077
COL5A3	down	-10,5	8,0	0,1710	CYFIP2	up	4,0	0,8	0,0577
COL8A2	down	-5,5	0,2	0,0095	CYP17A1	up	3,7	0,6	0,0498
COL9A3	down	-9,6	8,8	0,1987	CYP19A1	up	2,1	0,0	0,0032
COLEC11	down	-2,3	0,2	0,0288	CYP1B1	up	24,5	14,3	0,1289
COQ10A	up	2,1	0,2	0,0332	CYP21A2	up	3,8	1,4	0,1058
COQ9	down	-2,1	0,5	0,0967	CYP26B1	down	-4,2	1,1	0,0791
CPE	up	6,5	1,7	0,0700	CYP27A1	up	2,8	0,2	0,0268
CPM	up	3,0	0,7	0,0793	CYP2A13	up	2,9	1,5	0,1665
CPN1	up	2,4	1,1	0,1604	CYP2A6	up	3,1	2,5	0,2171
CPNE2	up	5,2	0,7	0,0385	CYP2A7	up	3,0	2,4	0,2217
CPNE7	down	-2,4	0,2	0,0350	CYP2B6	up	2,1	0,8	0,1515
CPNE8	down	-2,1	0,4	0,0769	CYP2C9	up	3,3	2,1	0,1787
CPS1	down	-4,8	3,5	0,1854	CYP2D6	up	2,3	0,7	0,1071
CREB3L3	up	2,8	0,0	0,0025	CYP2E1	up	6,9	4,0	0,1413
CREB5	down	-3,4	0,8	0,0707	CYP2U1	up	2,2	0,7	0,1223
CREG1	up	2,2	0,8	0,1424	CYP3A4	down	-2,3	0,3	0,0492
CRIM1	down	-2,3	0,3	0,0498	CYP3A5	down	-2,8	0,2	0,0260
CRIP3	down	-5,7	4,9	0,2007	CYP3A7	down	-2,1	0,4	0,0813
CROCCL2	down	-2,3	0,1	0,0128	CYP4A11	up	2,8	1,2	0,1451
CRYM	up	2,4	0,7	0,1040	CYP4F12	up	2,3	0,1	0,0172
CSNK2A2	up	2,1	0,5	0,1045	CYP4F2	up	2,3	0,1	0,0247
CSPP1	down	-2,2	0,5	0,1013	CYP7A1	up	6,9	0,9	0,0356
CSRNP3	down	-2,7	0,9	0,1144	CYR61	down	-3,4	2,4	0,1946
CSRP1	down	-2,7	1,6	0,1939	CYTSB	up	6,3	0,1	0,0048
CSTF2T	up	2,0	0,3	0,0703	DAB2	down	-2,1	0,0	0,0050
CTBP2	down	-3,5	1,2	0,1087	DAB2IP	up	12,5	8,5	0,1537
CTDSP2	up	2,2	0,2	0,0450	DAPK1	up	2,3	0,4	0,0638
CTDSPL	down	-2,0	0,1	0,0318	DCDC2	down	-5,9	0,8	0,0387
CTHRC1	down	-5,4	2,3	0,1118	DCLK3	up	3,2	0,5	0,0480
CTNNBIP1	down	-2,7	0,7	0,0893	DCP2	down	-2,1	0,4	0,0890
CTSD	up	2,2	0,4	0,0689	DDAH1	up	2,0	0,4	0,0849
CUBN	up	2,5	0,1	0,0152	DDO	up	2,8	0,5	0,0588
CUL5	up	2,2	0,0	0,0085	DDX10	down	-2,1	0,0	0,0073
CUX2	up	2,1	0,3	0,0531	DDX17	down	-2,3	0,6	0,0911
CWC22	down	-2,1	0,3	0,0677	DDX26B	up	9,4	4,2	0,1083
CX3CL1	up	2,9	0,4	0,0451	DDX52	down	-2,1	0,6	0,1192
CX3CR1	up	6,4	3,1	0,1228	DDX60	up	5,6	3,2	0,1441
CXADR	down	-2,1	0,0	0,0052	DENND1B	down	-2,7	0,1	0,0078
CXCL1	down	-3,3	2,7	0,2204	DENND2A	up	8,6	2,2	0,0647

DENND2C	up	2,2	0,5	0,0893
DENND4A	down	-2,8	0,0	0,0040
DES	down	-2,9	0,9	0,1028
DFNB59	down	-2,5	0,5	0,0662
DGCR8	down	-2,8	0,2	0,0281
DGKB	down	-14,5	1,1	0,0182
DGKG	down	-8,7	4,5	0,1255
DHCR24	up	2,0	0,2	0,0426
DHDPSL	up	5,4	1,4	0,0696
DHRS2	up	3,3	0,1	0,0088
DIAPH2	down	-2,4	0,1	0,0110
DIAPH3	down	-3,1	0,0	0,0039
DICER1	down	-2,3	0,1	0,0250
DIO1	up	2,9	0,4	0,0512
DIP2C	up	57,2	22,4	0,0875
DIS3	down	-2,6	0,1	0,0164
DISC1	down	-6,7	4,1	0,1510
DISP2	up	6,5	1,7	0,0674
DKFZP434L187	up	6,2	0,4	0,0168
DKFZP547L112	up	14,3	7,3	0,1170
DKFZP564C152	down	-2,6	0,5	0,0703
DKFZp667E0512	down	-3,0	0,4	0,0438
DKK4	down	-10,6	0,1	0,0015
DLC1	up	2,2	0,2	0,0396
DLG3	up	6,3	0,5	0,0231
DLK2	up	3,1	0,4	0,0475
DLX1	down	-6,6	3,9	0,1432
DLX2	down	-2,6	0,7	0,0916
DMKN	up	3,0	1,5	0,1523
DMTF1	down	-2,2	0,6	0,1151
DNA2	down	-2,3	0,4	0,0691
DNAH14	down	-2,2	0,2	0,0474
DNAJA4	up	5,3	4,7	0,2101
DNAJB14	down	-2,3	0,5	0,0803
DNAJB2	up	2,1	0,3	0,0726
DNAJC2	down	-3,0	0,6	0,0660
DNAJC25	up	2,1	0,3	0,0526
DNAJC3	down	-2,1	0,3	0,0710
DNM1L	down	-2,4	0,5	0,0835
DNMBP	up	2,2	0,1	0,0245
DNMT3B	up	3,1	0,3	0,0300
DNMT3L	up	3,6	2,3	0,1772
DNTTIP2	down	-2,5	0,5	0,0721
DOCK7	down	-2,3	0,1	0,0152
DOK1	up	3,0	0,7	0,0760
DOK3	up	2,9	0,5	0,0594
DOLPP1	up	2,2	0,3	0,0615
DPF3	up	2,6	0,4	0,0578
DPY19L1P1	down	-2,6	0,4	0,0582
DPY19L2P4	down	-2,7	0,1	0,0119
DPYD	up	2,1	0,3	0,0537
DPYS	down	-8,6	8,5	0,2133
DPYSL2	up	2,3	0,1	0,0110
DPYSL5	up	13,4	12,4	0,1957
DQX1	down	-5,2	1,3	0,0699
DSE	up	2,9	1,2	0,1383
DST	down	-2,3	0,0	0,0053
DTNA	down	-3,8	0,5	0,0396
DUSP26	up	16,8	5,9	0,0819
DUSP6	down	-3,8	1,9	0,1405
DYDC2	up	2,8	0,2	0,0241
DYNLT3	down	-2,6	0,2	0,0257
DZIP1L	up	7,7	1,3	0,0425
EBF3	down	-3,2	2,7	0,2300
ECE1	up	2,2	0,2	0,0371
ECHDC3	down	-4,0	2,0	0,1409
EDEM3	down	-2,0	0,3	0,0720
EDNRB	down	-4,0	3,0	0,1974
EEA1	down	-2,2	0,2	0,0283
EEF1E1	down	-2,0	0,1	0,0307
EFEMP1	down	-35,6	47,7	0,2461
EFHD1	up	2,5	0,6	0,0919
EFR3B	up	13,9	6,5	0,1084
EFTUD1	down	-2,7	0,3	0,0435
EGFL7	up	2,0	0,1	0,0204
EGR1	down	-2,3	0,6	0,1006
EHBP1	down	-2,2	0,1	0,0222
EHD3	up	4,2	2,0	0,1310
EIF3A	down	-2,3	0,7	0,1200
EIF4EBP2	up	2,0	0,2	0,0409
EIF5	down	-2,9	0,9	0,1093
EIF5B	down	-2,5	0,8	0,1213
ELOVL6	down	-3,1	1,3	0,1290
ELOVL7	up	2,8	1,3	0,1476
EMID1	up	3,0	0,2	0,0269
EMILIN2	up	2,2	1,3	0,2078
EML1	up	2,7	1,2	0,1453
EML4	down	-4,2	0,2	0,0174
EMP2	up	9,2	4,9	0,1285
EMR1	up	10,4	7,5	0,1649
ENAH	down	-2,5	0,2	0,0241
ENC1	down	-6,5	2,8	0,1091
ENDOD1	up	6,5	4,7	0,1734
ENPP4	down	-3,5	2,8	0,2116

ENPP6	down	-9,5	0,0	0,0008
ENTPD8	up	2,9	0,2	0,0192
EP400	up	2,2	0,3	0,0567
EPB41L1	up	5,1	1,6	0,0868
EPB41L3	up	19,2	16,6	0,1819
EPB41L4B	up	2,1	0,4	0,0870
EPCAM	down	-8,1	8,8	0,2286
EPHA10	up	4,0	0,4	0,0279
EPM2AIP1	down	-2,5	1,1	0,1567
EPN3	down	-2,8	0,8	0,1017
EPRS	down	-2,0	0,2	0,0524
EPS8	down	-3,1	0,1	0,0131
EPSTI1	up	4,4	1,2	0,0784
ERAP1	down	-4,9	0,0	0,0005
ERAP2	down	-3,4	0,0	0,0019
EREG	down	-2,2	0,0	0,0038
ERMAP	up	2,8	0,1	0,0185
ESPN	up	2,4	0,3	0,0419
ESPNL	up	2,4	0,2	0,0243
ETAA1	down	-2,4	0,5	0,0731
ETNK2	up	2,5	0,5	0,0681
ETS1	down	-2,9	0,3	0,0338
ETS2	down	-2,2	0,1	0,0190
ETV1	down	-3,7	0,8	0,0622
ETV4	down	-4,3	0,3	0,0220
ETV5	down	-3,2	0,2	0,0206
EVC2	down	-3,1	0,3	0,0280
EVI5	down	-2,0	0,2	0,0418
EXOC5	down	-2,0	0,5	0,1114
EXPH5	up	2,8	0,2	0,0285
EXT1	down	-2,4	0,1	0,0201
EYA3	down	-2,7	0,0	0,0046
EYA4	down	-10,5	0,7	0,0158
F9	up	89,3	105,2	0,2229
FAAH	up	2,4	0,4	0,0673
FABP6	up	2,3	0,6	0,1112
FADS1	up	2,6	0,1	0,0128
FADS6	up	3,5	1,1	0,0951
FAM105A	down	-10,0	10,0	0,2115
FAM111B	down	-3,7	1,5	0,1161
FAM129A	down	-2,6	0,1	0,0193
FAM133A	down	-68,5	26,6	0,0865
FAM133B	down	-2,0	0,1	0,0274
FAM135A	down	-3,9	0,1	0,0106
FAM13A	down	-2,5	0,8	0,1124
FAM13AOS	down	-3,1	0,0	0,0016
FAM150A	down	-2,9	0,0	0,0044
FAM153A	down	-2,4	0,1	0,0183
FAM153B	down	-2,9	0,1	0,0114
FAM155B	down	-2,3	0,7	0,1126
FAM167A	up	5,1	1,1	0,0590
FAM171A1	up	7,3	4,2	0,1412
FAM171B	down	-5,4	3,8	0,1761
FAM174B	down	-3,4	1,8	0,1594
FAM178A	down	-2,1	0,8	0,1485
FAM183A	up	3,5	1,5	0,1225
FAM184A	down	-2,0	0,6	0,1251
FAM188B	down	-8,9	8,3	0,2030
FAM189A1	up	8,7	5,3	0,1435
FAM20A	up	7,9	2,0	0,0654
FAM20C	up	8,5	1,6	0,0479
FAM22A	up	2,2	0,5	0,0940
FAM22D	up	5,0	1,5	0,0804
FAM38B	down	-9,5	5,5	0,1365
FAM3B	down	-3,1	2,7	0,2392
FAM40B	down	-2,3	0,1	0,0231
FAM50B	up	2,3	0,3	0,0427
FAM60A	down	-2,1	0,2	0,0380
FAM78A	up	4,1	0,4	0,0290
FAM81A	down	-2,2	0,2	0,0365
FAM9B	down	-186,7	108,2	0,1244
FAM9C	down	-31,3	0,5	0,0041
FANCB	down	-2,9	0,4	0,0493
FANCD2	down	-2,3	0,3	0,0520
FANCI	down	-2,0	0,4	0,0822
FANCL	down	-3,0	0,6	0,0711
FANCM	down	-2,7	0,4	0,0573
FAR1	down	-2,0	0,2	0,0545
FAR2	up	3,2	1,6	0,1491
FASTKD1	down	-2,5	0,2	0,0258
FAT1	down	-2,6	0,1	0,0167
FBLN7	up	3,7	2,3	0,1717
FBN1	up	2,3	0,4	0,0630
FBP1	up	5,8	1,0	0,0470
FBXL17	up	2,3	0,5	0,0893
FBXL21	up	11,2	1,3	0,0293
FBXL7	up	9,5	4,0	0,1021
FBXO38	down	-2,2	0,6	0,1077
FBXO4	down	-2,8	1,3	0,1459
FBXW10	down	-2,8	1,0	0,1199
FBXW2	up	2,9	0,0	0,0057
FCGBP	up	2,5	1,1	0,1553
FCGR2A	up	2,4	0,3	0,0401
FCGR3A	up	22,6	14,5	0,1409

FCRLA	up	7,1	2,1	0,0758
FCRLB	up	4,4	1,5	0,0937
FER	down	-2,0	0,7	0,1391
FER1L4	up	4,3	2,5	0,1547
FES	up	5,8	1,0	0,0474
FEZ1	up	8,0	3,7	0,1126
FGD5	up	3,8	0,9	0,0709
FGF13	down	-7,3	6,3	0,1967
FGF19	down	-10,7	7,8	0,1645
FGF2	up	11,0	4,8	0,1044
FGF9	down	-4,5	1,8	0,1117
FGFR4	up	7,7	7,1	0,2050
FGR	up	3,6	0,2	0,0163
FHL1	up	10,6	8,6	0,1793
FHOD3	up	5,4	2,1	0,1037
FILIP1	down	-4,0	0,3	0,0255
FLI1	down	-59,3	31,6	0,1166
FLJ11235	up	2,0	0,3	0,0584
FLJ13744	down	-2,2	0,1	0,0285
FLJ23834	down	-3,5	0,1	0,0132
FLJ36031	up	2,2	0,1	0,0219
FLJ37644	down	-4,0	0,1	0,0108
FLJ40330	down	-6,6	0,9	0,0365
FLJ40852	up	3,4	0,5	0,0493
FLJ42875	up	3,0	1,2	0,1261
FLJ45244	down	-2,4	0,2	0,0303
FLNC	down	-13,8	13,1	0,1996
FLRT1	up	2,5	0,2	0,0242
FLRT3	down	-8,1	6,9	0,1900
FLYWCH2	up	2,0	0,6	0,1274
FMNL1	down	-4,2	2,5	0,1575
FMO1	up	15,7	10,7	0,1511
FMO3	down	-20,5	2,6	0,0301
FMO4	up	3,4	1,0	0,0919
FMO5	down	-3,9	0,3	0,0224
FNBP1L	down	-2,8	0,5	0,0644
FNIP2	down	-2,7	0,5	0,0646
FOLR1	up	3,6	1,7	0,1381
FOXC1	down	-2,1	0,3	0,0520
FOXG1	down	-2,3	0,0	0,0067
FOXN4	up	4,8	0,1	0,0053
FOXO1	down	-2,1	0,4	0,0782
FOXO3	up	2,0	0,4	0,0896
FRAS1	down	-2,1	0,8	0,1488
FRMD3	down	-3,7	2,0	0,1549
FRMD6	down	-3,1	0,1	0,0116
FRRS1	down	-2,7	0,1	0,0082
FRY	down	-2,1	0,5	0,1007
FRYL	down	-2,5	0,6	0,0829
FST	down	-3,6	0,7	0,0593
FSTL5	down	-18,0	13,6	0,1639
FUT8	down	-2,3	0,3	0,0444
FUZ	down	-3,8	0,2	0,0166
FZD2	up	2,0	0,2	0,0330
FZD3	down	-2,4	0,8	0,1155
FZD4	down	-2,1	1,4	0,2316
FZD7	up	2,6	0,8	0,1084
G0S2	up	2,1	0,8	0,1559
G6PC	up	3,6	1,2	0,0981
GABARAPL1	up	2,0	0,8	0,1633
GABRA5	up	4,6	2,8	0,1603
GABRE	down	-3,5	0,4	0,0367
GABRG2	down	-2,2	0,9	0,1577
GAD1	up	2,4	0,3	0,0498
GADD45B	up	2,5	0,0	0,0061
GAFA3	down	-4,7	0,1	0,0079
GALNS	up	5,5	1,9	0,0913
GALNT6	up	6,7	3,0	0,1128
GALNTL1	up	13,8	6,6	0,1121
GARNL3	up	5,7	0,3	0,0142
GAS5	down	-2,1	0,1	0,0258
GATA3	down	-3,3	1,5	0,1355
GATM	up	3,8	2,0	0,1510
GBA3	up	6,2	5,0	0,1907
GBP2	down	-2,7	0,7	0,0829
GBP3	down	-2,8	0,5	0,0591
GCNT4	down	-3,3	2,3	0,1940
GCOM1	up	5,6	1,3	0,0644
GDA	down	-3,3	0,1	0,0062
GDF1	up	2,5	0,8	0,1184
GDF10	up	20,0	8,0	0,0923
GDF15	down	-2,5	0,3	0,0381
GDPD3	down	-2,2	0,7	0,1261
GEM	up	2,6	0,0	0,0061
GEN1	down	-2,1	0,2	0,0465
GGT8P	down	-2,2	0,2	0,0355
GHR	down	-2,1	0,4	0,0812
GIGYF2	down	-2,1	0,4	0,0892
GIMAP7	up	3,4	0,6	0,0596
GIPC2	down	-2,2	1,2	0,1915
GJA1	down	-7,4	0,1	0,0047
GJA3	up	8,9	4,8	0,1298
GLA	down	-2,2	0,1	0,0268
GLE1	up	2,1	0,0	0,0063

GLI1	up	5,2	2,1	0,1097
GLIPR1	down	-2,1	0,0	0,0027
GLIPR2	down	-4,0	3,9	0,2368
GLS	down	-3,8	0,1	0,0117
GLT1D1	up	6,7	5,7	0,1971
GLT8D3	down	-2,4	0,6	0,0994
GLT8D4	up	2,7	0,0	0,0028
GLUD1	up	2,0	0,3	0,0639
GLUD2	up	2,4	0,4	0,0695
GM2A	up	2,1	0,1	0,0239
GNB4	up	9,2	0,2	0,0049
GNGT1	down	-5,2	0,3	0,0168
GNPDA2	down	-2,2	0,3	0,0524
GNRH1	down	-2,3	0,6	0,1054
GNS	up	2,7	0,0	0,0043
GOLGA2LY1	down	-2,3	0,7	0,1164
GOLGA4	down	-4,7	0,8	0,0491
GOLGA6A	down	-2,3	0,1	0,0120
GOLGA6L10	down	-2,2	0,7	0,1359
GOLGA6L9	down	-2,2	0,5	0,0866
GOLGA8A	down	-2,4	0,0	0,0067
GOLGA8F	down	-2,1	0,8	0,1515
GOLGB1	down	-2,4	0,6	0,0958
GOLM1	down	-8,8	9,2	0,2217
GON4L	down	-2,1	0,0	0,0081
GOT1	down	-2,2	0,0	0,0055
GPATCH4	down	-2,3	0,3	0,0548
GPBP1	down	-2,1	0,3	0,0658
GPC1	up	3,4	0,1	0,0140
GPC4	up	5,1	1,9	0,1022
GPC5	up	8,3	6,9	0,1863
GPD1	up	2,4	0,5	0,0709
GPD1L	down	-2,5	0,8	0,1171
GPR109B	down	-2,7	1,4	0,1681
GPR110	down	-5,4	2,7	0,1310
GPR126	down	-3,4	0,3	0,0243
GPR128	up	2,2	0,6	0,1007
GPR133	up	2,3	0,4	0,0636
GPR146	up	2,1	0,3	0,0530
GPR158	down	-2,4	0,5	0,0858
GPR176	up	2,8	0,1	0,0071
GPR177	down	-3,1	0,6	0,0610
GPR68	up	6,8	0,0	0,0008
GPR81	down	-2,7	0,5	0,0695
GPRC5B	up	2,8	1,6	0,1767
GPRIN1	up	2,0	0,1	0,0172
GPSM1	up	3,7	1,8	0,1374
GPX7	down	-8,8	0,1	0,0017
GPX8	up	3,5	0,8	0,0702
GRAMD3	down	-2,1	0,1	0,0268
GRB14	down	-3,3	1,3	0,1175
GREM1	down	-4,5	2,8	0,1597
GSN	up	6,7	0,3	0,0109
GSTA1	up	16,0	6,4	0,0932
GSTA2	up	14,2	4,1	0,0696
GSTA3	up	12,8	4,2	0,0787
GSTA5	up	13,2	4,6	0,0826
GSTO2	up	2,7	0,5	0,0718
GTDC1	up	2,7	1,7	0,1997
GTF2H5	down	-2,1	0,5	0,0925
GTF2IRD2	up	5,5	1,3	0,0659
GUCA1B	down	-2,2	0,1	0,0148
GUCY2C	up	2,8	2,1	0,2219
GULP1	down	-4,1	0,0	0,0005
H2AFY2	up	6,5	2,7	0,1074
HAO2	up	7,9	6,5	0,1855
HAUS6	down	-2,1	0,2	0,0415
HAVCR2	down	-5,6	1,9	0,0889
HBE1	down	-4,9	2,1	0,1140
HBG1	down	-5,0	2,0	0,1089
hCG_1817306	down	-2,1	0,0	0,0041
hCG_1993592	down	-2,0	0,1	0,0209
HCG27	down	-2,5	1,3	0,1651
HCP5	up	2,7	0,1	0,0116
HDAC6	down	-2,3	0,4	0,0661
HDGFRP3	up	36,9	22,7	0,1342
HDHD3	up	2,3	0,3	0,0468
HEATR1	down	-2,1	0,4	0,0830
HECA	up	3,5	0,6	0,0537
HERC2P2	down	-2,1	0,3	0,0637
HERC6	up	3,2	0,8	0,0783
HERV-FRD	down	-2,5	0,0	0,0018
HEY1	up	2,7	0,9	0,1161
HEY2	down	-4,0	2,9	0,1922
HEYL	up	7,0	1,2	0,0461
HHAT	up	3,7	0,1	0,0119
HIBCH	down	-2,1	0,1	0,0297
HIST2H2BE	up	2,6	0,2	0,0332
HK2	down	-2,6	0,7	0,0907
HLA-DQB1	up	8,7	4,1	0,1145
HLTF	down	-3,0	0,8	0,0845
HMGCS2	up	3,0	1,0	0,1074
HMGN1	down	-3,8	0,8	0,0642
HMGN5	down	-3,3	0,2	0,0212

HNRNPA3	down	-2,2	0,3	0,0646
HNRNPU	down	-2,5	0,1	0,0210
HOMER2	up	5,0	0,5	0,0251
HOOK1	down	-3,2	0,2	0,0167
HOXA13	up	2,6	2,1	0,2436
HOXB5	down	-12,0	2,0	0,0402
HOXC13	down	-7,5	2,7	0,0914
HOXD10	down	-2,4	0,0	0,0058
HOXD8	down	-2,4	0,6	0,0966
HP	up	2,8	1,1	0,1307
HPGD	down	-3,5	0,9	0,0825
HPR	up	3,9	1,9	0,1354
HPSE	down	-5,2	0,5	0,0265
HRASLS	up	8,3	3,1	0,0923
HRC	down	-4,4	0,9	0,0592
HRCT1	down	-2,2	0,4	0,0767
HRG	up	2,5	0,7	0,0998
HSD17B11	down	-2,4	0,1	0,0231
HSD17B12	down	-2,0	0,2	0,0389
HSD17B6	up	3,5	2,2	0,1727
HSD3B1	up	4,6	3,5	0,1892
HSP90AA1	down	-2,2	0,1	0,0253
HSP90B1	down	-2,4	0,4	0,0723
HSPA12A	up	9,2	7,4	0,1802
HSPA12B	up	24,1	14,3	0,1318
HSPA4L	down	-3,3	0,5	0,0517
HSPA6	up	2,5	1,1	0,1481
HSPH1	down	-2,0	0,6	0,1279
HTRA1	up	7,3	0,9	0,0328
HYAL4	down	-5,6	3,7	0,1657
HYLS1	up	2,6	0,1	0,0099
ICA1	up	2,0	0,3	0,0576
ICA1L	down	-2,2	1,2	0,1896
ICAM5	down	-2,4	0,0	0,0032
IDS	down	-2,3	0,0	0,0046
IER3	down	-4,2	0,5	0,0358
IER5L	down	-2,3	0,4	0,0656
IFI16	up	2,4	1,0	0,1425
IFRD1	down	-2,7	0,2	0,0303
IFT80	down	-2,4	0,2	0,0331
IFT81	down	-2,3	0,5	0,0758
IFT88	down	-2,3	0,3	0,0477
IGFBP2	up	6,2	6,5	0,2298
IGFBP3	up	2,5	0,2	0,0377
IGFBP4	up	5,9	1,7	0,0766
IGFBPL1	down	-2,1	0,3	0,0610
IGSF1	up	2,1	0,8	0,1530
IGSF11	up	6,9	0,1	0,0028
IGSF9	up	6,4	2,1	0,0873
IKBKAP	up	3,2	1,2	0,1148
IL11RA	up	2,2	0,1	0,0159
IL13RA2	down	-8,0	0,1	0,0023
IL18	down	-13,3	16,0	0,2369
IL18R1	up	21,4	5,6	0,0615
IL1F7	up	2,4	0,7	0,1101
IL1R2	up	2,4	0,0	0,0027
IL1RAP	down	-2,3	0,1	0,0236
IL1RN	up	6,0	0,7	0,0317
IL22RA1	up	2,2	0,6	0,1058
IL23R	down	-10,2	6,4	0,1449
IL2RB	down	-5,2	4,0	0,1864
IL2RG	down	-5,2	1,1	0,0591
IL6ST	down	-2,4	0,4	0,0723
IL8	down	-6,1	4,4	0,1734
IMPA2	up	2,3	1,0	0,1568
INHBE	up	5,4	0,7	0,0377
INPP1	down	-2,9	0,5	0,0518
INPP5D	up	17,9	5,7	0,0747
INPP5K	up	2,1	0,3	0,0546
INTS6	down	-2,2	0,1	0,0127
IPO7	down	-2,0	0,5	0,1042
IPW	down	-3,1	1,5	0,1474
IQCA1	up	30,2	5,7	0,0438
IQCK	up	2,8	0,2	0,0289
IQGAP2	down	-2,8	1,5	0,1672
IQSEC2	up	2,2	0,6	0,1055
IRF8	up	3,6	2,1	0,1609
IRF9	up	2,6	0,3	0,0471
IRS2	up	2,2	0,8	0,1313
IRX3	up	5,2	3,8	0,1807
ISCA1	up	2,1	0,3	0,0555
ISX	up	4,1	0,7	0,0525
ITGA1	down	-2,3	0,1	0,0119
ITGA2	down	-6,7	0,1	0,0023
ITGA3	up	4,0	2,7	0,1779
ITGAM	up	4,0	3,5	0,2212
ITGAV	down	-2,7	0,2	0,0301
ITGB1BP2	up	2,2	0,7	0,1278
ITGB2	up	9,0	9,5	0,2220
ITIH1	up	7,5	4,5	0,1463
ITIH3	up	3,4	2,6	0,2069
ITIH4	up	3,3	1,9	0,1675
ITLN1	up	2,0	0,4	0,0861
ITPR3	up	6,1	2,0	0,0841

ITPRIPL1	down	-2,2	0,5	0,0957
ITSN2	down	-2,5	0,9	0,1255
IYD	up	8,7	1,3	0,0373
JAG1	down	-5,0	4,2	0,2041
JAZF1	up	5,4	0,3	0,0163
JMJD1C	down	-2,7	0,4	0,0573
JUN	down	-3,0	0,7	0,0749
KALRN	down	-8,4	2,2	0,0674
KANK1	up	2,1	0,4	0,0773
KANK3	up	2,0	0,5	0,1087
KANK4	up	54,9	26,3	0,1059
KBTBD11	up	40,0	24,9	0,1347
KCNC1	up	6,1	0,5	0,0237
KCNC3	up	3,4	0,3	0,0247
KCNE1L	down	-3,1	1,2	0,1165
KCNE3	up	10,6	5,8	0,1293
KCNJ15	down	-2,7	0,1	0,0171
KCNJ16	up	187,5	13,2	0,0159
KCNJ8	up	2,4	0,7	0,1014
KCNK10	up	6,3	2,9	0,1163
KCNK5	up	7,4	2,0	0,0681
KCNQ1OT1	down	-2,4	0,4	0,0621
KCTD5	up	2,1	0,1	0,0136
KCTD7	down	-2,1	0,5	0,0926
KDM4D	up	2,1	0,2	0,0432
KHDC1	up	2,7	0,3	0,0354
KIAA0040	up	5,6	2,8	0,1290
KIAA0125	up	2,6	0,5	0,0708
KIAA0232	down	-2,3	0,8	0,1303
KIAA0319	up	5,3	4,2	0,1909
KIAA0564	down	-2,2	0,1	0,0161
KIAA0802	down	-2,8	1,6	0,1804
KIAA0907	down	-2,2	0,1	0,0135
KIAA0947	down	-2,7	0,4	0,0510
KIAA1009	down	-2,8	0,6	0,0725
KIAA1107	down	-2,3	1,0	0,1632
KIAA1109	down	-4,1	0,4	0,0261
KIAA1147	down	-2,4	0,3	0,0550
KIAA1161	up	3,8	0,6	0,0498
KIAA1199	up	18,8	23,2	0,2366
KIAA1377	up	5,5	3,1	0,1443
KIAA1430	down	-2,3	0,0	0,0023
KIAA1549	down	-3,0	0,4	0,0479
KIAA1656	up	3,7	0,6	0,0482
KIAA1683	down	-2,1	0,0	0,0052
KIAA1712	down	-2,6	0,0	0,0008
KIAA1731	down	-3,4	0,5	0,0449
KIAA1804	down	-2,6	0,5	0,0737
KIAA1908	up	2,4	0,0	0,0045
KIAA1967	up	2,5	0,3	0,0498
KIF14	down	-3,1	0,5	0,0533
KIF15	down	-3,8	0,1	0,0115
KIF20B	down	-2,6	0,6	0,0822
KIF21A	down	-2,1	0,5	0,0973
KIF3A	down	-2,5	0,8	0,1081
KIF6	up	2,5	1,0	0,1370
KIRREL	down	-2,2	1,0	0,1668
KLC4	up	2,4	0,0	0,0038
KLF2	up	2,8	0,6	0,0701
KLHL24	up	3,0	1,5	0,1606
KLHL3	up	2,2	0,3	0,0661
KLHL34	down	-5,7	2,0	0,0947
KLHL5	down	-2,3	0,6	0,1067
KNG1	up	10,5	0,0	0,0001
KRAS	down	-2,1	0,0	0,0097
KRCC1	down	-3,3	0,9	0,0852
KREMEN1	up	3,3	0,0	0,0035
KRT222	down	-2,3	0,9	0,1489
KRT23	down	-15,1	13,6	0,1897
KRT6A	up	10,9	3,9	0,0871
KRT86	down	-2,0	0,1	0,0283
KRTAP19-1	down	-3,1	1,2	0,1215
KRTCAP3	down	-2,0	0,3	0,0601
KRTDAP	up	4,9	2,2	0,1232
KTN1	down	-3,2	0,9	0,0882
KYNU	down	-2,9	0,3	0,0324
L3MBTL3	up	3,5	0,8	0,0739
LAMA4	down	-19,9	22,9	0,2255
LAMB1	down	-4,9	2,1	0,1174
LAMB3	up	2,3	0,1	0,0234
LANCL2	up	2,7	0,3	0,0431
LARGE	up	10,3	1,9	0,0457
LARP1B	down	-2,5	0,6	0,0846
LARP7	down	-3,0	0,8	0,0826
LARS	down	-2,3	0,7	0,1161
LAT2	up	2,1	0,4	0,0737
LBP	up	9,0	6,7	0,1695
LCA5	down	-4,1	2,6	0,1745
LCAT	up	2,9	0,2	0,0256
LCORL	down	-2,5	0,5	0,0782
LCP1	down	-10,3	3,0	0,0707
LDHD	up	2,0	0,0	0,0079
LDLRAD1	up	8,7	3,2	0,0894
LDOC1L	up	2,1	0,2	0,0456

LEF1	up	20,9	14,2	0,1490
LEFTY1	up	5,2	3,5	0,1710
LEO1	down	-2,2	0,3	0,0564
LEPR	up	2,9	0,5	0,0620
LFNG	down	-6,5	2,7	0,1075
LGALS1	down	-2,2	0,0	0,0083
LGALS2	up	2,8	0,1	0,0100
LHPP	up	2,4	0,0	0,0077
LHX1	down	-4,9	0,9	0,0529
LHX2	up	4,7	2,4	0,1353
LHX6	up	5,4	1,6	0,0794
LIFR	up	13,7	7,1	0,1207
LIG4	down	-2,2	0,0	0,0009
LILRB3	down	-2,3	0,2	0,0294
LIMA1	down	-3,8	1,8	0,1345
LIMCH1	down	-2,1	0,1	0,0232
LIMD2	up	2,2	0,4	0,0700
LIN54	down	-2,5	0,2	0,0252
LINGO1	down	-40,6	11,1	0,0620
LIPG	down	-2,1	1,1	0,1970
LITAF	up	23,3	9,9	0,0967
LMBRD2	down	-2,1	0,4	0,0812
LNPEP	down	-2,4	0,6	0,0997
LNX1	down	-2,0	0,2	0,0349
LOC100127983	down	-3,5	1,4	0,1205
LOC100128164	up	10,8	9,4	0,1893
LOC100128842	down	-2,1	0,6	0,1158
LOC100129104	down	-2,5	0,4	0,0570
LOC100129291	down	-4,5	1,5	0,0940
LOC100129488	down	-3,4	0,3	0,0253
LOC100130506	down	-2,1	0,2	0,0513
LOC100130967	up	3,2	1,0	0,1008
LOC100131067	up	2,5	0,2	0,0246
LOC100131504	up	4,4	2,5	0,1524
LOC100131564	down	-2,1	0,5	0,1070
LOC100131646	up	2,3	0,4	0,0741
LOC100131929	down	-2,4	0,3	0,0488
LOC100132247	down	-2,4	0,1	0,0138
LOC100134228	down	-2,0	0,3	0,0747
LOC100134229	up	2,1	0,6	0,1265
LOC100170939	down	-2,2	0,7	0,1243
LOC100286895	down	-2,1	0,7	0,1346
LOC100286909	down	-2,4	0,7	0,1100
LOC100287412	up	2,0	0,0	0,0037
LOC100287869	up	2,2	0,6	0,1102
LOC100288367	down	-3,0	0,6	0,0713
LOC100288671	down	-2,1	0,1	0,0149
LOC100288846	up	3,2	0,3	0,0275
LOC100289058	down	-2,5	0,3	0,0395
LOC100289169	down	-2,7	0,9	0,1074
LOC100289490	up	2,9	0,3	0,0360
LOC100289574	down	-2,0	0,7	0,1378
LOC100292427	up	2,3	0,3	0,0434
LOC100293208	down	-2,4	0,0	0,0037
LOC134466	down	-2,6	1,0	0,1350
LOC145783	down	-4,0	0,1	0,0068
LOC150759	down	-4,2	1,8	0,1201
LOC151438	up	4,9	1,6	0,0883
LOC157562	down	-2,2	0,5	0,0897
LOC221442	down	-7,8	4,9	0,1492
LOC283352	up	2,9	0,8	0,0944
LOC283663	down	-2,6	0,2	0,0262
LOC283788	down	-3,0	0,3	0,0320
LOC284232	up	2,9	0,0	0,0009
LOC284542	down	-2,2	1,1	0,1804
LOC284561	up	2,1	0,6	0,1104
LOC285216	down	-2,6	0,7	0,0900
LOC285441	down	-2,9	0,0	0,0040
LOC338620	down	-3,3	1,2	0,1089
LOC339240	down	-2,9	0,3	0,0353
LOC339524	down	-4,2	1,6	0,1088
LOC340888	down	-2,4	1,2	0,1752
LOC344887	down	-6,7	0,9	0,0359
LOC346887	down	-3,1	1,2	0,1200
LOC348751	up	4,5	0,0	0,0031
LOC374491	down	-2,2	0,5	0,0822
LOC387895	down	-3,3	1,7	0,1506
LOC388242	down	-2,1	0,5	0,0958
LOC388630	down	-2,8	1,8	0,1990
LOC389634	up	4,8	0,7	0,0405
LOC389831	down	-2,1	0,1	0,0300
LOC399815	down	-2,6	0,5	0,0642
LOC400027	up	2,2	0,2	0,0375
LOC400987	down	-2,1	0,2	0,0387
LOC439949	up	7,7	0,7	0,0243
LOC440173	up	2,0	0,2	0,0402
LOC441208	up	3,5	0,1	0,0066
LOC441601	down	-2,1	0,0	0,0074
LOC441666	down	-4,5	0,8	0,0514
LOC552889	up	12,1	3,4	0,0687
LOC642413	up	2,1	0,2	0,0313
LOC644662	up	3,0	0,1	0,0081
LOC646509	up	2,1	0,1	0,0160
LOC646936	down	-4,6	2,3	0,1333

LOC646976	up	2,1	0,4	0,0717
LOC650226	up	2,1	0,6	0,1160
LOC723809	down	-17,9	0,3	0,0035
LOC727758	down	-2,2	0,0	0,0093
LOC727916	up	2,4	0,3	0,0502
LOC729683	up	2,3	0,1	0,0136
LOC729806	down	-3,9	1,9	0,1347
LOC729817	down	-2,4	0,1	0,0226
LOC730098	up	3,0	0,7	0,0744
LOC84740	down	-4,1	3,9	0,2298
LOH3CR2A	down	-2,1	0,5	0,0984
LONRF1	down	-2,0	0,1	0,0110
LOXL1	up	9,5	7,7	0,1805
LOXL2	up	27,6	15,6	0,1252
LOXL4	up	5,4	1,4	0,0689
LPA	up	3,1	0,8	0,0787
LPAL2	up	3,4	0,3	0,0283
LPCAT3	up	2,7	0,3	0,0420
LPGAT1	down	-2,2	0,4	0,0718
LPP	down	-2,0	0,0	0,0057
LRFN5	down	-4,2	0,0	0,0013
LRMP	up	4,1	2,0	0,1369
LRP11	up	2,5	0,4	0,0655
LRP12	down	-3,9	0,0	0,0031
LRP4	up	2,3	1,3	0,1911
LRRC16A	up	7,0	4,4	0,1503
LRRC27	up	4,5	2,3	0,1362
LRRC31	up	4,5	0,6	0,0355
LRRC39	down	-3,7	1,2	0,0933
LRRC4	down	-2,1	0,5	0,0900
LRRC47	up	2,5	0,0	0,0031
LRRC48	up	2,3	0,1	0,0114
LRRC6	up	12,0	1,1	0,0231
LRRCC1	down	-3,5	0,6	0,0560
LRRFIP1	down	-2,2	0,6	0,1083
LSAMP	down	-2,1	0,0	0,0057
LTB	down	-2,8	2,1	0,2203
LTBP1	up	137,0	2,8	0,0047
LUC7L3	down	-3,6	0,8	0,0652
LUM	down	-6,8	3,5	0,1296
LUZP4	up	8,5	1,2	0,0371
LY6G5C	up	3,1	0,6	0,0641
LY6K	up	2,1	0,2	0,0313
LY75	down	-8,2	4,3	0,1274
LY96	down	-6,2	0,7	0,0307
LYG1	down	-2,4	0,5	0,0791
LYNX1	down	-2,8	0,6	0,0713
LYPD1	up	8,2	4,4	0,1297
LYSMD3	down	-2,9	0,6	0,0649
LYST	down	-3,2	0,1	0,0129
LYZ	down	-4,8	0,3	0,0182
MACF1	down	-2,2	0,5	0,0981
MACROD2	down	-12,1	0,4	0,0078
MAF	up	2,7	0,4	0,0536
MAFB	up	3,6	0,2	0,0207
MAFF	down	-2,9	0,8	0,0987
MAG	up	2,1	0,5	0,0971
MAGEA10	up	9,6	0,8	0,0204
MAGEA9	up	12,1	4,4	0,0863
MAGEB2	up	17,7	2,4	0,0325
MAGEC1	up	20,7	10,3	0,1130
MAGEC2	up	6,1	0,6	0,0272
MALAT1	down	-4,4	1,7	0,1125
MAN1C1	up	5,6	3,0	0,1386
MANBA	down	-2,1	0,2	0,0472
MAP3K8	down	-2,1	0,9	0,1711
MAP4K3	down	-2,2	0,2	0,0396
MAPK13	up	3,4	0,2	0,0175
MAPKAP1	up	2,1	0,1	0,0226
MAPT	down	-2,8	0,6	0,0681
MARCO	up	8,5	7,7	0,1986
MARK1	up	2,6	0,5	0,0639
MARVELD1	up	12,6	0,9	0,0172
MASP2	up	2,6	0,8	0,1032
MAT2A	down	-2,5	0,3	0,0429
MATN2	up	2,0	0,6	0,1319
MBD2	up	2,7	0,2	0,0288
MBL2	up	2,1	0,1	0,0232
MBNL1	down	-2,5	0,1	0,0128
MBNL2	down	-2,8	1,4	0,1644
MBOAT2	up	4,7	2,0	0,1182
MBP	down	-15,3	12,8	0,1799
MBTPS1	up	2,0	0,1	0,0111
MCC	down	-10,5	1,4	0,0330
MCM3APAS	down	-2,8	0,1	0,0128
MCTS1	down	-3,3	1,7	0,1547
ME3	down	-2,1	0,9	0,1747
MEG3	down	-2,0	0,1	0,0126
MEIS2	down	-2,1	0,3	0,0676
MESP1	up	3,3	0,2	0,0211
MET	down	-2,4	0,4	0,0646
METTL7A	up	3,5	2,0	0,1626
MFAP2	up	3,2	1,0	0,0994
MFGE8	up	2,4	0,0	0,0002

MFNG	up	2,4	0,9	0,1276
MFSD8	down	-2,4	0,7	0,1013
MGC23270	up	2,3	0,2	0,0290
MGC24125	down	-2,7	0,9	0,1097
MGC70870	down	-3,2	0,8	0,0808
MIB2	up	3,3	0,2	0,0191
MID2	down	-2,6	0,4	0,0512
MIPOL1	down	-2,0	0,7	0,1391
MIR17HG	down	-2,6	1,1	0,1459
MKKS	down	-2,0	0,2	0,0335
MKLN1	down	-3,2	0,7	0,0720
MLF1	down	-2,1	0,4	0,0867
MLH3	down	-3,1	0,7	0,0744
MLLT11	down	-2,8	0,6	0,0796
MLLT3	down	-2,0	0,3	0,0631
MLXIP	up	2,8	0,5	0,0674
MMD	down	-2,1	0,6	0,1175
MMP11	up	2,1	0,3	0,0511
MMP15	down	-2,9	1,3	0,1402
MMP23B	down	-2,1	0,6	0,1172
MNS1	down	-2,2	0,7	0,1271
MOBKL1A	down	-2,2	0,6	0,1082
MOBKL2B	up	3,0	1,1	0,1207
MOGAT2	down	-3,2	0,0	0,0018
MORC3	down	-2,4	0,4	0,0732
MORC4	down	-2,3	0,3	0,0438
MOSPD2	down	-2,2	0,8	0,1405
MOXD1	up	5,1	2,0	0,1061
MPDZ	down	-2,2	0,4	0,0704
MPHOSPH10	down	-2,7	0,5	0,0691
MPP1	up	3,2	1,4	0,1294
MPP7	up	6,0	1,7	0,0764
MPV17L	up	2,5	1,1	0,1550
MRC1L1	down	-3,5	0,4	0,0368
MRPL30	up	2,3	0,3	0,0567
MRPL42P5	up	2,0	0,3	0,0733
MSH2	down	-2,0	0,2	0,0416
MSH3	down	-2,0	0,2	0,0391
MSRA	up	2,7	0,2	0,0227
MST1R	down	-5,3	2,7	0,1318
MT1B	up	2,1	0,1	0,0214
MT1F	up	4,1	0,1	0,0048
MT1G	up	2,2	0,0	0,0031
MT1H	up	2,1	0,0	0,0067
MT1X	up	2,2	0,1	0,0107
MTBP	down	-2,5	0,1	0,0181
MTHFD2	down	-2,6	0,5	0,0634
MTMR11	up	2,4	1,4	0,1976
MTMR6	down	-2,0	0,1	0,0290
MTMR8	down	-3,8	0,5	0,0419
MTMR9L	down	-4,4	0,9	0,0575
MUC15	down	-2,1	0,1	0,0122
MUC4	down	-2,0	0,2	0,0440
MVK	up	2,3	0,2	0,0387
MVP	up	3,7	0,1	0,0105
MXRA8	down	-2,8	1,3	0,1485
MYCBP2	down	-3,8	1,3	0,0971
MYCN	down	-95,7	112,8	0,2228
MYH10	down	-2,0	0,3	0,0547
MYH3	down	-2,0	0,4	0,0843
MYL5	up	2,6	0,6	0,0865
MYO10	down	-2,2	0,1	0,0151
MYO1D	up	4,9	0,9	0,0485
MYO5A	down	-2,4	1,2	0,1683
MYO5C	down	-2,2	0,3	0,0511
MYO6	down	-2,6	0,3	0,0415
MYO9A	down	-2,9	0,3	0,0350
MYOM2	up	6,3	3,9	0,1526
MYSM1	down	-3,1	0,9	0,0943
N4BP2	down	-2,7	0,5	0,0610
N4BP2L2	down	-2,5	0,1	0,0181
NAAA	down	-2,2	0,7	0,1357
NARG1	down	-2,5	0,2	0,0241
NARG1L	down	-2,2	0,7	0,1253
NAT8	down	-2,7	1,0	0,1276
NAT8L	up	2,1	0,8	0,1597
NBN	down	-2,1	0,1	0,0285
NCALD	up	3,2	1,7	0,1548
NCAPG	down	-2,2	0,5	0,0951
NCOA7	down	-3,9	1,4	0,1052
NCRNA00087	up	2,0	0,2	0,0409
NCRNA00164	down	-2,5	1,6	0,2062
NDRG1	up	4,4	0,3	0,0221
NDRG4	up	3,5	1,1	0,0997
NEAT1	down	-2,2	0,7	0,1263
NEBL	up	3,5	0,5	0,0408
NECAB1	down	-5,0	3,3	0,1700
NEK1	down	-2,5	0,5	0,0761
NEK6	up	2,2	0,3	0,0560
NES	down	-4,4	0,3	0,0225
NETO2	up	3,8	0,4	0,0351
NEURL1B	up	3,0	0,1	0,0150
NEXN	down	-2,7	0,4	0,0566
NFASC	up	6,4	5,9	0,2091

NFATC4	up	2,1	0,5	0,1082
NFIB	down	-2,4	0,1	0,0103
NFKBIE	down	-2,3	0,8	0,1347
NHS	down	-16,3	5,4	0,0773
NIN	down	-2,1	0,6	0,1283
NIPBL	down	-2,3	0,3	0,0495
NKTR	down	-3,2	0,7	0,0688
NKX2-1	up	2,2	0,2	0,0413
NLGN2	up	3,1	0,6	0,0632
NLRC5	up	2,6	0,1	0,0144
NLRP2	up	2,1	0,1	0,0111
NLRP5	down	-5,2	3,7	0,1783
NNMT	down	-2,4	0,7	0,1091
NOC3L	down	-2,4	0,6	0,0930
NOL8	down	-2,1	0,7	0,1322
NOM1	down	-2,2	0,1	0,0136
NOSTRIN	down	-3,1	0,8	0,0846
NOTCH1	up	2,6	1,5	0,1912
NPAS1	down	-2,2	0,5	0,0876
NPEPPS	down	-2,0	0,2	0,0468
NPHP1	up	3,2	1,7	0,1532
NPM2	down	-2,7	1,0	0,1273
NPNT	up	16,7	11,6	0,1529
NR0B2	down	-8,9	5,5	0,1455
NR1I3	up	3,8	0,7	0,0591
NR2E3	down	-3,0	0,2	0,0229
NRCAM	down	-2,0	0,5	0,1049
NRG4	up	4,4	1,0	0,0651
NRIP1	down	-2,4	0,0	0,0053
NRXN3	up	21,4	15,8	0,1597
NSD1	up	2,5	0,1	0,0131
NT5E	down	-2,9	1,4	0,1545
NTN5	up	4,6	2,4	0,1430
NUAK2	down	-2,9	1,7	0,1778
NUDT13	down	-3,4	0,0	0,0003
NUDT9	down	-2,7	0,1	0,0150
NUFIP2	down	-2,6	0,7	0,0946
NUP205	down	-2,2	0,4	0,0842
NXF2	up	6,0	2,9	0,1232
NXF5	up	6,0	2,8	0,1215
NXN	up	2,2	0,0	0,0017
NYNRIN	up	2,3	0,7	0,1210
OASL	up	3,6	1,6	0,1353
OAT	up	2,1	0,2	0,0518
OBFC1	up	2,3	0,3	0,0582
OBSCN	up	2,2	0,4	0,0801
OCA2	up	2,8	0,4	0,0518
ODF2L	down	-2,8	1,1	0,1309
OFD1	down	-2,2	0,6	0,1121
ONECUT1	up	2,1	0,6	0,1177
ONECUT2	down	-3,1	0,8	0,0811
OPHN1	down	-3,5	0,3	0,0251
OPN3	down	-4,1	1,6	0,1145
OR2A9P	down	-2,0	0,2	0,0463
OR51B4	down	-4,0	2,8	0,1847
ORM2	up	2,4	0,2	0,0333
OSBPL10	down	-3,6	3,2	0,2273
OSBPL3	down	-2,2	0,7	0,1287
OSBPL6	up	2,6	1,2	0,1530
OSCAR	up	3,3	1,5	0,1394
OTC	down	-2,1	0,2	0,0317
OTUD4	down	-2,2	0,5	0,0825
OTUD7B	down	-2,9	0,3	0,0312
OXCT1	up	3,7	0,2	0,0167
OXT	up	7,2	1,4	0,0495
OXTR	down	-2,5	0,6	0,0940
P2RX5	down	-2,6	1,1	0,1469
P2RY2	up	2,0	0,2	0,0350
PABPC1L	down	-7,3	0,5	0,0180
PABPC4L	down	-4,1	1,3	0,0919
PAGE4	up	3,4	1,8	0,1561
PAICS	down	-2,3	0,2	0,0273
PAIP2B	up	3,7	1,4	0,1090
PAK6	up	5,7	0,2	0,0117
PALLD	down	-2,1	0,6	0,1203
PALMD	down	-6,1	3,8	0,1542
PAM	down	-2,0	0,6	0,1282
PAQR8	down	-3,1	1,3	0,1285
PARD3B	down	-3,8	3,5	0,2267
PARD6A	down	-2,3	0,3	0,0507
PARP11	up	2,5	0,7	0,0987
PARP14	down	-2,1	0,6	0,1183
PARVA	up	4,7	1,9	0,1101
PAX3	down	-2,0	0,2	0,0451
PBRM1	down	-2,0	0,5	0,1127
PBX3	up	2,0	0,3	0,0635
PBX4	down	-3,0	1,9	0,1836
PC	up	2,0	0,1	0,0218
PCDH1	down	-3,6	0,1	0,0110
PCDH24	up	4,5	0,9	0,0548
PCDHA1	up	2,5	0,1	0,0092
PCDHB12	up	2,8	0,2	0,0229
PCDHB2	up	2,1	0,1	0,0179
PCDHB5	up	3,2	0,7	0,0679

PCID2	down	-5,1	1,6	0,0865
PCK1	up	2,5	0,6	0,0827
PCM1	down	-2,3	1,2	0,1804
PCP4L1	up	2,4	0,6	0,0974
PCSK1N	up	2,3	0,7	0,1213
PCSK7	up	2,0	0,3	0,0741
PDCD7	down	-2,1	0,0	0,0023
PDE4D	down	-12,5	9,4	0,1668
PDE4DIP	down	-2,2	0,3	0,0594
PDE5A	down	-6,1	4,3	0,1716
PDE6A	up	11,9	0,0	0,0008
PDE6B	up	43,4	5,1	0,0268
PDGFRL	up	2,1	0,6	0,1114
PDK4	up	9,6	2,2	0,0566
PDLIM3	down	-3,1	1,2	0,1213
PDLIM4	up	3,3	0,4	0,0366
PDS5B	down	-2,4	0,1	0,0226
PDZD3	up	3,9	0,2	0,0127
PDZRN3	up	11,9	6,4	0,1254
PECAM1	down	-4,7	0,2	0,0141
PFKFB2	down	-2,7	0,5	0,0676
PFN3	up	2,6	0,3	0,0444
PGC	down	-4,0	1,8	0,1241
PGLYRP2	up	3,6	1,3	0,1046
PGRMC1	up	2,9	0,0	0,0010
PHF11	down	-2,4	0,7	0,1120
PHF6	down	-2,4	0,6	0,0959
PHIP	down	-4,9	0,7	0,0389
PHLDA1	down	-2,6	0,8	0,1061
PHLDA2	down	-2,8	0,3	0,0341
PHTF2	down	-2,6	0,3	0,0383
PI4K2A	up	2,0	0,1	0,0273
PI4K2B	down	-2,1	0,6	0,1205
PIBF1	down	-2,5	0,4	0,0551
PIGA	down	-2,3	0,2	0,0255
PIK3C2A	down	-2,3	0,1	0,0225
PIK3CA	down	-2,1	0,1	0,0144
PIK3IP1	up	2,2	0,3	0,0657
PINK1	up	2,1	0,4	0,0892
PION	down	-2,3	0,4	0,0612
PIPOX	up	2,2	0,5	0,0996
PITPNC1	up	4,2	0,9	0,0644
PITX2	down	-4,5	3,4	0,1929
PIWIL4	down	-89,0	102,3	0,2191
PKD2	up	4,7	2,4	0,1339
PKHD1L1	down	-2,4	1,1	0,1609
PKIB	down	-4,5	1,7	0,1029
PKIG	up	2,2	0,2	0,0425
PKN2	down	-2,1	0,9	0,1680
PLA2G1B	up	4,5	0,1	0,0041
PLAC2	up	3,8	1,0	0,0768
PLAC8	down	-6,4	3,0	0,1200
PLAGL1	up	3,5	0,1	0,0115
PLCB1	down	-2,7	0,6	0,0747
PLCD1	up	2,1	0,1	0,0199
PLCG2	up	25,8	11,7	0,1024
PLCH1	down	-3,1	0,0	0,0013
PLD1	down	-2,9	0,0	0,0050
PLD6	down	-2,1	0,3	0,0569
PLEKHA1	down	-2,1	0,3	0,0662
PLEKHA6	down	-2,1	0,6	0,1116
PLEKHG1	up	4,3	3,4	0,2015
PLEKHG6	up	2,3	0,4	0,0741
PLEKHN1	down	-2,2	0,4	0,0639
PLG	up	3,5	1,2	0,1001
PLGLB1	up	2,7	1,4	0,1642
PLIN1	up	6,2	2,1	0,0871
PLK3	down	-3,4	0,4	0,0337
PLOD2	down	-2,7	0,1	0,0194
PLXND1	down	-2,9	1,6	0,1690
PMFBP1	down	-2,2	0,1	0,0164
PML	up	2,1	0,0	0,0005
PMS1	down	-2,5	0,4	0,0600
PNMA2	up	2,9	0,2	0,0264
PNMAL1	up	2,8	1,4	0,1662
PNN	down	-4,1	0,6	0,0445
PNPLA7	up	3,5	0,4	0,0345
PNPLA8	down	-2,4	1,0	0,1524
PODXL	down	-2,4	0,9	0,1349
POF1B	down	-2,1	0,0	0,0020
POLK	down	-2,8	0,6	0,0799
POLQ	down	-2,3	0,7	0,1145
POP1	down	-2,0	0,0	0,0106
POU2AF1	down	-3,8	1,6	0,1258
POU6F1	up	2,7	0,7	0,0880
PPARGC1A	up	7,1	7,6	0,2302
PPFIBP1	down	-2,5	0,0	0,0058
PPIG	down	-2,2	0,2	0,0358
PPIL6	up	3,9	1,2	0,0923
PPM1E	up	11,4	6,9	0,1396
PPM1K	down	-2,7	0,2	0,0228
PPM1L	down	-6,0	0,7	0,0313
PPP1R14A	up	7,4	2,9	0,0994
PPP1R1A	up	2,1	0,9	0,1752

PPP1R3B	down	-2,8	0,5	0,0634
PPP1R3C	up	3,2	0,6	0,0629
PPP1R3F	up	3,3	0,2	0,0195
PPP1R9A	down	-2,9	0,0	0,0022
PPP2R1B	up	3,7	1,3	0,1074
PPP2R2B	down	-2,6	0,6	0,0787
PPP2R2C	down	-3,7	0,1	0,0078
PPP4R2	down	-2,1	0,1	0,0132
PPWD1	down	-2,2	0,2	0,0326
PQLC3	down	-2,0	0,6	0,1245
PRAGMIN	down	-2,5	1,1	0,1584
PRAME	up	2,2	0,1	0,0143
PRAP1	up	3,0	0,4	0,0417
PRDM13	up	2,6	0,3	0,0421
PRDM6	up	13,2	3,1	0,0560
PRDXDD1P	down	-3,1	1,0	0,1012
PRELID2	down	-2,5	0,1	0,0083
PREX1	down	-5,6	3,6	0,1604
PRG4	up	3,4	0,5	0,0436
PRKAA1	down	-2,2	0,1	0,0244
PRKAB1	up	2,1	0,2	0,0314
PRKAB2	down	-2,6	0,5	0,0692
PRKAG2	up	3,6	1,7	0,1383
PRKD1	up	3,9	1,8	0,1328
PROM1	down	-9,2	9,2	0,2139
PRPF39	down	-3,1	0,2	0,0200
PRPF4B	down	-3,1	1,2	0,1220
PRPH	up	2,2	1,0	0,1726
PRPH2	down	-6,5	2,9	0,1118
PRR13	up	2,1	0,0	0,0081
PRR15	up	18,1	0,2	0,0027
PRR22	up	2,1	0,0	0,0072
PRR5-ARHGAP8	up	3,3	1,1	0,1040
PRSS16	up	3,9	0,1	0,0076
PRSS23	down	-2,7	1,9	0,2131
PRSS7	down	-10,6	2,2	0,0504
PRTG	up	3,1	0,0	0,0050
PSKH2	up	3,1	0,4	0,0442
PSMD9	up	2,4	0,4	0,0593
PTGIS	up	4,9	1,2	0,0697
PTK6	up	5,0	1,6	0,0878
PTK7	up	4,5	1,0	0,0637
PTPN22	down	-2,7	0,1	0,0184
PTPN4	down	-6,0	0,5	0,0222
PVRL1	up	5,7	2,8	0,1259
PYGO1	up	15,4	5,5	0,0835
PYY2	up	2,1	0,2	0,0458
QKI	up	2,0	0,0	0,0090
QSER1	down	-2,2	0,2	0,0297
R3HCC1	up	2,2	0,2	0,0419
RAB11FIP2	down	-2,1	0,8	0,1528
RAB11FIP4	up	3,1	1,8	0,1792
RAB26	down	-2,0	0,3	0,0697
RAB27B	down	-7,7	1,6	0,0549
RAB28	down	-2,0	0,6	0,1207
RAB31	down	-4,6	3,9	0,2078
RAB37	up	5,1	0,8	0,0428
RAB3B	down	-3,9	0,2	0,0157
RAB3D	down	-7,6	1,5	0,0517
RAB7B	down	-2,4	0,1	0,0094
RAB8B	down	-3,0	0,9	0,1004
RABEP1	down	-2,3	1,0	0,1552
RAC2	up	2,1	0,6	0,1233
RAD50	down	-2,4	0,2	0,0364
RAD54B	down	-2,6	0,4	0,0555
RADIL	up	3,4	0,6	0,0560
RAG1	up	3,8	1,9	0,1427
RALGPS1	up	22,6	1,5	0,0158
RAMP1	down	-2,3	1,0	0,1588
RANBP2	down	-2,2	0,5	0,0994
RAPGEF5	down	-3,0	1,6	0,1641
RAPGEF6	down	-2,5	0,3	0,0479
RAPH1	up	2,2	0,1	0,0230
RASA2	down	-3,0	0,6	0,0698
RASD1	down	-4,2	1,3	0,0929
RASD2	down	-4,0	1,4	0,1055
RASEF	up	6,2	1,0	0,0443
RASGEF1B	down	-3,4	0,1	0,0064
RASL11A	up	3,2	1,5	0,1414
RASL12	down	-13,0	9,9	0,1675
RASSF5	up	2,9	0,1	0,0089
RASSF8	down	-2,4	0,7	0,1103
RAVER2	up	17,3	2,9	0,0403
RB1CC1	down	-2,1	0,7	0,1367
RBBP6	down	-2,4	0,7	0,1028
RBBP8	down	-2,0	0,3	0,0645
RBM25	down	-2,1	0,3	0,0559
RBM27	down	-2,1	0,4	0,0722
RBM41	down	-3,1	0,1	0,0094
RBMS1	up	6,6	0,4	0,0164
RBP1	up	4,7	1,6	0,0969
RBP2	up	6,7	0,2	0,0071
RBP5	up	2,9	0,7	0,0759
RCN1	down	-2,6	1,4	0,1771

RDH12	down	-4,6	1,3	0,0796
RDH16	up	2,5	0,7	0,0965
RDH5	up	2,5	0,5	0,0754
RDX	down	-2,6	0,1	0,0202
RELN	down	-2,3	0,9	0,1442
RENBP	down	-4,0	0,0	0,0008
REPS2	up	6,9	5,3	0,1788
REV3L	down	-2,2	0,3	0,0656
RFC1	down	-2,2	0,5	0,0921
RFK	up	2,2	0,0	0,0018
RFTN1	up	18,4	3,6	0,0461
RFX3	down	-3,2	1,5	0,1401
RGAG4	up	5,7	4,2	0,1788
RGNEF	down	-2,1	0,1	0,0226
RGP1	up	2,2	0,2	0,0299
RGPD5	down	-2,4	0,6	0,0975
RGS20	down	-5,1	3,1	0,1544
RGS3	down	-2,9	0,1	0,0174
RHBG	down	-2,9	1,6	0,1681
RHOBTB1	down	-2,9	2,1	0,2102
RHOF	up	2,3	0,1	0,0191
RHOH	down	-4,3	0,6	0,0389
RHOV	up	4,4	0,0	0,0031
RHPN1	up	5,0	1,3	0,0728
RIC3	up	4,1	1,2	0,0850
RICH2	up	5,0	2,0	0,1051
RICTOR	down	-2,4	1,0	0,1475
RIF1	down	-2,4	0,1	0,0130
RILPL2	up	2,0	0,0	0,0090
RIMBP3	up	2,0	0,0	0,0069
RIMKLB	up	2,7	0,2	0,0218
RIMS3	up	2,8	0,4	0,0435
RIN1	down	-7,7	5,7	0,1726
RIN2	up	2,3	0,1	0,0255
RIPK2	down	-2,1	0,1	0,0116
RNASE2	up	12,9	1,8	0,0330
RNASE4	up	2,4	0,9	0,1328
RND1	up	2,6	0,6	0,0814
RND3	down	-7,7	4,7	0,1459
RNF148	down	-3,9	3,2	0,2102
RNF152	up	4,2	0,9	0,0634
RNF160	down	-2,8	0,3	0,0316
RNF17	down	-3,8	0,0	0,0014
RNF217	up	7,6	0,4	0,0121
RNF6	down	-2,1	0,4	0,0773
RNLS	up	5,0	0,5	0,0256
RNU12	up	2,0	0,3	0,0711
ROBO1	down	-4,6	3,1	0,1756
ROCK1	down	-2,7	0,2	0,0248
ROCK2	down	-2,2	0,7	0,1328
ROR1	down	-4,7	3,4	0,1838
RPGRIP1L	down	-2,3	0,7	0,1229
RPL10	down	-4,4	1,0	0,0659
RPL27A	up	2,1	0,3	0,0690
RPRML	up	2,5	1,1	0,1476
RPS6KA3	down	-2,7	0,8	0,1018
RPS6KA5	up	3,8	1,3	0,1047
RPS6KB1	down	-2,1	0,9	0,1734
RRAGD	up	31,2	9,0	0,0662
RRP15	down	-2,1	0,2	0,0505
RSF1	down	-2,5	0,2	0,0265
RTDR1	up	2,7	0,1	0,0072
RTKN2	down	-2,4	0,5	0,0841
RTN1	up	10,6	6,8	0,1482
RTN4RL1	up	3,3	0,6	0,0586
RTP3	up	15,2	15,2	0,2058
RTP4	up	2,1	0,6	0,1129
RUFY2	down	-2,4	0,7	0,1103
RUFY3	down	-2,3	0,1	0,0220
RUNDC2B	down	-2,8	0,3	0,0403
RUNX1	down	-2,4	0,4	0,0675
RXRA	up	2,2	0,1	0,0114
S100P	down	-3,9	1,5	0,1109
S1PR1	up	10,6	0,2	0,0046
SAA4	up	5,1	0,2	0,0122
SACS	down	-3,3	0,9	0,0883
SAGE1	down	-2,0	0,4	0,0768
SAMD12	down	-5,4	0,0	0,0019
SAMD9	down	-3,0	1,7	0,1733
SAPS2	down	-2,2	0,1	0,0245
SBF2	down	-2,3	0,1	0,0235
SC5DL	down	-2,0	0,0	0,0037
SCCPDH	down	-2,1	0,1	0,0308
SCD5	up	8,8	2,2	0,0618
SCLT1	down	-2,9	0,9	0,1008
SCN9A	down	-2,1	0,3	0,0532
SDAD1	down	-2,7	0,8	0,0998
SDCBP2	up	6,1	0,1	0,0033
SDCCAG1	down	-3,3	0,5	0,0460
SEC31A	down	-4,3	0,3	0,0201
SECTM1	up	4,8	1,4	0,0833
SEL1L3	down	-5,3	1,7	0,0845
SELV	up	4,3	1,9	0,1244
SEMA3B	down	-3,4	1,7	0,1486

SEMA3D	down	-3,9	3,8	0,2365	SLC13A3	up	10,2	0,2	0,0037
SEMA3G	down	-2,1	0,2	0,0419	SLC13A4	down	-14,7	0,5	0,0086
SEMA6A	down	-3,4	2,6	0,2066	SLC13A5	up	2,0	0,4	0,0793
SENP3	down	-2,1	0,4	0,0804	SLC16A10	up	3,8	0,7	0,0523
SENP7	down	-2,7	0,3	0,0388	SLC16A12	up	6,6	4,3	0,1590
SEPP1	down	-2,4	0,0	0,0001	SLC16A2	up	9,4	1,7	0,0454
SEPT4	up	4,2	2,9	0,1807	SLC16A3	down	-3,9	1,6	0,1180
SEPT5	up	2,5	0,0	0,0058	SLC17A1	up	6,2	1,8	0,0763
SEPT6	up	2,6	0,2	0,0326	SLC17A2	up	7,5	1,3	0,0453
SERINC2	up	2,0	0,0	0,0054	SLC1A2	up	32,5	29,2	0,1849
SERINC5	up	2,5	0,9	0,1193	SLC1A3	up	8,0	0,2	0,0068
SERPINA10	up	2,5	0,5	0,0749	SLC1A7	up	2,4	1,2	0,1754
SERPINA11	up	2,0	0,8	0,1617	SLC22A15	down	-2,1	0,2	0,0320
SERPINA4	up	2,7	0,0	0,0053	SLC22A4	up	2,5	1,0	0,1419
SERPINA5	up	2,1	0,4	0,0745	SLC22A7	up	5,0	2,7	0,1409
SERPINA6	up	2,0	0,3	0,0557	SLC22A9	up	2,4	0,2	0,0262
SERPINA7	up	3,9	2,6	0,1821	SLC23A3	up	7,6	2,4	0,0799
SERPINB9	up	8,6	4,4	0,1242	SLC25A12	down	-2,8	0,5	0,0633
SERPING1	up	3,7	1,3	0,1045	SLC25A18	up	2,7	0,4	0,0544
SERPINI1	up	2,0	0,8	0,1617	SLC25A36	down	-2,1	0,3	0,0534
SESN1	up	2,7	0,2	0,0314	SLC25A42	up	2,1	0,6	0,1087
SETBP1	down	-5,3	4,0	0,1861	SLC2A10	up	2,1	0,8	0,1613
SETD8	up	2,0	0,0	0,0002	SLC2A13	down	-2,4	0,8	0,1192
SETX	down	-2,1	0,6	0,1229	SLC2A2	up	2,8	0,2	0,0218
SF1	down	-2,3	0,1	0,0111	SLC2A3	up	2,4	0,5	0,0731
SFMBT2	up	6,7	1,0	0,0400	SLC30A1	up	2,4	0,5	0,0811
SFN	down	-2,5	0,5	0,0726	SLC30A3	up	2,3	1,3	0,1985
SFRP4	up	2,2	0,3	0,0522	SLC30A4	up	22,2	0,1	0,0011
SFRS11	down	-2,2	0,3	0,0582	SLC30A8	up	2,8	1,0	0,1221
SFRS12	down	-2,9	0,4	0,0498	SLC35F2	up	3,8	1,2	0,0899
SFRS18	down	-2,6	0,3	0,0462	SLC38A1	up	2,1	0,2	0,0437
SGK2	up	2,0	0,4	0,0895	SLC38A11	down	-3,5	2,1	0,1713
SGMS1	up	2,1	0,4	0,0802	SLC38A2	down	-2,7	0,7	0,0911
SGOL1	down	-2,0	0,3	0,0575	SLC38A5	down	-3,3	1,2	0,1133
SGOL2	down	-2,4	0,4	0,0647	SLC39A14	up	2,3	0,1	0,0138
SGSM1	down	-3,6	2,8	0,2071	SLC39A5	up	2,2	0,5	0,0957
SH3BGRL	down	-2,4	0,5	0,0703	SLC41A1	up	2,5	0,8	0,1159
SH3GLB1	down	-2,3	1,0	0,1622	SLC44A3	down	-2,1	0,7	0,1324
SH3RF1	down	-2,6	0,9	0,1173	SLC44A5	down	-3,6	0,4	0,0320
SH3TC1	down	-2,5	0,0	0,0009	SLC45A4	down	-4,0	0,9	0,0660
SHPRH	down	-2,2	0,6	0,1060	SLC4A4	down	-5,9	2,3	0,1034
SHROOM2	up	12,6	6,0	0,1116	SLC4A7	down	-6,3	0,3	0,0147
SIK2	up	2,2	0,2	0,0290	SLC5A11	down	-2,6	0,8	0,1090
SIX2	up	2,4	0,6	0,0996	SLC5A3	down	-2,5	0,7	0,1065
SKAP1	up	4,1	2,2	0,1457	SLC6A11	down	-2,5	0,1	0,0211
SLC10A1	up	4,2	1,5	0,0999	SLC6A13	up	2,1	0,2	0,0382
SLC12A2	down	-2,2	0,1	0,0208	SLC6A20	down	-3,5	0,8	0,0697

SLC6A6	down	-3,3	1,5	0,1398
SLC7A11	down	-4,0	0,1	0,0040
SLCO2B1	up	2,8	0,2	0,0272
SLCO4C1	up	2,1	0,3	0,0558
SLFN11	down	-22,3	17,2	0,1656
SLK	down	-2,0	0,6	0,1242
SLPI	up	7,8	3,3	0,1036
SLTM	down	-2,5	0,5	0,0746
SMAD9	down	-2,1	1,0	0,1875
SMARCA1	down	-2,5	0,9	0,1239
SMARCAD1	down	-2,4	0,9	0,1398
SMC1A	down	-3,5	0,1	0,0097
SMC2	down	-2,1	0,3	0,0676
SMC4	down	-2,5	0,5	0,0749
SMC5	down	-2,3	0,2	0,0306
SMC6	down	-3,3	0,9	0,0821
SMCHD1	down	-2,2	0,4	0,0746
SMG1	down	-2,3	0,5	0,0871
SMO	down	-2,6	0,6	0,0783
SMS	down	-2,1	0,6	0,1159
SMYD1	up	3,9	0,2	0,0190
SNAP25	down	-2,4	1,0	0,1518
SNHG1	down	-3,1	0,6	0,0571
SNORD123	up	2,2	0,2	0,0292
SNRK	down	-2,2	0,1	0,0166
SNRPN	down	-3,0	2,3	0,2130
SNURF	down	-2,2	0,4	0,0692
SNX13	down	-2,6	0,7	0,0969
SNX25	down	-2,2	0,5	0,0964
SOCS1	down	-3,1	1,4	0,1429
SOCS3	up	2,0	0,2	0,0361
SOHLH2	down	-2,2	0,4	0,0684
SORBS2	down	-2,1	0,8	0,1517
SORCS3	up	4,5	1,4	0,0866
SORD	up	2,2	0,1	0,0143
SOX2	up	11,4	0,1	0,0012
SOX4	down	-2,2	0,9	0,1540
SOX5	down	-3,5	1,2	0,1042
SOX6	down	-15,4	16,9	0,2199
SOX9	down	-6,6	3,2	0,1208
SP4	down	-2,1	0,1	0,0128
SP5	up	18,2	0,2	0,0020
SPAG8	down	-2,4	0,1	0,0132
SPARC	up	8,9	1,8	0,0520
SPG20	down	-3,6	0,8	0,0717
SPINK4	down	-6,9	2,4	0,0886
SPINK5	down	-2,1	0,9	0,1651
SPINK5L3	down	-3,7	0,6	0,0523
SPINT1	up	2,2	1,4	0,2106
SPINT2	up	2,1	0,4	0,0859
SPOCK2	up	2,2	0,8	0,1369
SPP2	up	36,8	42,4	0,2218
SPRED1	down	-2,0	0,5	0,1102
SPRY1	down	-3,5	2,1	0,1682
SPRY2	down	-3,1	2,0	0,1937
SPRY4	down	-6,9	1,9	0,0727
SPTBN5	up	2,7	0,0	0,0037
SRC	up	2,4	0,0	0,0032
SRCRB4D	up	3,7	2,4	0,1794
SRGN	down	-11,9	6,5	0,1263
SRP72	down	-2,2	0,5	0,0861
SRPX	up	9,1	3,2	0,0876
SSB	down	-2,0	0,4	0,0873
SSBP2	up	8,4	1,4	0,0418
SSFA2	down	-2,8	0,1	0,0080
SSTR1	up	5,7	2,1	0,0959
SSTR2	down	-25,2	2,9	0,0268
SSTR5	down	-6,3	0,1	0,0046
SSX1	down	-9,6	8,9	0,2006
SSX2IP	down	-2,6	0,4	0,0623
SSX8	down	-6,8	3,0	0,1122
ST6GAL1	up	2,4	0,6	0,0924
STAG2	down	-3,3	0,8	0,0724
STARD6	up	3,7	2,5	0,1815
STAT3	up	2,0	0,5	0,1080
STEAP1	down	-2,0	0,2	0,0484
STEAP2	down	-2,6	0,3	0,0385
STEAP3	up	2,2	0,4	0,0710
STH	down	-2,6	0,6	0,0792
STK39	down	-8,4	1,3	0,0399
STOM	up	2,7	0,3	0,0407
STRN	down	-2,4	1,0	0,1450
STX11	up	2,0	0,8	0,1542
STXBP1	up	18,9	6,2	0,0768
STXBP4	down	-2,1	0,1	0,0150
STXBP5	down	-2,2	0,2	0,0360
STXBP5L	down	-2,7	0,0	0,0064
SUCLA2	down	-2,2	0,4	0,0792
SUGT1L1	down	-2,6	0,1	0,0104
SULF2	up	209,5	121,3	0,1243
SULT2A1	up	3,6	0,1	0,0078
SUOX	up	2,0	0,0	0,0073
SUZ12	down	-2,5	0,1	0,0143
SUZ12P	down	-2,1	0,2	0,0458

SV2B	up	6,0	1,0	0,0435
SVOP	up	5,4	1,4	0,0718
SVOPL	up	2,3	0,4	0,0638
SYDE2	down	-2,6	0,2	0,0248
SYNC	down	-2,0	0,2	0,0525
SYNM	down	-2,9	0,1	0,0153
SYT1	down	-3,4	1,3	0,1172
SYT13	up	13,8	6,9	0,1162
SYT15	up	2,2	0,0	0,0065
SYT7	up	2,9	0,3	0,0401
SYTL1	down	-2,6	1,3	0,1679
SYTL3	up	3,2	0,5	0,0539
SYTL5	down	-2,6	1,4	0,1759
TACC1	down	-3,0	0,0	0,0003
TAF15	down	-2,1	0,3	0,0690
TAF1A	down	-2,2	0,5	0,0913
TAF2	down	-2,7	0,4	0,0459
TAF5L	down	-2,0	0,8	0,1601
TAF7	up	2,5	0,7	0,0981
TANC2	up	5,6	4,4	0,1887
TANK	down	-2,1	0,2	0,0413
TAS2R14	down	-2,9	0,9	0,0999
TBC1D12	down	-2,9	0,8	0,0907
TBC1D2	up	3,3	0,9	0,0825
TBC1D4	down	-6,2	3,5	0,1409
TBC1D8B	down	-3,0	0,5	0,0543
TBX18	down	-3,9	0,4	0,0350
tcag7.1307	up	10,5	3,3	0,0763
TCEA2	up	5,4	1,0	0,0521
TCEAL3	down	-3,5	0,6	0,0528
TCEAL5	down	-2,4	1,3	0,1852
TCEAL6	down	-3,8	0,7	0,0559
TCF12	down	-2,3	0,1	0,0114
TCF25	up	2,0	0,5	0,0997
TCIRG1	down	-2,1	1,0	0,1864
TCTEX1D2	up	2,3	0,3	0,0578
TDH	up	8,2	6,2	0,1736
TDO2	down	-3,9	0,3	0,0237
TDRD10	up	3,9	1,9	0,1378
TERF1	down	-2,2	0,1	0,0277
TESC	down	-5,6	3,5	0,1590
TEX11	down	-15,7	7,3	0,1082
TEX15	down	-6,5	0,0	0,0019
TEX19	up	3,0	1,8	0,1833
TFCP2	down	-52,9	0,9	0,0037
TFEB	down	-4,1	0,1	0,0056
TFPI	down	-14,5	3,1	0,0519
TFR2	up	2,3	0,4	0,0621
TGFB3	down	-3,0	1,4	0,1436
TGM2	up	2,2	0,4	0,0661
TH1L	up	2,1	0,2	0,0318
THAP5	down	-2,3	0,3	0,0450
THBS1	down	-3,9	0,8	0,0586
THBS4	down	-2,1	0,8	0,1472
THG1L	up	2,2	0,2	0,0293
THOC2	down	-3,7	0,9	0,0721
THSD4	down	-4,2	1,6	0,1058
THUMPD2	down	-2,3	0,4	0,0752
TIA1	down	-2,2	0,6	0,1112
TIMD4	down	-3,4	0,8	0,0788
TLE2	up	3,9	2,4	0,1682
TLE4	down	-5,1	3,6	0,1794
TLL2	up	3,9	1,3	0,0993
TLR2	up	3,4	1,7	0,1498
TLR4	down	-2,2	0,9	0,1524
TM4SF1	down	-7,9	7,0	0,1992
TM4SF4	up	2,4	0,5	0,0763
TMBIM1	up	2,2	0,4	0,0691
TMC6	down	-5,2	0,8	0,0414
TMCC3	up	8,2	1,1	0,0338
TMEM108	up	4,4	1,8	0,1134
TMEM127	up	2,1	0,2	0,0429
TMEM150C	up	9,5	4,6	0,1161
TMEM159	up	8,8	4,9	0,1325
TMEM19	up	2,1	0,5	0,1100
TMEM2	down	-2,7	0,1	0,0180
TMEM200A	up	2,8	0,0	0,0051
TMEM217	up	2,6	0,4	0,0504
TMEM220	down	-15,1	8,9	0,1341
TMEM30B	down	-2,1	0,5	0,0936
TMEM42	down	-5,7	1,8	0,0862
TMEM45A	up	11,1	0,2	0,0053
TMEM45B	up	6,1	6,3	0,2291
TMEM47	down	-19,1	18,3	0,1978
TMEM55A	down	-2,9	0,1	0,0169
TMEM8B	up	4,6	0,3	0,0174
TMF1	down	-2,3	0,1	0,0196
TMOD1	up	2,5	0,3	0,0469
TMPRSS2	up	5,1	0,9	0,0470
TMPRSS6	up	4,8	0,3	0,0204
TMSB4X	down	-5,1	2,1	0,1099
TMSL3	down	-8,3	8,4	0,2163
TMX3	down	-2,0	0,4	0,0925
TNC	up	3,5	1,4	0,1239

TNF	down	-8,7	7,1	0,1846
TNFAIP8	down	-2,3	0,4	0,0617
TNFRSF11A	up	3,9	0,3	0,0256
TNFRSF11B	down	-15,1	0,4	0,0066
TNFRSF25	up	5,7	0,6	0,0290
TNFSF11	down	-21,5	5,4	0,0581
TNFSF13B	down	-4,1	1,1	0,0747
TNFSF4	down	-2,2	1,1	0,1862
TNIK	down	-2,8	1,7	0,1827
TNK1	down	-2,2	0,1	0,0157
TNN	up	2,7	0,2	0,0222
TNNC1	down	-5,7	3,4	0,1493
TNPO1	down	-2,7	0,8	0,1089
TNPO2	down	-5,7	0,3	0,0128
TNS1	up	3,9	0,1	0,0109
TNS3	up	2,0	0,4	0,0852
TOX2	up	4,6	0,7	0,0426
TP53I3	up	2,2	0,5	0,0999
TP53INP2	up	2,9	0,2	0,0235
TP53TG3	up	2,0	0,6	0,1240
TP73	up	3,2	0,1	0,0105
TPBG	up	2,1	0,6	0,1209
TPD52L1	up	11,9	8,5	0,1603
TPK1	down	-2,8	1,9	0,2034
TPP2	down	-2,1	0,3	0,0634
TPR	down	-2,6	0,5	0,0747
TPTE	down	-2,3	0,3	0,0521
TRAF3IP2	up	3,1	0,4	0,0456
TRAF5	down	-3,0	0,3	0,0309
TRANK1	up	2,3	0,4	0,0678
TRAPPC2L	up	2,3	0,6	0,0966
TRAPPC6A	up	2,6	0,2	0,0220
TRIB2	up	6,0	0,7	0,0304
TRIM13	down	-2,9	0,2	0,0189
TRIM14	up	2,3	0,1	0,0213
TRIM2	down	-2,1	0,3	0,0491
TRIM31	up	2,1	0,4	0,0753
TRIM32	up	2,2	0,1	0,0162
TRIM34	down	-2,6	1,2	0,1540
TRIM35	up	2,1	0,2	0,0485
TRIM36	up	2,4	0,1	0,0133
TRIM5	down	-2,7	1,7	0,1887
TRIM59	up	3,3	1,0	0,0997
TRIM60	up	6,2	0,5	0,0226
TRIM74	up	2,5	0,4	0,0584
TRIM9	down	-3,8	2,2	0,1610
TRIP11	down	-2,5	0,3	0,0474
TRNP1	down	-2,0	0,0	0,0030
TRNT1	down	-2,1	0,1	0,0133
TRO	up	17,0	5,7	0,0792
TRPM7	down	-2,4	0,1	0,0174
TRPV2	down	-7,1	3,5	0,1210
TSNARE1	up	2,3	0,2	0,0424
TSPAN13	down	-2,4	0,2	0,0385
TSPAN3	up	2,4	0,1	0,0172
TSPAN8	down	-2,2	0,7	0,1314
TSPAN9	up	2,0	0,1	0,0325
TSPYL1	up	2,1	0,1	0,0186
TSPYL4	up	2,8	0,3	0,0421
TTC13	down	-2,6	0,4	0,0616
TTC14	down	-2,1	0,4	0,0781
TTC21B	down	-2,1	0,4	0,0874
TTC22	down	-12,1	13,1	0,2210
TTC3	down	-3,2	1,0	0,0978
TTC37	down	-2,6	0,8	0,1051
TTC39C	up	2,0	0,1	0,0285
TTC7B	up	3,5	0,4	0,0317
TTC9	up	3,1	0,9	0,0931
TTLL11	up	2,3	0,3	0,0481
TTLL2	down	-5,6	1,1	0,0508
TTR	down	-2,4	1,5	0,2091
TUB	up	2,9	0,5	0,0544
TUBAL3	down	-11,8	11,7	0,2071
TUBB2B	up	3,7	1,5	0,1197
TUBB4	up	2,0	0,1	0,0240
TUSC3	up	4,8	0,8	0,0490
TWISTNB	down	-2,1	0,4	0,0756
TXLNA	up	2,0	0,0	0,0080
TXNDC11	up	2,1	0,1	0,0279
TXNL4B	up	2,0	0,3	0,0644
TYMP	up	3,9	0,8	0,0598
TYW3	down	-2,1	0,6	0,1194
UAP1L1	up	2,1	0,4	0,0788
UBA6	down	-3,6	0,7	0,0610
UBR1	down	-2,1	0,5	0,1045
UCHL5	down	-2,2	0,4	0,0715
UCP2	up	2,0	0,4	0,0924
UGGT2	down	-3,1	0,9	0,0985
UGT1A6	down	-4,7	3,2	0,1735
UGT2B11	down	-3,0	0,8	0,0905
UGT2B4	down	-3,4	0,7	0,0645
UGT2B7	down	-3,6	2,0	0,1571
ULK1	up	2,5	0,8	0,1067
ULK2	up	17,0	4,5	0,0620

UNC13C	down	-3,7	0,1	0,0058	WNK4	down	-2,5	0,2	0,0321
UNC5B	down	-8,3	9,6	0,2374	WNT5A	up	5,5	0,1	0,0035
UNC93A	up	2,9	0,5	0,0650	WRN	down	-2,2	0,1	0,0268
UNG	up	2,2	0,1	0,0226	WSCD1	up	2,1	0,1	0,0272
UPF2	down	-3,0	0,4	0,0412	WWOX	up	2,2	0,0	0,0084
UPF3B	down	-4,1	0,9	0,0641	XAF1	down	-2,9	2,0	0,2002
USHBP1	down	-4,0	2,3	0,1606	XBP1	down	-2,3	0,6	0,1046
USO1	down	-2,1	0,7	0,1450	XIAP	down	-2,3	0,2	0,0420
USP16	down	-2,4	0,7	0,0996	XIST	down	-55,6	22,7	0,0911
USP25	down	-2,5	0,1	0,0187	XK	up	4,9	0,2	0,0140
USP46	down	-2,0	0,4	0,0938	XKR6	up	7,8	2,2	0,0722
USP47	down	-2,3	0,3	0,0515	XPR1	down	-2,3	0,1	0,0171
USP48	down	-2,4	0,0	0,0052	XRCC2	down	-2,4	0,0	0,0039
USP53	down	-3,1	1,2	0,1203	XYLB	up	3,1	0,4	0,0411
USP6NL	down	-2,3	0,6	0,0975	YIF1B	up	5,2	2,2	0,1136
UTP14A	down	-2,0	0,0	0,0012	YPEL1	up	2,6	0,7	0,0937
UTP15	down	-2,0	0,3	0,0615	YPEL2	up	2,2	0,0	0,0044
UTP20	down	-2,2	0,7	0,1277	YTHDC2	down	-3,0	0,7	0,0764
UTRN	down	-2,0	0,2	0,0512	ZADH2	down	-2,0	0,4	0,0936
UTS2	down	-5,9	6,1	0,2308	ZBTB20	down	-2,8	0,2	0,0216
VAMP4	down	-2,6	0,5	0,0754	ZBTB41	down	-2,6	0,3	0,0422
VASH1	up	3,5	0,4	0,0313	ZC3H10	up	2,1	0,0	0,0004
VAV2	up	2,0	0,1	0,0227	ZC3H11A	down	-2,0	0,0	0,0043
VCX	up	8,4	3,1	0,0910	ZC3H12C	up	35,9	0,1	0,0006
VCX2	up	5,4	1,7	0,0848	ZC3H13	down	-3,9	1,0	0,0747
VCX3A	up	10,0	4,1	0,1007	ZC3H6	down	-3,9	0,0	0,0007
VCY	up	5,8	2,0	0,0902	ZCCHC3	up	2,4	0,6	0,0922
VDR	up	10,5	3,0	0,0696	ZDHHC2	up	5,8	0,1	0,0036
VPS13A	down	-5,3	0,5	0,0276	ZDHHC8P	up	2,1	0,5	0,0946
VPS13B	down	-2,1	0,7	0,1267	ZEB1	down	-2,9	1,3	0,1390
VPS13C	down	-2,6	1,0	0,1312	ZER1	up	2,7	0,3	0,0441
VPS54	down	-2,3	0,2	0,0410	ZFAND2A	up	2,0	0,2	0,0522
VSNL1	down	-2,2	0,1	0,0267	ZFC3H1	down	-2,1	0,4	0,0832
VTN	up	2,3	0,3	0,0435	ZFHX4	down	-2,2	0,1	0,0178
VWCE	up	2,1	0,2	0,0399	ZFYVE16	down	-2,1	0,0	0,0016
VWF	up	2,2	0,7	0,1317	ZIC5	down	-2,6	1,3	0,1683
WBP5	down	-2,0	0,6	0,1306	ZIM2	up	2,0	1,2	0,2154
WDHD1	down	-2,4	0,3	0,0495	ZMYM5	down	-2,2	0,1	0,0180
WDR66	up	5,0	1,5	0,0827	ZMYM6	down	-2,1	0,3	0,0667
WDR67	down	-2,2	0,3	0,0606	ZMYND12	up	2,2	0,1	0,0195
WDR72	down	-3,0	0,2	0,0208	ZNF100	down	-2,6	1,1	0,1500
WFIKKN1	up	2,4	0,6	0,0983	ZNF107	down	-3,6	0,4	0,0326
WFS1	down	-2,0	0,2	0,0434	ZNF138	down	-2,5	0,3	0,0395
WHSC1	down	-2,5	0,1	0,0220	ZNF146	down	-2,2	0,1	0,0138
WIPF1	up	2,8	0,0	0,0005	ZNF148	down	-2,2	0,3	0,0519
WNK2	down	-9,2	0,0	0,0000	ZNF177	up	2,4	1,0	0,1421
WNK3	up	10,5	1,4	0,0341	ZNF182	down	-2,1	0,3	0,0680

ZNF195	down	-2,1	0,0	0,0072
ZNF207	down	-2,6	0,7	0,0992
ZNF215	down	-2,0	0,1	0,0300
ZNF229	up	2,3	0,3	0,0561
ZNF248	down	-3,0	0,1	0,0070
ZNF25	down	-2,8	1,5	0,1699
ZNF254	down	-2,2	0,2	0,0295
ZNF267	down	-2,4	0,1	0,0240
ZNF273	down	-2,3	0,1	0,0229
ZNF280C	down	-2,1	0,2	0,0340
ZNF280D	down	-2,7	0,4	0,0521
ZNF292	down	-2,8	0,5	0,0685
ZNF323	down	-2,0	0,1	0,0263
ZNF326	down	-2,5	0,3	0,0430
ZNF37B	down	-2,3	0,5	0,0780
ZNF385A	up	2,2	0,5	0,0994
ZNF395	up	2,0	0,0	0,0047
ZNF41	down	-2,0	0,0	0,0076
ZNF449	down	-2,1	0,7	0,1391
ZNF451	down	-2,1	0,0	0,0012
ZNF488	up	2,8	0,5	0,0614
ZNF492	down	-2,2	0,3	0,0513
ZNF493	down	-2,8	1,0	0,1176
ZNF502	down	-3,3	1,0	0,0987
ZNF513	up	5,4	0,8	0,0407
ZNF518B	down	-2,6	0,2	0,0349
ZNF519	down	-2,0	0,2	0,0487
ZNF541	up	4,9	2,5	0,1360
ZNF560	down	-2,9	0,0	0,0041
ZNF599	up	2,4	0,6	0,0905
ZNF608	down	-2,1	0,4	0,0704
ZNF614	down	-2,2	0,1	0,0239
ZNF615	down	-2,2	0,6	0,1098
ZNF618	up	12,8	0,4	0,0068
ZNF619	up	2,9	0,9	0,0964
ZNF624	down	-2,0	0,3	0,0582
ZNF630	down	-2,6	0,9	0,1188
ZNF638	down	-2,6	0,7	0,0956
ZNF644	down	-2,3	0,6	0,0945
ZNF660	down	-6,9	1,4	0,0515
ZNF670	down	-2,3	0,2	0,0437
ZNF678	down	-2,4	0,7	0,1036
ZNF702P	up	2,6	1,5	0,1811
ZNF711	down	-2,7	0,8	0,1041
ZNF718	down	-3,7	0,6	0,0501
ZNF721	down	-3,1	0,9	0,0958
ZNF726	down	-2,0	0,7	0,1452
ZNF747	up	2,0	0,1	0,0250
ZNF783	down	-2,2	0,1	0,0228
ZNF800	down	-2,7	0,5	0,0602
ZNF876P	down	-18,7	12,4	0,1465
ZNF92	down	-2,2	0,1	0,0262
ZNF99	down	-2,0	0,5	0,1116
ZRANB2	down	-2,1	0,6	0,1132
ZSCAN18	up	2,1	0,4	0,0790
ZSCAN5A	up	2,1	0,2	0,0398

Supplementary Table 3. Genes being deregulated in HepG2-cells expressing solFGFR4. *Data were processed as described in Experimental Procedures and are means of fold-vector control values of 2 different experiments. Fold-change cutoffs of ≥2 and ≤0.5 were used to select upregulated and downregulated genes, respectively.*

Gene	reg.	Mean x Control	S.D.	p-value
ABLIM3	up	2,24	0,39	0,070
ABTB1	up	2,80	0,19	0,024
ACAD10	up	20,14	2,21	0,026
ADC	up	5,34	2,91	0,141
ADH4	down	-2.03	0.22	0.047
AKAP9	down	-2.02	0.72	0.147
ALB	down	-2.34	0.97	0.150
ALG10B	down	-2.07	0.32	0.066
ANGPTL1	down	-2.51	0.64	0.093
ANGPT2	up	3,81	2,95	0,203
ANKRD32	down	-2.33	0.12	0.020
AQP3	up	2,37	0,84	0,130
BRCA2	down	-2.19	0.66	0.119
C12orf60	down	-2.02	0.63	0.132
C6orf167	down	-2.03	0.00	0.000
C13orf15	up	2,07	0,89	0,169
C14orf72	up	2,13	0,49	0,095
C7orf58	down	-2.20	0.56	0.101
CASP8AP2	down	-2.11	0.49	0.096
CCDC150	down	-2.05	0.48	0.098
CCDC41	down	-2.06	0.35	0.073
CENPC1	down	-2.36	0.21	0.035
CENPE	down	-2,39	1,03	0,154
CEP290	down	-2,01	0,63	0,131
CHMP4B	up	2,43	1,17	0,167
COG6	down	-2,31	0,21	0,035
CUL5	down	-2,21	0,09	0,017
CYB561	up	2,03	0,21	0,046
CYTH4	up	2,08	0,00	0,000
DLEU2	down	-2,09	1,11	0,199
DLGAP5	down	-2,01	0,30	0,066
DNAJB4	down	-2,08	0,45	0,091
EGR2	up	2,91	1,70	0,179
EIF4A2	down	-2,01	0,23	0,051
FANCM	down	-2,04	0,50	0,104
FLNB	up	2,00	0,71	0,148
FPGT	down	-2,09	0,66	0,129
FUT1	up	3,79	2,11	0,157
GNPDA2	down	-2,02	0,40	0,086
G0S2	up	4,76	0,80	0,048
GPAM	down	-2,00	0,70	0,146
HLTF	down	-2,52	0,24	0,036
HMMR	down	-2,10	0,46	0,092
HSPA6	down	-2,29	0,14	0,024
IER3IP1	down	-2,13	0,17	0,034
IFIT1	down	-2,56	0,89	0,121
IGF2	up	2,97	1,36	0,145
IGFBP1	up	2,04	0,19	0,041
IGFBP3	up	2,24	0,21	0,039
INHBE	up	2,41	0,51	0,079
IQCG	up	2,44	0,53	0,082
ITGB3BP	down	-2,05	0,89	0,171
KLHDC7B	up	2,18	0,56	0,103
KLHL29	up	4,56	0,41	0,026
LARP6	up	4,13	2,46	0,162
LENG8	up	9,72	1,11	0,029
LOC100129113	up	4,12	1,77	0,121
LOC401397	down	-2,11	0,68	0,130
LRRC47	up	2,09	0,13	0,026
MANEA	down	-2,34	0,22	0,037
MEI1	up	2,41	0,09	0,014
NDC80	down	-2,04	0,47	0,098
NUP107	down	-2,04	0,72	0,145
NXT2	down	-2,07	0,39	0,081
OSCAR	up	2,25	0,06	0,011
PAEP	up	2,00	0,01	0,002
PHIP	down	-2,00	0,64	0,136
PI4K2B	down	-2,04	0,08	0,018
PIGK	down	-2,28	0,45	0,078
PLXND1	up	2,38	0,61	0,097
PSG2	up	4,06	2,40	0,161
RAB39B	up	10,47	1,26	0,030
RAC2	up	2,08	0,14	0,029
RAD54B	down	-2,09	0,22	0,046
RASD1	up	2,04	0,04	0,008

RNF160	down	-2,40	0,17	0,028	SSTR3	up	12,74	2,33	0,044
ROBO3	up	3,62	0,23	0,020	TBL1XR1	down	-2,01	0,21	0,047
RRAD	up	2,55	0,96	0,131	TNFRSF10D	up	2,05	0,51	0,105
SERPINE1	up	2,01	0,03	0,007	TNPO1	down	-2,08	0,42	0,086
SFRS12IP1	down	-2,14	0,47	0,089	TTK	down	-2,13	0,11	0,021
SGOL2	down	-2,40	0,38	0,060	UNC5B	up	4,25	0,49	0,034
SLC25A36	down	-2,05	0,46	0,096	USP15	down	-2,29	0,43	0,074
SLCO4C1	down	-2,25	0,48	0,085	ZDHHC14	up	2,64	1,67	0,199
SNORD22	down	-2,26	0,09	0,015	ZNF267	down	-2,02	0,08	0,018
SPRR2C	up	3,57	1,23	0,104	ZNF292	down	-2,09	0,67	0,130
SPRR2D	up	6,51	4,20	0,157	ZNF418	up	2,25	0,11	0,020

Supplementary Table 4. Genes being deregulated in HepG2-cells expressing kdFGFR4. *Data were processed as described in Experimental Procedures and are means of fold-vector control values of 2 different experiments. Fold-change cutoffs of ≥2 and ≤0.5 were used to select upregulated and downregulated genes, respectively.*

Gene	reg.	mean x Control	S.D.	p-value
ACADM	down	-2.02	0.16	0.035
AIMP1	down	-2.02	0.36	0.078
AKAP9	down	-2.75	1.48	0.171
ANKRD12	down	-3.03	1.63	0.164
ANKRD32	down	-2.67	0.34	0.045
ANLN	down	-2.15	0.48	0.092
ARHGAP18	down	-2.04	0.16	0.035
ARL6IP1	down	-2.17	0.43	0.081
ASNSD1	down	-2.13	0.28	0.055
BDP1	down	-2.51	1.17	0.159
BLZF1	down	-2.18	0.20	0.039
BRIX1	down	-2.06	0.05	0.011
C12orf4	down	-2.15	0.67	0.125
C12orf60	down	-2.07	0.69	0.137
C14orf106	down	-2.36	0.85	0.132
C1orf156	down	-2.10	0.22	0.045
C5	down	-2.17	0.92	0.161
C6orf211	down	-2.10	0.26	0.052
CASP8AP2	down	-2.61	0.85	0.113
CCDC41	down	-2.36	0.41	0.066
CCDC77	down	-2.13	0.08	0.016
CCDC99	down	-2.06	0.57	0.115
CCNL1	down	-2.99	2.43	0.227
CCPG1	down	-2.08	0.06	0.012
CDC40	down	-2.14	0.36	0.071
CDC7	down	-2.06	0.24	0.051
CDC73	down	-2.04	0.22	0.048
CEBPZ	down	-2.39	0.34	0.054
CENPC1	down	-3.29	0.55	0.054
CENPE	down	-3.86	2.55	0.179
CENPK	down	-2.36	0.62	0.100
CENPQ	down	-2.14	0.47	0.089
CFI	down	-2.16	0.02	0.003
CHD9	down	-2.15	0.57	0.107
COG6	down	-3.03	0.07	0.007
COMMD8	down	-2.03	0.37	0.079
CUL5	down	-2.63	0.02	0.002
CUZD1	down	-2.33	0.10	0.017
DCUN1D4	down	-2.13	0.53	0.102
DDX18	down	-2.13	0.59	0.112
DDX6	down	-2.05	0.97	0.184
DLGAP5	down	-2.39	0.20	0.033
DNA2	down	-2.51	0.37	0.054
DNTTIP2	down	-2.38	0.35	0.056
DOPEY1	down	-2.17	0.64	0.117
EEA1	down	-2.13	0.31	0.060
EIF2A	down	-2.08	0.38	0.077
EIF3E	down	-2.21	0.95	0.161
EIF4A2	down	-2,52	0,12	0,018
ELMOD2	down	-2,14	0,14	0,027
ERBB2IP	down	-2,04	0,53	0,111
ERGIC2	down	-2,19	0,33	0,062
ESCO1	down	-2,26	0,02	0,004
ESF1	down	-2,13	0,74	0,139
EXOC6	down	-2,05	0,23	0,048
FAM133B	down	-2,49	0,10	0,015
FAM35A	down	-2,06	0,13	0,027
FASTKD1	down	-2,00	0,07	0,015
FASTKD3	down	-2,03	0,04	0,008
G2E3	down	-2,32	0,04	0,007
GFM2	down	-2,03	0,47	0,099
GNPDA2	down	-2,10	0,19	0,039
GOLGA4	down	-2,53	1,09	0,149
HLTF	down	-2,35	0,35	0,058
HMMR	down	-2,48	0,50	0,075
HOOK1	down	-2,63	0,54	0,073
HSP90AA1	down	-2,48	0,94	0,134
IER3IP1	down	-2,10	0,10	0,021
IFIT1	down	-2,59	0,46	0,064
IL6ST	down	-2,24	0,22	0,040
ITGB3BP	down	-2,12	0,84	0,155
KIAA0528	down	-2,53	0,11	0,016
KIAA0776	down	-2,43	0,14	0,022
KIAA1033	down	-2,05	0,14	0,031
KIAA1524	down	-2,18	0,22	0,041
KIF15	down	-2,09	1,01	0,184
KPNA5	down	-2,32	0,65	0,106
KRR1	down	-2,05	0,07	0,014
KRT37	up	2,53	0,03	0,005
KTN1	down	-2,20	0,55	0,099
LARP7	down	-2,52	0,21	0,031
LOC401397	down	-2,39	0,81	0,125
LPAR6	down	-2,32	0,71	0,115
LRRC58	down	-2,45	0,17	0,027

LTV1	down	-2,06	0,17	0,036
LUC7L3	down	-2,00	0,02	0,005
MAD2L1	down	-2,19	0,24	0,044
MANEA	down	-2,68	0,05	0,006
MBNL3	down	-2,25	0,71	0,122
MORC3	down	-2,11	0,02	0,003
MPHOSPH10	down	-2,39	0,73	0,114
MRPL50	down	-2,07	0,59	0,119
MTERF	down	-2,42	0,10	0,016
MTTP	down	-2,18	0,04	0,008
NARG2	down	-2,32	0,33	0,056
NBEAL1	down	-2,05	0,48	0,099
NCAPG	down	-2,08	0,49	0,099
NDC80	down	-2,33	0,40	0,066
NEK7	down	-2,45	0,15	0,023
NOC3L	down	-2,29	0,47	0,081
NOL11	down	-2,46	0,47	0,072
NOL8	down	-2,25	0,46	0,081
NOP58	down	-2,07	0,10	0,021
NUDCD1	down	-2,00	0,36	0,080
NUF2	down	-2,14	0,53	0,100
NUP107	down	-2,24	0,70	0,122
NXT2	down	-2,21	0,55	0,099
PAK1IP1	down	-2,01	0,05	0,012
PBK	down	-2,12	0,08	0,016
PGM3	down	-2,05	0,62	0,126
PIBF1	down	-2,81	0,68	0,083
PIK3C3	down	-2,09	0,59	0,115
PION	down	-2,08	0,53	0,107
PLK4	down	-2,30	0,31	0,053
PLS1	down	-2,25	0,52	0,091
PMS1	down	-2,46	0,52	0,079
PPIG	down	-2,22	0,04	0,008
PPWD1	down	-2,04	0,01	0,003
PRKRIR	down	-2,05	0,39	0,082
PTAR1	down	-2,04	0,09	0,019
RAC2	up	2,14	0,66	0,123
RAD51AP1	down	-2,35	0,11	0,018
RAD54B	down	-2,29	0,07	0,012
RARS	down	-2,06	0,87	0,168
RASD1	up	2,32	0,88	0,140
RB1CC1	down	-2,07	0,17	0,035
RBM41	down	-2,72	1,18	0,143
RECQL	down	-2,00	0,27	0,060
RIF1	down	-2,76	0,91	0,112
RNMT	down	-2,12	0,63	0,121
RPAP3	down	-2,36	0,09	0,015
RRAD	up	2,86	2,05	0,211
SAMD9	down	-3,93	0,12	0,009
SCOC	down	-2,08	0,73	0,142
SDCCAG1	down	-2,29	0,40	0,069
SEPP1	down	-2,22	0,17	0,030
SEPT7	down	-2,05	0,05	0,011
SFRS12IP1	down	-3,18	0,65	0,066
SGOL2	down	-3,56	0,71	0,062
SHOC2	down	-2,08	0,58	0,116
SLC25A36	down	-2,13	0,15	0,030
SMC2	down	-2,34	0,10	0,017
SMC6	down	-2,38	0,05	0,008
SPP1	down	-2,02	0,14	0,031
SSX2IP	down	-2,22	0,34	0,062
STXBP4	down	-2,03	0,04	0,008
TAF1B	down	-2,29	0,09	0,016
TANK	down	-2,13	0,62	0,119
TAX1BP1	down	-2,09	0,56	0,110
TBC1D23	down	-2,29	0,71	0,118
TBC1D8B	down	-2,21	0,13	0,024
TBK1	down	-2,50	0,03	0,005
TBL1XR1	down	-2,08	0,08	0,016
TGDS	down	-2,15	0,27	0,052
THUMPD2	down	-2,01	0,14	0,030
TMEM161B	down	-2,20	0,07	0,013
TMEM87A	down	-2,02	0,60	0,125
TMTC3	down	-2,10	0,55	0,109
TNFAIP2	up	2,11	0,59	0,114
TNFRSF10D	up	2,04	0,16	0,035
TNPO1	down	-2,44	0,39	0,059
TTC37	down	-2,26	0,17	0,030
TXNDC9	down	-2,04	0,60	0,123
UBA3	down	-2,07	0,54	0,109
UPF3B	down	-2,02	0,36	0,077
USP15	down	-2,58	0,80	0,110
WDR36	down	-2,17	0,56	0,104
ZC3H11A	down	-2,00	0,83	0,169
ZNF146	down	-2,82	0,55	0,066
ZNF195	down	-2,05	0,01	0,003
ZNF24	down	-2,29	0,92	0,148
ZNF267	down	-2,87	0,52	0,062
ZNF292	down	-2,58	0,85	0,116
ZNF600	down	-2,01	0,05	0,011
ZNF644	down	-2,53	0,91	0,127
ZNF823	down	-2,05	0,37	0,077
ZRANB2	down	-2,20	0,09	0,016
ZRANB3	down	-2,21	0,56	0,100

ZWILCH	down	-2,56	1,07	0,143

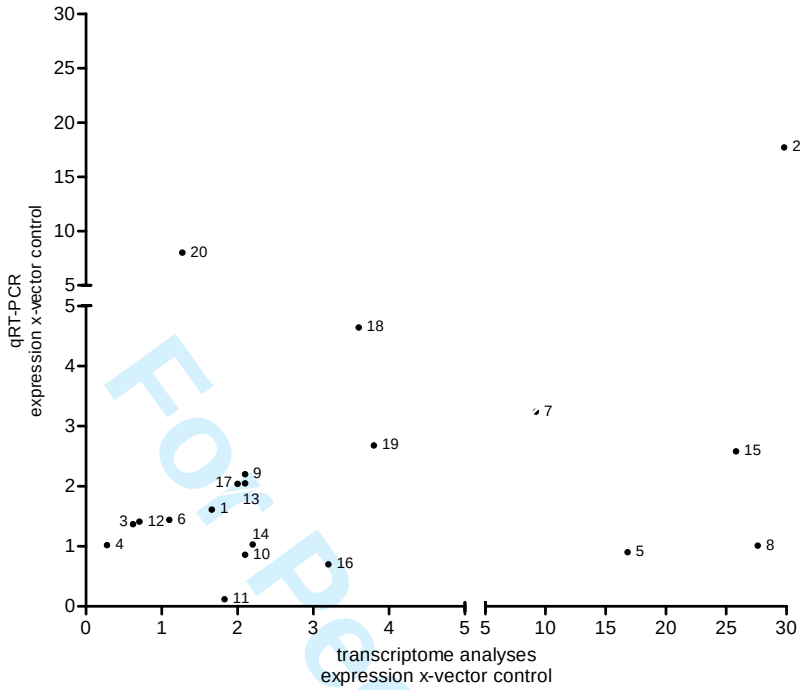

Supplementary Figure 6. Validation of transcriptome data by quantitative RT-PCR (qRT-PCR). *Correlation of the relative expression of selected genes determined by transcriptome analysis and qRT-PCR. FGFR4-overexpressing clones and vector controls were subjected to the analysis. Each data point represents the expression level of a given gene, expressed as fold vector control, and is the mean of ≥2 independent determinations per method applied. Symbols: 1, ACAD10; 2, AFP; 3, CDC7, 4, CENPE; 5, DUSP26; 6, GAPDH; 7, GNB4; 8, LOXL2, 9, MAPKAP1; 10, MMP11; 11, MMP14; 12, NDC80; 13, PI4K2A; 14, PIK3IP1; 15, PLCG2; 16, PPP1R3C; 17, PRKAB1; 18; PRKAG2; 19; RPS6KA5; 20, ZNF14. Statistics by GraphPad Prism (Version 5.0):* $r^2 = 0.7818$; $p < 0.01$.

Supplementary Table 5. Most significant gene sets in GSEA analysis of hepatoma/hepatocarcinoma cells showing FGFR4-overexpression or subjected to interference with FGFR-4 mediated signaling by solFGFR4 or kdFGFR4. *For further details on GSEA see http://www.broadinstitute.org/gsea/doc/GSEAUserGuideFrame.html. Gene sets were considered to be significantly deregulated in case of a FDR q-value of less than 0.25 and/or a p-value of less than 0.05.*

TREATMENT	SOURCE[1]	GENESET[2]	ES[3]	NES[4]	p-value[5]	FDR q-value[6]	up/dwn[7]
METABOLISM							
FGFR4 Overexpr.	reactome	integration of energy metabolism	432	16443998	0,010	0,143	Up
Bile Acid & Phase I / II Metabolism							
FGFR4 Overexpr.	reactome	glutathione conjugation	762	20704389	0,000	0,003	Up
SolFGFR4	reactome	glutathione conjugation	-0,391	-16707102	0,000	0,004	down
kdFGFR4	reactome	glutathione conjugation	-391	-1551765	0,000	0,003	down
FGFR4 Overexpr.	reactome	xenobiotics	737	18618722	0,010	0,029	up
FGFR4 Overexpr.	reactome	phase1 functionalization of compounds	716	25428765	0,000	0,000	up
FGFR4 Overexpr.	reactome	phase ii conjugation	431	14801257	0,039	0,277	up
FGFR4 Overexpr.	kegg	drug metabolism cytochrome p450	604	20455685	0,000	0,003	up
FGFR4 Overexpr.	kegg	primary bile acid biosynthesis	756	19609323	0,000	0,009	up
FGFR4 Overexpr.	reactome	synthesis of bile acids and bile salts	729	19394598	0,000	0,012	up
Carbohydrate Metabolism							
FGFR4 Overexpr.	kegg	glycolysis gluconeogenesis	535	18168197	0,000	0,044	up
kdFGFR4	reactome	glycolysis	-340	-11867602	0,000	0,085	down
solFGFR4	reactome	regulation of glucokinase by glucokinase regulatory protein	-340	-18091897	0,000	0,002	down
kdFGFR4	reactome	regulation of glucokinase by glucokinase regulatory protein	-341	-15361433	0,000	0,004	down
kdFGFR4	kegg	pentose phosphate pathway	-246	-13278433	0,000	0,028	down
FGFR4 Overexpr.	reactome	regulation of insulin secretion	381	13782212	0,047	0,342	up
solFGFR4	signal transduction ke	g alpha s pathway	-408	-15892403	0,000	0,007	down
Lipid Metabolism							
FGFR4 Overexpr.	reactome	metabolism of lipids and lipoproteins	408	18155632	0,000	0,044	up
FGFR4 Overexpr.	kegg	ppar signaling pathway	479	16627568	0,006	0,143	up
FGFR4 Overexpr.	kegg	fatty acid metabolism	534	16547354	0,004	0,144	up
FGFR4 Overexpr.	reactome	fatty acid triacylglycerol and ketone body metabolism	374	14658921	0,014	0,276	up
kdFGFR4	reactome	activated ampk stimulates fatty acid oxidation in muscle	-445	-15405483	0,000	0,003	down
FGFR4 Overexpr.	reactome	lipoprotein metabolism	517	15096359	0,027	0,249	up
solFGFR4	reactome	cholesterol biosynthesis	-0,341	-1348732	0,000	0,045	down
kdFGFR4	reactome	cholesterol biosynthesis	-347	-19267347	0,000	0,000	down
solFGFR4	kegg	steroid biosynthesis	-409	-18535615	0,000	0,001	down
FGFR4 Overexpr.	kegg	steroid biosynthesis	758	19486688	0,000	0,010	up
kdFGFR4	kegg	steroid biosynthesis	-431	-1532288	0,000	0,004	down
FGFR4 Overexpr.	kegg	glycerophospholipid metabolism	422	1476495	0,021	0,279	up
kdFGFR4	reactome	peroxisomal lipid metabolism	-557	-29659848	0,000	0,000	down
solFGFR4	reactome	peroxisomal lipid metabolism	-359	-15086856	0,042	0,014	down

GROWTH FACTORS & SIGNALING							
FGFR4 Overexpr.	reactome	signaling by fgfr	372	13992958	0,026	0,328	up
FGFR4 Overexpr.	reactome	signaling by ngf	377	15654117	0,000	0,200	up
FGFR4 Overexpr.	kegg	neurotrophin signaling pathway	342	13113501	0,050	0,380	up
FGFR4 Overexpr.	pathway interaction db	hnf3b pathway	575	185707	0,000	0,030	up
FGFR4 Overexpr.	biocarta	wnt pathway	548	1544899	0,029	0,215	up
FGFR4 Overexpr.	signal transduction ke	wnt ca2 cyclic gmp pathway	677	18498185	0,002	0,030	up
FGFR4 Overexpr.	kegg	vegf signaling pathway	471	16928533	0,000	0,136	up
FGFR4 Overexpr.	kegg	insulin signaling pathway	421	16532453	0,004	0,143	up
FGFR4 Overexpr.	reactome	dag and ip3 signaling	542	16121129	0,006	0,166	up
FGFR4 Overexpr.	pathway interaction db	foxo pathway	455	14477632	0,038	0,283	up
FGFR4 Overexpr.	molecular signature db	neighbourhood of egfr	486	18112922	0,000	0,017	up
FGFR4 Overexpr.	kegg	erbb signaling pathway	448	16314427	0,006	0,153	up
FGFR4 Overexpr.	pathway interaction db	erbb1 receptor proximal pathway	535	16491752	0,014	0,139	up
FGFR4 Overexpr.	reactome	pi3k events in erbb2 signaling	473	1462234	0,045	0,277	up
FGFR4 Overexpr.	reactome	signaling by erbb2	457	16867846	0,002	0,134	up
FGFR4 Overexpr.	reactome	grb2 sos provides linkage to mapk signaling for intergrins	619	15648876	0,032	0,198	up
FGFR4 Overexpr.	pathway interaction db	myc represspathway	416	14346324	0,041	0,290	up
FGFR4 Overexpr.	literature[8]	growth factors	291	15379304	0,000	0,051	up
FGFR4 Overexpr.	molecular signature db	neighbourhood of igfbp1	469	18355389	0,003	0,021	up
solFGFR4	pathway interaction db	smad2, 3 pathway	-445	-16881058	0,045	0,004	down
FGFR4 Overexpr.	reactome	regulation of insulin like growth factor igf activity by insulin like growth factor binding proteins igfbps	755	19594024	0,000	0,009	up
FGFR4 Overexpr.	molecular signature db	neighbourhood of igf1	615	22455778	0,000	0,000	up
FGFR4 Overexpr.	biocarta	igf1r pathway	512	14718565	0,043	0,277	up
FGFR4 Overexpr.	pathway interaction db	mtor 4pathway	499	17298361	0,004	0,110	up
kdFGFR4	biocarta	igf1 mtor pathway	-461	-16046475	0,000	0,002	down
solFGFR4	biocarta	mtor pathway	-387	-16303421	0,000	0,005	down
kdFGFR4	biocarta	mtor pathway	-562	-2946386	0,000	0,000	down
kdFGFR4	pathway interaction db	smad2, 3 pathway	-576	-21198254	0,000	0,000	down
kdFGFR4	reactome	pkb mediated events	-499	-21047058	0,000	0,000	down
solFGFR4	signal transduction ke	erk1 erk2 mapk pathway	-250	-13145965	0,000	0,058	down
kdFGFR4	signal transduction ke	erk1 erk2 mapk pathway	-389	-16336486	0,000	0,001	down
FGFR4 Overexpr.	biocarta	erk pathway	547	16009966	0,018	0,165	up
FGFR4 Overexpr.	reactome	p130cas linkage to mapk signaling for integrins	601	15549306	0,047	0,206	up
FGFR4 Overexpr.	pathway interaction db	p53 downstream pathway	364	1408855	0,016	0,314	up
DNA REPLICATION							
solFGFR4	kegg	dna replication	-355	-16250973	0,000	0,005	down
solFGFR4	reactome	scf skp2 mediated degradation of p27 p21	-328	-17479932	0,000	0,002	down
kdFGFR4	reactome	e2f mediated regulation of dna replication	-320	-12472445	0,000	0,054	down
kdFGFR4	biocarta	raccycd pathway	-248	-10537288	0,000	0,195	down
kdFGFR4	gene ontology	regulation of mitotic cell cycle	-326	-11982346	0,133	0,040	down
FGFR4 Overexpr.	reactome	deposition of new cenpa containing nucleosomes at the centromere	501	1692985	0,000	0,140	up

FGFR4 Overexpr.	reactome	meiotic recombination	442	16039301	0,008	0,166	up
kdFGFR4	gene ontology	cytokinesis	-277	-14520413	0,000	0,009	down
CELL ADHESION							
FGFR4 Overexpr.	kegg	adherens junction	445	161398	0,004	0,166	up
FGFR4 Overexpr.	reactome	integrin alphaiib beta3 signaling	536	15740358	0,033	0,192	up
FGFR4 Overexpr.	reactome	signal transduction by l1	532	1608842	0,016	0,167	up
FGFR4 Overexpr.	signal transduction ke	integrin signaling pathway	397	14292204	0,036	0,293	up
FGFR4 Overexpr.	kegg	n glycan biosynthesis	455	14559896	0,039	0,280	up
FGFR4 Overexpr.	reactome	formation of fibrin clot clotting cascade	487	14463629	0,046	0,277	up
FGFR4 Overexpr.	reactome	glycosaminoglycan metabolism	391	14483864	0,018	0,286	up
FGFR4 Overexpr.	kegg	cell adhesion molecules cams	334	16972758	0,000	0,031	up
FGFR4 Overexpr.	literature[9]	cell adhesion	354	14507823	0,031	0,082	up
FGFR4 Overexpr.	reactome	hs gag biosynthesis	518	1536494	0,049	0,221	up
FGFR4 Overexpr.	geneontology	leukocyte cell-cell adhesion	464	16197507	0,013	0,040	up
FGFR4 Overexpr.	reactome	chondroitin sulfate dermatan sulfate metabolism	523	1618145	0,016	0,163	up
MALIGNANT PHENOTYPE							
FGFR4 Overexpr.	kegg	non small cell lung cancer	508	16354848	0,014	0,150	up
FGFR4 Overexpr.	kegg	endometrial cancer	487	15982684	0,014	0,166	up
FGFR4 Overexpr.	kegg	thyroid cancer	506	14910656	0,041	0,259	up
FGFR4 Overexpr.	pathway interaction db	upa upar pathway	527	16548454	0,006	0,147	up
solFGFR4	biocarta	ndkdynamin pathway	-326	-13396149	0,043	0,048	down
kdFGFR4	molecular signature db	breuhahn - growth factor signaling in liver cancer	-237	-0, 922641	0,750	0,195	down

1. The source of the geneset.
2. The name of the geneset listed in the molecular signature database or gene ontology.
3. ES: Enrichment score for the gene set is the degree to which this gene set is overrepresented at the top or bottom of the ranked list of genes in the expression dataset.
4. NES: Normalized enrichment score is the enrichment score for the gene set after it has been normalized across analyzed gene sets.
5. p-value: the statistical significance of the enrichment score not adjusted for gene set size or multiple hypothesis testing.
6. FDR q-value: the estimated probability that the normalized enrichment score represents a false positive finding.
7. up/down: whether the geneset is enriched in the up-regulated or the down-regulated portion of the array
8. This geneset was constructed from literature and encompasses: AGT, AMBN, AMELX, AMH, ANGPTL3, AREG, ARTN, BDNF, BMP1, BMP10, BMP15, BMP2, BMP3, BMP4, BMP5, BMP6, BMP7, BMP8A, BMP8B, BTC, CD320, CECR1, CLCF1, CLEC11A, CSF1, CSF2, CSF3, CSPG5, CTGF, CXCL1, CXCL12, DKK1, EFEMP1, EGF, EREG, ESM1, F2, FGF1, FGF10, FGF11, FGF12, FGF13, FGF14, FGF16, FGF17, FGF18, FGF19, FGF2, FGF20, FGF21, FGF22, FGF23, FGF3, FGF4, FGF5, FGF6, FGF7, FGF8, FGF9, FIGF, GDF1, GDF10, GDF11, GDF15, GDF2, GDF3, GDF5, GDF6, GDF9, GDNF, GFER, GH1, GKN1, GMFB, GMFG, GPI, GRN, HBEGF, HDGF, HDGFRP3, HGF, IGF1, IGF2, IL10, IL11, IL12A, IL12B, IL1B, IL2, IL3, IL4, IL5, IL6, IL7, IL9, INHA, INHBA, INHBB, INHBC, INHBE, JAG1, JAG2, KGFLP1, KITLG, LACRT, LEFTY1, LEFTY2, LEP, LIF, MDK, MIA, NDP, NENF, NODAL, NOV, NRG1, NRG2, NRG4, NRTN, NTF3, NUDT6, OGN, OSM, PDGFA, PDGFB, PDGFC, PDGFD, PGF, PPBP, PROK1, PSPN, PTN, RABEP1, RABEP2, REG1A, TDGF1, TFF1, TGFA, TGFB1, TGFB2, TGFB3, THPO, VEGFB, VEGFC, VGF and WISP3.
9. This geneset was manually constructed from literature and consists of: CEACAM6, L1CAM, EFEMP1, NCAM1, CHL1, VCAM1, DSCAM, TCAM1, DSCAML1, ECM1, CEACAM4, CEACAM5, SDK1,

OPCML, ECM2, CEACAM7, GLYCAM1, ALCAM, CEACAM8, MATN1, SPON1, MADCAM1, CEACAM21, PECAM1, AMBN, NRCAM, COMP, CEACAM3, BSN, EFEMP2, MCAM, FREM1, ESAM, CEACAM1, CEACAM20, CEACAM19, SPON.

Supplementary Table 6. Ingenuity Pathway Analysis of hepatoma/hepatocarcinoma cells showing FGFR4-overexpression or subjected to interference with FGFR4-mediated signaling by solFGFR4 or kdFGFR4. *The functional significance of differentially expressed genes was evaluated using Ingenuity Pathway analysis software (Ingenuity Systems Version 8.8, Redwood City, CA; www.ingenuity.com). GenBank IDs of all genes with at least a two-fold change and $p < 0.05$ were imputed for network generation and pathway analyses and mapped to canonical pathways and functional networks available in the Ingenuity Pathway Knowledge Base. A score was determined for each network, reflecting the negative logarithm of the p-value based on the chance that the focus genes were grouped in the network by random chance. Abbreviations: TCP, top canonical pathway; TN, top networks.*

TREATMENT	Cat.		p-value	Ratio	Score
METABOLISM					
solFGFR4	TCP	Superpathway of Methionine Degradation	4,47E-07	15/65 (0,231)[8)]	
FGFR4 Overexpr.	TCP	Protein Ubiquitination Pathway	3,61E-06	99/270 (0,367)	
solFGFR4	TCP	Protein Ubiquitination Pathway	7,49E-11	67/270 (0,248)	
kdFGFR4	TCP	Protein Ubiquitination Pathway	3,67E-10	65/270 (0,241)	
solFGFR4	TN	Small Molecule Biochemistry[1)]			36[9)]
kdFGFR4	TN	Small Molecule Biochemistry[1)]			34
Bile Acid & Phase I / II Metabolism					
FGFR4 Overexpr.	TCP	LXR/RXR Activation	4,05E-08	60/123 (0,488)	
FGFR4 Overexpr.	TCP	CAR/RXR Activation	1,93E-04	17/29 (0,586)	
FGFR4 Overexpr.	TCP	PXR/RXR Activation	1,15E-05	34/67 (0,507)	
FGFR4 Overexpr.	TCP	LXR/RXR Activation	1,47E-07	58/139 (0,417)	
kdFGFR4	TN	Drug Metabolism [2)]			34
Carbohydrate Metabolism					
solFGFR4	TN	Carbohydrate Metabolism [2)]			36
kdFGFR4	TN	Carbohydrate Metabolism [2)]			34
Lipid Metabolism					
solFGFR4	TCP	Superpathway of Methionine Degradation	4,47E-07	15/65 (0,231)	
FGFR4 Overexpr.	TN	Lipid Metabolism[3)]			27
GROWTH FACTORS & SIGNALING					

solFGFR4	TCP	Role of BRCA1 in DNA Damage Response	5,82E-10	26/71 (0,366)	
kdFGFR4	TCP	Role of BRCA1 in DNA Damage Response	3,6E-07	22/71 (0,31)	
solFGFR4	TCP	Hereditary Breast Cancer Signaling	6,32E-08	35/134 (0,261)	
solFGFR4	TCP	p53 Signaling	3,34E-04	24/99 (0,242)	
kdFGFR4	TCP	p53 Signaling	3,92E-03	21/99 (0,212)	
kdFGFR4	TCP	ATM Signaling	1,6E-06	21/66 (0,318)	
solFGFR4	TCP	Hypoxia-Inducible Factor Signaling	9,56E-05	20/70 (0,286)	
FGFR4 Overexpr.	TCP	Production of Nitric Oxide and Reactive Oxygen Species in Macrophages	9,12E-06	73/212 (0,344)	
FGFR4 Overexpr.	TN	Cell-To-Cell Signaling and Interaction[4)]			27
DNA REPLICATION					
solFGFR4	TN	Cell Cycle, DNA Replication [5)]			36
kdFGFR4	TN	Cell Cycle, DNA Replication [5)]			34
FGFR4 Overexpr.	TN	Cell Cycle, DNA replication [5)]			27
kdFGFR4	TCP	Mitotic Roles of Polo-Like Kinase	7,99E-09	26/74 (0,351)	
FGFR4 Overexpr.	TCP	Mitotic Roles of Polo-Like Kinase	3,68E-06	35/74 (0,473)	
solFGFR4	TCP	Cell Cycle: G1/S Checkpoint Regulation	7,66E-05	20/69 (0,29)	
kdFGFR4	TCP	Cell Cycle: G1/S Checkpoint Regulation	1,74E-03	17/69 (0,246)	
solFGFR4	TCP	Cell Cycle: G2/M DNA Damage Checkpoint Regulation	3,29E-06	18/48 (0,375)	
kdFGFR4	TCP	Cell Cycle: G2/M DNA Damage Checkpoint Regulation	5,48E-05	16/48 (0,333)	
kdFGFR4	TCP	Liver Necrosis/Cell Death	1,56E-03	48/271 (0,177)	
FGFR4 Overexpr.	TCP	Liver Necrosis/Cell Death	1,25E-05	102/271 (0,376)	
CELL ADHESION					

FGFR4 Overexpr.	TN	Connective Tissue Development and Function [6]			27
solFGFR4	TCP	Remodeling of Epithelial Adherens Junctions	1,43E-08	26/70 (0,371)	
kdFGFR4	TCP	Remodeling of Epithelial Adherens Junctions	1,03E-06	23/70 (0,329)	
FGFR4 Overexpr.		Cellular Movement [7]			27
MALIGNANT PHENOTYPE					
solFGFR4	TCP	Hereditary Breast Cancer Signaling	6,32E-08	35/134 (0,261)	

1) Part of the TN: Carbohydrate Metabolism, Small Molecule Biochemistry, Nephrosis
2) Part of the TN: Carbohydrate Metabolism, Drug Metabolism, Small Molecule Biochemistry
3) Part of the TN: Developmental Disorder, Hereditary Disorder, Lipid Metabolism
4) Part of the TN: Cell-To-Cell Signaling and Interaction, Cellular Assembly and Organization, Cellular Function and Maintenance
5) Cell Cycle, Cellular Assembly and Organization, DNA Replication, Recombination, and Repair
6) Part of the TN: Organ Morphology, Skeletal and Muscular System Development and Function, Connective Tissue Development and Function
7) Part of the TN: Dermatological Diseases and Conditions, Cell Cycle, Cellular Movement.
8) indicates the ratio between deregulated genes to the total number of genes being grouped to a pathway given.
9) A score of 2 corresponds with a 1 in 100 chance that the focus genes are grouped together by random chance. As such, scores of 2 or higher indicate at least a 99% confidence that a true molecular relationship exists.

Human hepatocellular carcinoma and FGFR4-overepxressing hepatocarcinoma cells exhibit similar alterations in signaling cascades

Following ligand binding and FGFR4 dimerization, the kinase domains transphosphorylate each other. As a result, several downstream pathways may be activated: RAS–RAF–MAPK, PI3K–AKT, signal transducer and activator of transcription (STAT), and phospholipase Cγ (PLCG) (Turner et al., Nat Rev Cancer 2010). FGFRs also phosphorylate ribosomal S6 kinase (Kang *et al., Mol Cell Biol* 2009). Signaling can be negatively regulated at several levels, e.g., by receptor internalization or the induction of negative regulators, including sproutys or MAPK phosphatases, which may interfere through modulation of the MAPK pathway (Turner et al., Nat Rev Cancer 2010).

In FGFR4-overexpressing hepatocarcinoma cells enhanced phosphorylation of PLCG1 and ERK became evident, which indicates activation of the PLCG- and RAS-RAF-MAPK-pathways (suppl.fig.3C and 3D). Interestingly, AKT phosphorylation appeared to be somewhat reduced. Analyzing the transcriptome of these cells and the subsequent validation of the data by qRT-PCR revealed deregulations of several further genes, involved directly or indirectly in FGFR4-mediated signaling, which is outlined in the following.

In one of the clones we found elevated mRNA levels of 1-phosphatidylinositol-4,5-bisphosphate phosphodiesterase gamma-2 **(PLCG2).** Like PLCG1, PLCG2 hydrolyzes phosphatidylinositol 4,5-bisphosphate (PtdIns(4,5)P_2 or PIP_2) to form inositol 1,4,5-triphosphate and diacylglycerol. The former product promotes the intracellular mobilization of calcium, whereas the latter one activates protein kinase C isoforms. Generally, the functionality of PLCG isoenzymes is based on the products of phosphoinositide metabolism and phosphatidylinositol 4-kinase type 2-alpha **(PI4K2A)** phosphorylates PtdIns at the D-4 position, an essential step in the biosynthesis of PtdInsPs (Barylko et al., JBC 2001). This indicates that apart from the enhanced phosphorylation of PLCG1 further components of the PLCG-pathway were affected occassionally by FGFR4-overexpression.

With regard to the RAS-RAF-MAPK pathway, we found unchanged levels of the serine/threonine kinase, PDZ binding kinase **(PBK),** and enhanced expression of the target of rapamycin complex 2 subunit **(MAPKAP1).** PBK is related to the dual specific mitogen-activated protein kinase kinase (MAPKK) family. Evidence suggests that mitotic phosphorylation is required for its catalytic activity (Gaudet et al., PNAS 2000). MAPKAP1

binds to both ATF-2 and p38, enhances ATF-2-dependent transcription in the MAPK-pathway and inhibits RAS-mediated signaling (Makino et al., Genes Cells 2006; Schroder et al., Cell Sign 2007).

The activation of ribosomal S6 kinase by FGFR4 appeared to be active as well, since the ribosomal protein S6 kinase polypeptide 5 **(RPS6KA5)** wase found to be upregulated in two of three FGFR4-overexpressing hepatocarcinoma cell clones. As members of the RSK family of serine/threonine kinases it phosphorylates various substrates, including members of the mitogen-activated kinase (MAPK) signaling pathway. The activity of these proteins has been implicated in controlling cell growth and differentiation (Xing et al.,Science 1996). In response to growth factors or stress RPS6KA5 is activated by either ERK or SAPK2 proteins, which in turn mediates activation of the CREB (cAMP response element-binding protein) and ATF1 (Activating Transcription Factor-1). The growth-factor induced activation of RPS6KA5 can be blocked by inhibitors for the MAPK pathways. Dual specificity protein phosphatase 26 (**DUSP26**) inactivates MAPK1 and MAPK3 which leads to dephosphorylation of heat shock factor protein 4 and a reduction in its DNA-binding activity. In dependence of the context, DUSP26 can also induce activation of MAP kinase p38 and c-Jun N-terminal kinase (Yu et al., Oncogene 2007). The level of this gene appeared to be altered by FGFR4-overexpression.

Also couterregulations appear to be active. Li et al (Mol Cell Biochem 2008) show that zinc finger protein 418 (**ZNF418)** is a transcriptional repressor with the KRAB motif as the basal repressive domain. Overexpression of ZNF418 inhibits the transcriptional activity of SRE and AP-1 and may act as a negative regulator in MAPK signaling pathway. Phosphoinositide-3-kinase-interacting protein 1 **(PIK3IP1)** shares homology with the p85 regulatory PI3K subunit. It directly binds to the p110 catalytic subunit and down modulates PI3K activity (Zhu et al., Biochem Biophys Res Commun 2007). The upregulation in clone 4 may explain the somewhat reduced phosphorylation of AKT (see suppl.fig. 3C and 3D).

In samples of human hepatocellular carcinoma (HCC) we studied the expression of genes, which were found to be deregulated in FGFR4-overexpressing clones. We discriminated between HCC with low and high FGFR4-expression. In the latter group mRNA deregulations of PLCG2, PI4K2A, MAPKAP1, DUSP26, ZNF418, and PIK3IP1 were evident. This may be indirect evidence that in FGFR4-overexpressing HCC and FGFR4-overexpressing hepatocarcinoma cells similar signaling cascades are activated.

Supplementary Table 7. FGFR4-overexpressing hepatocarcinoma cells and human hepatocellular

carcinoma (HCC): Expression of genes related to FGFR4-mediated signaling. *Details on FGFR4-overexpressing clones and vector controls see figure 2. Patients were subjected to surgical resection of HCC. Written informed consent was obtained from each patient. The study protocol conformed to the ethical guidelines of the 1975 Declaration of Helsinki, as reflected by the approval of the "Ethic Committee of the Medical University of Vienna". Details on age and sex of the patients, histopathological grade and pTNM stage of HCCs see below. Abbreviations: m, male; f, female; HCC1, HCC grade 1; HCC2, HCC grade 2. The classification of the tumour grade followed the criteria published by Edmondson et al. (Cancer 7: 462-503, 1954). For further details see Gauglhofer et al. (Hepatology, 2011). Messages were quantified by real time RT-PCR using assay kits (Applied Biosystems) according to the manufacturers instructions. For details see Methods. Bold numbers indicate message levels in HCC elevated at least 1.5-fold above the levels in the surrounding tissue or vector control.*

Expression in FGFR4-overexpressing clones (x vector control)[a)]

	FGFR4	PLCG2	PI4K2A	PBK	MAPKAP1	RPS6KA3	RPS6KA5	DUSP26	ZNF418	PIK3IP1
Clone 1	**10,4**	0,13	0,61	0,85	0,83	0,86	0,55	0,64	1,07	0,17
Clone 3	**18,3**	0,56	1,32	0,43	**2,27**	1,27	**1,8**	1,08	**7,27**	0,47
Clone 4	**16,5**	**4,61**	**2,76**	1,33	**2,14**	1,26	**3,56**	0,72	**8,77**	**1,59**

Expression in HCC (x surrounding tissue)[b)]

Age	Sex	Disease	FGFR4	PLCG2	PI4K2A	PBK	MAPKAP1	RPS6KA3	RPS6KA5	DUSP26	ZNF418	PIK3IP1
54	m	HCC1, pT1, pNx, pMx	**5,2**	0,54	**2,97**	**11,2**	**1,82**	1,36	1,2	**31,71**	**2,01**	0,91
67	m	HCC2, pT2, pN0, pMx	**4,9**	0,78	0,98	1,18	1,17	1,1	0,41	**1,57**	**1,65**	**6,05**
67	m	HCC2, pT1, pNx, pMx	**4,5**	**2,74**	**4,72**	0,13	**2,19**	**2,05**	0,35	**2,72**	0,56	**7,32**
68	m	HCC2, pT1, pNx, pMx	**4,1**	0,46	0,81	0,64	**2,46**	0,14	0,79	**2,24**	0,26	**2,77**
77	f	HCC2, pT1, pNx, pMx	**3,3**	**1,85**	**1,77**	**1,52**	**1,85**	1,19	1,32	0,08	0,14	**1,81**

82	f	HCC2, pT1, pNx, pMx	0,4	0,32	0,94	0,11	0,48	1,05	0,17	0,36	0,34	**1,96**
62	m	HCC2, pT1, pN0, pMx	0,6	0,36	0,09	**11,23**	0,41	0,29	**3,42**	0,17	**2,13**	0,55
56	m	HCC2, pT1, pNx, pMx	0,6	1,17	1,45	0,53	0,47	0,79	0,47	0,22	0,46	0,73
48	m	HCC2, pT2, pNx, pMx	0,7	0,6	1,01	**1,56**	0,78	**1,56**	0,27	0,09	0,52	0,4
59	m	HCC2, pT2, pN0, pMx	0,6	**2,12**	1,15	0,62	0,78	0,62	1,09	**3,19**	0,29	**2,24**

a) The expression level in FGFR4-overexpressing clone, relative to that in the vector control, has been expressed as $2^{-\text{deltadeltaCT}}$, which reflects deltaCT of the FGFR4-overexpressing clone minus deltaCT of the vector control (normalized to 1).

b) The expression level in HCC, relative to that in the surrounding liver tissue, has been expressed as $2^{-\text{deltadeltaCT}}$, which reflects deltaCT of the HCC minus deltaCT of the surrounding non-tumorous liver tissue (normalized to 1).